Investigation of a Novel Façade-Based Solar Loop Heat Pipe Water Heating System

Zhangyuan Wang, BEng., MSc.

Thesis submitted to the University of Nottingham

for the degree of Doctor of Philosophy

December 2011

Abstract

Solar thermal is one of the most cost-effective renewable energy technologies, and solar water heating is one of the most popular solar thermal systems. Based on the considerations on the existing barriers of the solar water heating, this research will propose a novel façade-based solar water heating system employing a unique loop heat pipe (LHP) structure with top-level liquid feeder, which will lead to a façade-integrated, low cost, aesthetically appealing and highly efficient solar system and has considerable potential to provide energy savings and reduce carbon emissions to the environment.

The research initially involved the conceptual design of the proposed system. The prefabricated external module could convert the solar energy to heat in the form of low-temperature vapour. The vapour will be transported to indoors through the transport line and condensed within the heat exchanger by releasing the heat to the service water. The heated water will then be stored in the tank for use.

An analytical model was developed to investigate six limits to the loop heat pipe's operation, i.e., capillary, entrainment, viscous, boiling, sonic and filled liquid mass. It was found that mesh-screen wick was able to obtain a higher capillary (governing) limit than sintered-powder. Higher fluid temperature, larger pipe diameter and larger exchanger-to-pipes height difference would lead to a higher capillary limit. Adequate system configuration and operating conditions were suggested as: pipe inner diameter of 16 mm, mesh-screen wick, heat transfer fluid temperature of 60^{o}C and height difference of 1.5 m.

This research further developed a computer model to investigate the dynamic performance of the system, taking into account heat balances occurring in different parts of the system, e.g., solar absorber, heat pipes loop, heat exchanger, and tank. Data extracted from two previously published papers were used to compare with the established model of the same setups, and an agreement could be achieved under a reasonable error limit.

This research further constructed a prototype system and its associated testing rig at the SRB (Sustainable Research Building) Laboratory, University of Nottingham and conducted testing through measurement of various operational parameters, i.e., heat transfer fluid temperature, tank water temperature, solar efficiency and system COP (Coefficient of Performance). Two types of glass covers, i.e., evacuated tubes and single glazing, were applied to the prototype, and each type was tested on two different days of 8 hours from 09:00:00 to 17:00:00. By comparison of the measurement data with the modelling results, reasonable model accuracy could be achieved in predicting the LHP system performance. The water temperature remained a steady growth trend throughout the day with an increase of 13.5^{o}C for the evacuated tube system and 10.0^{o}C for the single glazing system. The average testing efficiencies of the evacuated tube system were 48.8% and 46.7% for the two cases with the testing COPs of 14.0 and 13.4, respectively. For the single glazing system, the average testing efficiencies were 36.0% and 30.9% for the two cases with the COPs of 10.5 and 8.9, respectively. Experimental results also indicated that the evacuated tube based system was the preferred system compared to the single glazing system.

This research finally analysed the annual operational performance, economic and environmental impacts of the optimised evacuated tube system under real weather conditions in Beijing, China by running an approved computer model. It was concluded that the novel system had the potential to be highly-efficient, cost-effective and environmentally-friendly through comparison with a conventional flat-plate solar water heating system.

List of Published Papers

As a result of the PhD research work, the papers published/submitted to the journals are:

1. X. Zhao, **Z. Wang**, Q. Tang, Theoretical investigation of the performance of a novel loop heat pipe solar water heating system for use in Beijing, China, Applied Thermal Engineering 30 (2010) 2526-2536.
2. **Z. Wang**, X. Zhao, Analytical study of the heat transfer limits of a novel loop heat pipe system, International Journal of Energy Research 35 (2011) 404-414.
3. **Z. Wang**, Z. Duan, X. Zhao, M. Chen, Dynamic performance of a façade-based solar loop heat pipe water heating system, submitted to Solar Energy, October 2011.

Acknowledgements

I would sincerely like to thank my supervisor, Professor Xudong Zhao, for his invaluable and patient guidance with my research project.

I would like to thank the PEET/IT Power for the financial support.

I would like to thank the technical officer, David Oliver from Department of Architecture and Built Environment, for his technical instructions throughout the process of the project.

I would also like to thank all my friends for their continued support.

I would especially like to thank my parents for their encouragement and support during my study, and for giving me the courage and confidence to overcome the problems I encountered and carry on with my research.

List of Contents

List of Figures

List of Tables

Nomenclature

Chapter 2: Literature review

A	Area, m^2
C_p	Specific heat capacity, J/(kg·K)
F_R	Collector heat removal factor
F_R'	Exchanger heat removal factor
I	Total solar radiation on the surface of the collector, W/m^2
m	Mass, kg
$\dot{m}$	Mass flow rate, kg/s
Q	Energy flux, W
t	Time, s
T	Temperature, ^oC
T_r	Required temperature for room space or hot water, ^oC
T_t^+	Tank water temperature at the end of a time period, ^oC
U	Heat loss coefficient, $W/(m^2 \cdot K)$
U_1	Temperature-dependent heat loss coefficient, $W/(m^2 \cdot K)$
U_2	Temperature-dependent heat loss coefficient, $W/(m^2 \cdot K)$
Greek symbols	
α	Absorptivity
δ	Thickness, m
ε	Effectiveness
η	Efficiency
η_0	Optical efficiency
λ	Thermal conductivity, W/(m·K)
τ	Transmittance
Subscripts	
a	Ambient
back	Back of the collector
c	Collector
d	Symbol of differential coefficient
edge	Edges of the collector
f	Heat transfer fluid across the collector
i	Inlet
l	Heat loss
L	Heat load
min	Minimum values
o	Outlet
s	Secondary loop between the exchanger and storage
tk	Hot water tank
top	Top glass cover
u	Useful energy
w	Water

Chapter 4: Operating limits of the façade-based solar LHP water heating system

C	Constant
C_p	Specific heat capacity at a constant pressure, J/(kg·K)
C_v	Specific heat capacity at a constant volume, J/(kg·K)
D	Diameter, m
f	Friction factor
g	Gravitational acceleration, 9.81 m/s^2
h_{fg}	Latent heat of evaporation, J/kg
H	Height, m
K	Permeability, m^2
L	Length, m
m	Mass, kg
M	Mach number
N	Number/quantity
P	Pressure, Pa
ΔP	Pressure drop, Pa
Q	Energy flux, W
r_b	Critical radius of bubble generation, m
Re	Reynolds number
R_v	Vapour constant, J/(kg·K)
T	Temperature, ^{o}C
v	Velocity, m/s
x	Factor relating to the filled liquid mass, 0.8 for heat absorbing pipes and exchanger and 1 for adiabatic section
z	Shape factor, 1 for circular and 0.833 for rectangular shapes
Greek symbols	
γ	Specific heat ratio
δ	Thickness, m
θ	Contact angle, ^{o}
λ	Thermal conductivity, W/(m·K)
μ	Dynamic viscosity, Pa·s
ρ	Density, kg/m^3
σ	Surface tension, N/m
φ	Porosity
Φ	Absorber tilt angle, ^{o}
Subscripts	
BL	Boiling limit
CL	Capillary limit
EL	Entrainment limit
FL	Filled liquid mass limit
g	Gravity

he	Heat exchanger
hp	Heat absorbing pipes
l	Liquid
lf	Liquid film
lh	Liquid header
ll	Liquid line
max	Maximum values
min	Minimum values
ms	Mesh-screen wick
sp	Sintered-powder wick
SL	Sonic limit
v	Vapour
vh	Vapour header
vl	Vapour line
VL	Viscous limit
w	Wick

Chapter 5: Theoretical analysis and computer simulation of the dynamic performance of the façade-based solar LHP water heating system

A	Area, m^2
C_p	Specific heat capacity, J/(kg·K)
D	Diameter, m
g	Gravitational acceleration, 9.81 m/s^2
h	Convective heat transfer coefficient, $W/(m^2 \cdot K)$
h_{fg}	Latent heat of evaporation, J/kg
H_f	Frictional resistance loss, m
H_l	Local resistance loss, m
I	Total solar radiation on the surface of the collector, W/m^2
L	Length, m
$\dot{m}$	Mass flow rate, kg/s
N	Number/quantity
Nu	Nusselt number
Pr	Prandtl number
ΔP	Pressure drop, Pa
Q	Energy flux, W
R	Thermal resistance, K/W
Re	Reynolds number
t	Time, s
Δt	Time interval, s
T	Temperature, ^oC
v	Velocity, m/s
V	Volume, m^3

Greek symbols

α	Absorptivity
δ	Thickness, m
ε	Emissivity
ζ	Frictional resistance coefficient
η	Efficiency
λ	Thermal conductivity, W/(m·K)
μ	Dynamic viscosity, Pa·s
ξ	Local resistance coefficient
ρ	Density, kg/m^3
σ	Stefan Boltzmann constant, $5.67*10^{-8}$ $W/(m^2 \cdot K^4)$
τ	Transmittance
φ	Porosity

Subscripts

0	Initial values
ab	Absorbed energy by the solar collector
air	Air flow between the collector surface and inner glass cover
amb	Ambient
ave	Average values
bb	Backboard
c	Collector
COP	Coefficient of Performance
d	Symbol of differential coefficient
en	Solar energy entering across the glass cover
g	Evacuated tubes or single glazing
he	Heat exchanger
hp	Heat absorbing pipes
i	Inlet
l	Liquid
loop	Heat pipes loop
loss	Heat dispersed to the ambient from the collector surface
o	Outlet
pump	Water pump
s	Wick in the solid form
sb	Side board
tk	Hot water tank
v	Vapour
vh	Vapour header
vl	Vapour line
w	Saturated wick
wp	Water pipelines connecting the exchanger and tank

Chapter 7: Annual operational performance, economic and environmental evaluations of the solar façade LHP system with evacuated tubes

cf_{CO2}	CO_2 conversion factor, kgCO2/kWh
C	Cost, £
CR	CO_2 emission reduction, kg
CS	Life cycle cost saving, £
PP	Payback period, years
Q	Electrical energy, kWh
Subscripts	
c	Capital cost
el	Conventional electric water heater
m	Annual maintenance cost
o	Annual operating cost
sf	Façade-based solar loop heat pipe water heating system with evacuated tubes

Chapter 1: Introduction

1.1 Research background

Over the past several decades, global energy consumption has been steadily growing. In 2008, the total consumed primary energy reached 11,315 million tonnes of oil equivalent (equalling to 474 EJ) [1.1], of which 80-90% was from the burning of fossil fuels. Despite the latest energy review [1.2] indicating that owing to the unexpected global financial crisis the world's primary energy consumption dropped by 1.1% in 2009, energy consumptions in some developing countries, particularly in Asia, were still rising. In addition, overexploitation of the primary energy sources has caused the depletion of fossil fuels, and there will only be 119 years of coal production, 46 years of oil production and 63 years of natural gas flow left in the ground with the current proved reserves [1.3]. The principle of energy supply and demand suggests that as fossil fuel supplies diminish, rising energy prices will impact on the development of the global economy.

On the other hand, the combustion of fossil fuels for energy, industrial processes and transportation has caused a significant increase in the emissions of greenhouse gases to the atmosphere. It has been agreed by most scientists that this growth is the primary cause of global warming. Over the last 30 years of the twentieth century, global temperature has already risen 1.4°C [1.4], and it will continue to rise over the next 100 years. This warming will cause significant changes in sea levels, ecosystems and weather events, which will threaten people's health and way of life, and cause irreversible losses to species of both plants and animals.

Thus, the inflation of energy prices and the impact of climate change have led to the exploration of alternative, renewable energy sources for the purposes of energy savings and environmental protection.

Solar thermal is one of the most cost-effective renewable energy technologies and has enormous market potential globally. Since the beginning of the 1990s, the world solar thermal market has been continuously developing. In Europe,

the solar thermal market tripled from 2002 to 2006 and is still booming [1.5]. The European Solar Thermal Industry Federation (ESTIF) has predicted that, by 2020, the European Union (EU) will reach a total operational solar thermal capacity of between 91 and 320 GW; and by 2050, the EU will eventually achieve 1,200 GW of solar thermal capacity [1.6].

Solar water heating is one of the most popular solar thermal systems and makes up 80% of the solar thermal market worldwide [1.7]. Over the past four decades, solar water heating systems have gained wide applications in the building sector globally [1.8]. In the meantime, the systems have been identified with a number of technical problems that have become the barriers to their promotions, e.g., low existing efficiency, high heat loss and poor solar energy harvesting capability. Some challenges also relate to their installations to the buildings and capital costs.

Most solar water heaters for buildings are flat-plate types or conventional heat pipes array installed on roofs for layout convenience. This installation requires long runs of pipelines delivering water from the roof heaters to the outlet points and receiving water from the water mains. Thus, the cost of the system is high; most importantly, the installation detracts from the aesthetics of the building, particularly those multi-storey buildings containing a large number of end users.

In recent years, several façade-based solar heaters have been developed and used in practical projects [1.9 ~ 1.11]. These devices are simply positioned on the walls or balconies [1.12], which prevent the occupation of roof space and shorten the distance of piping runs, and thereby improve the building's aesthetic view. However, this layout still requires the transportation of water from the inside of the building to the outside, which may cause the hazard of pipes freezing during winter operation.

In general, the barriers for the use of the solar water heaters in buildings could be summarised as:

1. Heaters located on roof space detract from the aesthetics of the building;

2. Circulating water between the inside and outside of the building increases the risk of pipes freezing during winter operation;
3. Current heating devices are not truly integrated with building façade, which leads to an increase in construction cost and a less appealing building appearance.

In order to overcome the barriers listed above for the use of solar water heating systems in buildings, further research in this area is required.

In order to overcome barriers 1 and 3, a modular façade solar water heater, able to replace the façade wall or attained to the wall as the external decoration layer, is proposed. A prefabrication technique is applied in manufacturing the glazing-fitted heat pipe façade; the heat absorbing pipes could be embedded into a lightweight board, which could act as the replacement or exterior decoration layer of the current wall structure. This method will create a building integrated, low cost solar water heating system. Estimation suggests that using a combined modular façade will save 10-20% of construction cost, compared to conventional structure of separate arrangements of wall façade and overhung collector [1.13].

In order to overcome barrier 2, loop heat pipes have been proposed. Loop heat pipes (LHPs) are two-phase heat transfer devices separating the vapour and liquid flows and thus eliminating the entrainment friction between them. Entrainment is one of the dominant operating limits impacting on heat transfer in the pipes. These pipes are, therefore, able to transfer large amounts of heat for distances up to several metres or to several tens of metres in a horizontal or vertical position through the effect of capillary pumping or gravity [1.14]. For the façade water heating application, loop heat pipes will allow solar heat to be collected from the outer façade surface, transported to a heat exchanger inside the building and further transferred to the water across the heat exchanger. This prevents long-distance running of water from the building interior to exterior and protects the water pipes from freezing during winter operation. A specially designed liquid downward-feeding approach will be applied to allow the wicks

attained to the heat absorbing pipe walls to be fully saturated with water, thus increasing heat output by around 15-20% more than traditional loop heat pipes.

1.2 Research objectives

Based on the considerations above, the aim of the research is to develop a novel solar façade water heating system, employing a unique loop heat pipe structure with a top-level liquid feeder. This innovative solar system has the potential to overcome the difficulties associated with the existing solar water heaters, i.e., unpleasant architectural view due to use of the roof space, separate layout of the heat absorbing pipes and façade, high thermal losses through the long water piping, the hazard of pipes freezing due to indoor-outdoor water transportation and low efficiency in converting solar energy to heat for hot water. It is expected that this system is façade integrated, low cost, highly efficient and aesthetically appealing, and could contribute to the reduction of fossil fuel consumption and carbon emissions associated with building's hot water production and supply.

The detailed objectives are:

1. To conceptually design the proposed solar façade water heating system.
2. To develop computer models for the optimisation of the solar façade system configuration and prediction of its thermal performance.
3. To construct and test a prototype solar façade system in the laboratory.
4. To complete the annual operational performance, economic and environmental analyses on the new system.

1.3 Research methodology

The overall research methodology could be outlined as:

1. Raising questions and associated limitations (related to Objective 1);
2. Theoretical investigations to give answers (related to Objective 2);
3. Experimental validations (related to Objective 3);
4. Giving possible solutions for the limitations and scope of the questions to be applied (related to Objective 4).

In order to achieve the above listed objectives, various methodological approaches will be employed as follows:

1. Approach for Objective 1 – Conceptual design of the proposed solar façade water heating system (Task 1)

The approach employed for this objective is to:

(1) Select a sample building which has representative characteristics of buildings;
(2) Conduct a conceptual design of the façade water heating system based on the selected building;
(3) Make a list of system components and analyse the potential variations in material types and geometrical sizes.

These can be considered as the questions raised and to be solved in the subsequent actions.

A conceptual design of the proposed solar façade water heating system will be carried out. A typical 3-member flat in Beijing (China) will be initially selected due to the unique balcony/facade structure of the flat and the fast-growing solar thermal market in China. On this preset condition, the façade heater will be primarily designed by giving potential geometrical size, material and quantity of the components needed, e.g., thermal-clear glass covers, heat absorbing pipes and associated wick/liquid-feeding structures. Subsequently, the components within the indoor part, e.g., flat-plate heat exchanger and water tank, will also be designed or selected. It should be stressed that the design is a primary (conceptual) sketch which will leave potential variations in size, material type and quantity of these components. The magnitude of the system, including quantity of modular façade, can be scaled up or down depending upon geographic location and size of the building and number of occupants served.

2. Approach for Objective 2 – Development of computer models to optimise system configuration and predict its thermal performance (Task 2)

The approach employed for this objective is to develop computer models to analyse the fluid flow and heat transfer occurring in various parts of the system. The aims could be briefed as:

(1) To determine the most appropriate material for the system components to be used;
(2) To optimise the geometrical size and quantity of these components;
(3) To predict the performance of the components and the system considered as a whole.

This approach will theoretically answer the questions raised in the previous stage of the research (relative to Objective 1).

Based on the indicative design of the proposed system, a computer model will be developed to analyse the operating limits (heat transport capacity) of the system and determine six limits to the system's operation, i.e., capillary, entrainment, viscous, boiling, sonic and filled liquid mass (Task 2.1). The results of the simulation will be used to establish the relationship between the limits and several associated parameters, i.e., heat transfer fluid temperature, wick structure, heat pipe diameter and height difference between the absorbing pipes array and exchanger, and to identify the system's governing limit which is the minimum of the six limits.

In consideration of heat balances occurring in various parts of the proposed system such as the solar absorber, heat pipes loop and heat exchanger, a computer model will be developed to investigate the dynamic performance of the system (Task 2.2). This will involve four heat transfer processes, i.e., converting the solar radiation into the heat received by the absorbers, transporting the absorbed heat from the absorbers to the heat exchanger, transferring the heat from the exchanger to the service water, and transporting the heat carried by the service water into the tank. These processes will be

time-dependent and interrelated and can be represented by the classic heat transfer equations concerning conduction, convection and radiation. Solving these conjugate equations will generate various groups of solutions. By analysing the obtained solutions and comparing the simulation results to the experimental data, the optimal configuration for the system components will be selected. The most appropriate system operating conditions, including temperatures of the heat transfer fluid and water in the tank, will be recommended. The potential increase in solar efficiency of the new system and the electrical energy usage due to implementation of the electric pump will be identified. Previously published papers will be used to validate this model, by applying the same input parameters of the papers to the newly developed model and comparing the modelling and experimental data of the papers to the new simulation results.

3. Approach for Objective 3 - Construction and testing of a prototype solar façade system in the laboratory (Task 3)

The approach employed for this objective is to construct and test an experimental prototype under laboratory conditions. This aims to:

(1) Analyse the potential errors occurring in the computer simulations;
(2) Enhance the accuracy of the computer model's prediction;
(3) Approve/modify the theoretical answers to the questions raised by using the experimental method.

This will generate a laboratory-based façade water heating prototype that is a model of the real system to be used in buildings.

This approach will involve constructing the loop heat pipe solar façade system (Task 3.1), testing its performance and operating characteristics, and validating the modelling results using the test data (Task 3.2). One group of optimised façade, sized in 1 m^2 and expected to achieve the maximum heat output of 640 W under the summer peak irradiation condition (800 W/m^2), will be constructed. This prototype is flexibly structured to allow possible changes of the system components (e.g., glazing) in case that adjustment is needed during

performance measurement. The prototype will then be erected against a solar radiation simulator and linked to a compact indoor water cycle system comprising the water tank, flat-plate heat exchanger and electric pump. The whole system will be installed and tested in a controlled environment, i.e., the SRB (Sustainable Research Building) Laboratory, University of Nottingham, where a range of solar/ambient air conditions can be simulated. The temperatures of the heat transfer fluid and water across the heat exchanger will be measured using the embedded sensors, and the pressure of the heat pipes loop will also be measured using a pressure gauge. All measurement data will be logged into the computer system, and used to determine the solar efficiency of the system under various solar/ambient conditions and estimate the magnitude of system COP (Coefficient of Performance) by taking into account the pump power consumed during the system's operation.

The performance of the system will be verified based on the comparison between the computer prediction and experiment, thus determining the real figures of the system's solar efficiency and COP. As a result, an optimised model for the façade-based solar LHP water heating system and its associated experimental unit will be generated. These will be used to examine whether the expected increase in solar efficiency can be achieved and determine the system's COP when in operation. It should be noted that the modified computer model could be used for the prediction of the annual operational performance, economic and environmental analyses of the new system.

4. Approach for Objective 4 – Development of a computer model to evaluate the annual operational performance, economic and environmental impacts of the new system (Task 4)

The approach for this objective is to develop a dedicated computer model to evaluate the annual operational performance of using this technology in buildings, and analyse its economic and environmental (primarily CO_2 emission) impacts through comparison between the results obtained from the proposed solar system and a conventional flat-plate solar water heating system. The cost payback period will be calculated, indicating the feasibility of

applying this system. This will clarify the practicality and potential benefits to be achieved when converting this technology into a commercial product.

The annual operational performance of such a system will be analysed, taking the solar façade applied to the typical 3-member flat in Beijing (China) into account. The solar/ambient air conditions of a typical day for each month of the year will be considered. The temperatures of the heat transfer fluid within the loop and water flowing across the exchanger, solar conversion efficiency and system COP under these weather conditions will be computed using the model developed in Task 2.2. The system's capital and operating costs and cost saving during the system's life cycle period will be calculated and compared to the conventional flat-plate solar water heating system. The environmental benefit of the system will be examined with respect to the reduced amount of carbon dioxide emissions.

1.4 Novelty of the proposed research

The proposed research has the following innovative features:

1. Solar heat is transferred to indoor water tank through evaporation and condensation of a heat transfer fluid within the LHP, thus removing the need to transport water into a building from the outside, overcoming the risks in conventional systems of pipes freezing and improving the efficiency of solar-to-hot-water conversion.
2. Using prefabrication techniques to embed the heat absorbing pipes into building façades allows true integration of the heat absorbing pipes with the building façades, thus reducing the cost of the façade module and improving the aesthetic view of the building.
3. A unique liquid feeding structure through round-distributed mini-holes at the top of the heat absorbing pipe allows heat transfer liquid to be distributed evenly throughout the heat pipe wick, and enables control of liquid-feeding speed to balance liquid evaporation and supplement, thus maximising loop heat pipe heat transfer.

This research will lead to a new solar façade water heating system, which has reduced construction cost and increased solar efficiency relative to the conventional solar water heating systems. It is, therefore, timely in terms of its considerable capability of saving energy and reducing the amount of CO_2 released to the environment.

1.5 Thesis structure

The research involves different aspects for system conceptual design, computer model setup, prototype testing and performance evaluations, which could be categorised into 8 chapters.

Chapter 1 contained the background information of the research, explained the objectives, summarised how the research will be performed and stated the novelty of the research.

Chapter 2 provides a review of the relevant areas of research on developing the novel system including solar thermal market potential, classifications and mathematical analysis of solar water heating systems, practical applications of solar water heaters in buildings, technical background of LHP technology, numerical and experimental analyses on LHP heat transfer performance as well as the applications of LHP technology in solar water heating systems.

Chapter 3 describes the working principle of the novel system. Based on a selected 3-member flat in Beijing (China), the characteristic parameters of the system components, e.g., glass covers in the configurations of evacuated tubes and single glazing, mesh-screen or sintered-powder wicked heat absorbing pipes, flat-plate heat exchanger and water tank, will be conceptually designed.

Chapter 4 will theoretically investigate the operating limits (heat transport capacity) of the LHP employed in the novel system. A computer model will be developed to simulate the six operating limits, i.e., capillary, entrainment, viscous, boiling, sonic and filled liquid mass, and identify the governing limit of the LHP device. The optimised operational and geometrical parameters of the LHP system, i.e., heat transfer fluid temperature, wick structure, heat pipe

diameter and height difference between the heat absorbing pipes and exchanger, will be determined against the six limits.

Chapter 5 will analyse the dynamic performance of the novel system in the configurations of evacuated tubes and single glazing. A computer model will be established to illustrate the four heat transfer processes, i.e., solar energy absorbed by the collector surface, heat transferred to the exchanger, heat transferred to the water flowing across the exchanger and further to the service water in the storage. This model will be applied to compare with the testing and modelling data of two previously published papers by entering the same parameters used in these papers to the newly developed model.

Chapter 6 will describe the construction of the prototype solar façade in the configurations of evacuated tubes and single glazing and its associated testing rig in the laboratory. The time variations of the temperatures of the heat transfer fluid in the LHP and water flowing across the exchanger, system efficiency and COP will be analysed and discussed through comparison with the modelling results.

Chapter 7 gives the annual operational performance of the solar LHP system with evacuated tubes, which is predicted by the model developed in Chapter 5 with respect to the heat transfer fluid temperature, tank water temperature, solar conversion efficiency and system COP. The economic and environmental impacts of this system will also be evaluated through comparison with a conventional flat-plate solar water heating system. The cost payback period will also be estimated.

Chapter 8 will generalise the research project, present the conclusions obtained from the above chapters and indicate future work to be done.

Chapter 2: Literature review

2.0 Overview

In this chapter, a comprehensive review into the solar thermal and loop heat pipe (LHP) technologies will be carried out.

Solar thermal is the technology converting solar energy to usable heat for applications in water, space heating and cooling, electricity, fuels and agricultural and industrial processes. The global potential of the solar thermal market at the present time and in the near future will be discussed, as well as the driving forces and existing barriers to its expansion.

As the main application of solar thermal is for domestic hot water, the technical background of the solar water heating system will be introduced including working principle, classifications and associated mathematical theory. The practical applications of solar water heaters in buildings will be demonstrated. Compared with the roof-mounted or roof-integrated solar water heater, the building balcony/façade integrated solar system could represent improved building aesthetic view and reduced construction cost. However, some barriers including the long water pipes transporting and winter freezing problems still remain and could be potentially solved by LHP technology.

LHP is an efficient heat transfer device that could transport thermal energy over long distances, up to several tens of metres. It has some unique features over conventional heat pipe, e.g., gravity-unaffected and flexibility in its design and installation, which makes LHP particularly suitable for applications in solar water heating systems. Three components of the LHP device, i.e., working fluid, wick, and container, will be described relating to their influences on the performance of the LHP.

A significant literature review of the LHP technology will be illustrated, and the review results will be analysed in terms of the performance characteristics and research methodology. For the performance characteristics, the steady-state and transient behaviour of the LHP device will be examined. The research

methods, i.e., theoretical analyses and computer simulations, and experimental investigations, will be analysed.

Although substantial work has been done in solar thermal and LHP studies, the opportunities for further work will be identified.

This review will help recognise the problems remaining in the existing solar thermal systems, remove the barriers to solar applications, establish the standards related to the design and installation of the solar systems, identify new research subjects to improve the performance of the solar systems, and expand solar thermal market potential throughout the world.

2.1 Global solar thermal market

2.1.1 Current status and the global market potential for solar thermal

Solar energy is one of the primary energy sources, with 120,000 TW striking the Earth's surface excluding those reflected by the atmosphere directly to the outer space. Compared to the total primary energy supply of 433 EJ in 2002 equivalent to 13.75 TW of power consumption [2.1], solar energy exceeds 8,700 times the primary energy supply, meaning that the energy the Earth received from the Sun each hour is as much as humankind consumed in one year.

Heating consumes the largest share of primary energy supply and accounts for 40-50% of world energy demand, including cooking and high temperature industrial processes. The building sector consumes 35% of the final energy demand, of which 75% is for space and domestic water heating. In Europe, the final energy demand for heating (48%) is higher than for electricity (20%) or transport (32%) [2.1]. However, most of the heat supply currently comes from fossil fuels, indicating that there would be a significant market potential for replacement of these by renewable energy heating technologies.

Solar thermal designates all technologies that collect solar rays and convert the solar energy to usable heat for use in water, space heating and cooling, electricity, fuels and agricultural and industrial processes.

Over the last two decades, the global solar thermal market has increased significantly. Between 2000 and 2009, the global market of glazed solar collectors grew at an average rate of 20.8% as shown in Fig. 2-1 [2.2]. The annual installed capacity of glazed water collectors almost tripled between 2004 and 2009 worldwide, although it experienced a slight decrease of about 15% in 2007 [2.3]. China is the leader in the annual installed capacity as the largest solar thermal market globally with a sustained growth of 22%. It is recognised that the dominance of China is driven by its large population and the rapid growth of the solar heating sector. As the second largest market for glazed collectors, Europe showed an average annual growth rate of 20% [2.3], although a disappointing result (-9.9%) happened in 2009 due to a downturn of 23.1% in the largest European market, Germany. The US market, mostly of unglazed collectors, also dropped by 8.5% owing to the economic recession in 2009. Regardless of the above downturns, the Chinese (35.5%) and Australian (78.5%) markets were responsible for a global expansion of 27.3% in 2009 [2.2].

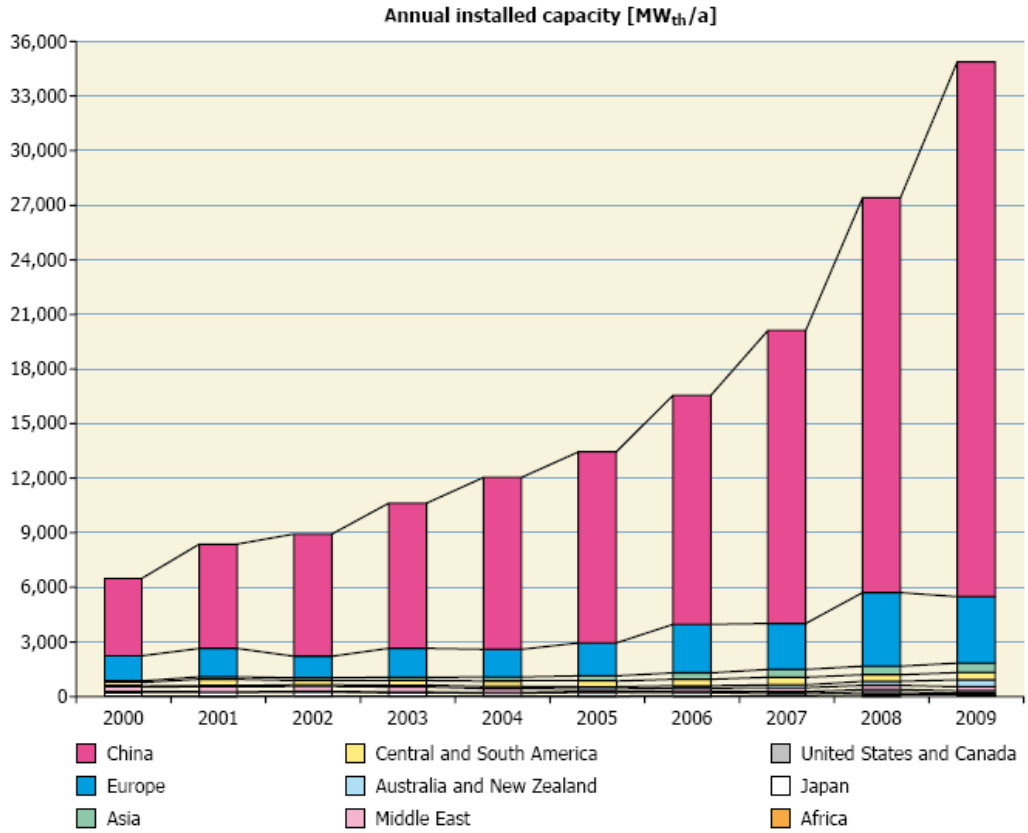

Fig. 2-1. Annual installed capacity of glazed water collectors from 2000 to 2009 [2.2].

By the end of 2009, the total capacity of the solar thermal collectors in operation equalled 172.4 GW worldwide, of which 58.9% (101 GW) was in China. Fig. 2-2 [2.2] shows an overview of the different types of collectors applied in the leading countries in 2009 in respect of the total installed solar thermal capacity. China was the world leader in total solar thermal capacity, focusing on evacuated-tube collectors for the purposes of preparing hot water and providing space heating. The United States (14.4 GW) ranked second owing to its high installation of unglazed collectors for swimming pool heating. With approximately 9 GW, Germany was holding third place, followed by Turkey, Australia, Japan, Brazil, Austria, Greece and Israel.

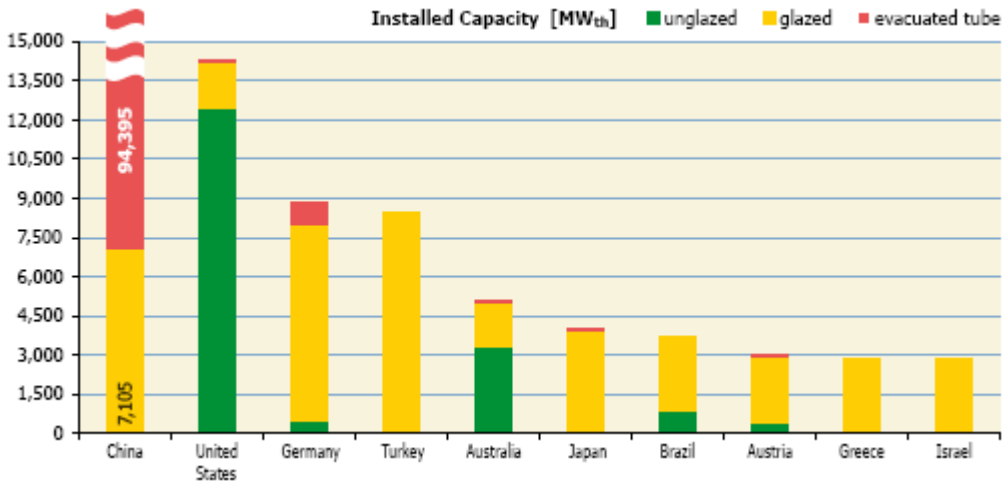

Fig. 2-2. Total installed capacity of water-based collectors by the end of 2009 [2.2].

The energy production of all water-based solar thermal systems in 2009 was 142 TWh, corresponding to 14.4 million tonnes of oil equivalent (Mtoe). Provisional numbers for 2010 suggested that 2010 witnessed a 162 TWh energy production with 23.6 GW newly installed solar thermal collectors. Compared with other forms of renewable energy sources, solar thermal energy was second to wind power, excluding biomass and hydropower (Fig. 2-3 [2.2]). Still, it represented less than 0.5% of the global final energy demand [2.4].

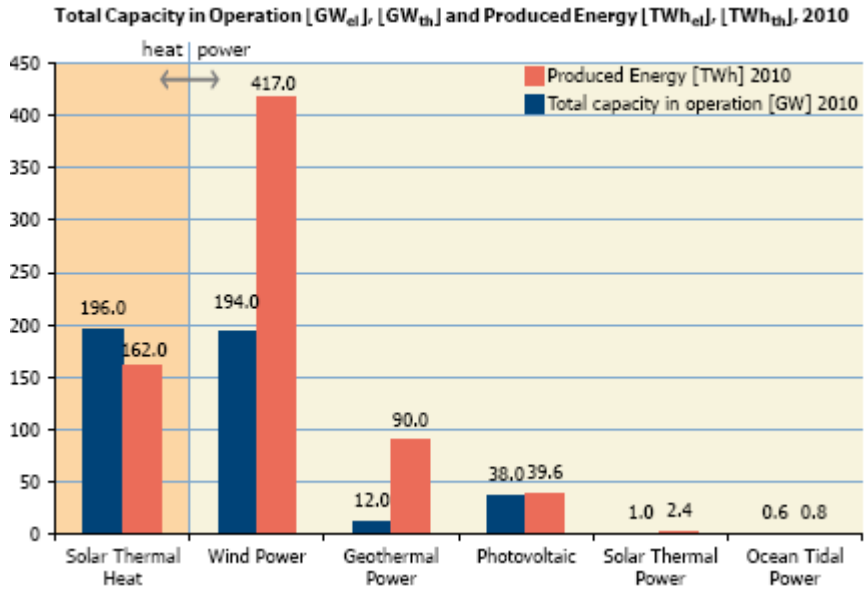

Fig. 2-3. Energy production of solar thermal in 2010 [2.2].

The IEA World Energy Outlook 2008 [2.4] has foreseen a contribution from solar thermal of 45 Mtoe to the final energy demand for domestic water and space heating by 2030, thus leading to a 0.6% of the total final energy demand, if current energy policies continue. It has also anticipated that if all the policies currently under consideration are implemented by 2030, solar thermal will provide 64 Mtoe to the global energy demand, 10 times greater than the 6.6 Mtoe in 2003. China, Europe and the United States will still be the leading markets in the total installed solar thermal capacity in 2030, according to the projected figures [2.5].

The European Solar Thermal Industry Federation (ESTIF) [2.6] has forecast that, under full R&D and policy scenarios, a total installed capacity of 1,019 GW in the EU will contribute about 15% of the low temperature heat demand by 2030. By 2050, the total capacity could reach 2,716 GW to provide about 129 Mtoe of solar heat, which is roughly 47% of the overall heat demand in the EU.

2.1.2 Driving forces to the expansion of solar thermal market

The fast-growing global solar thermal market could be driven by several factors, such as low costs (under certain circumstances), financial incentives, regulatory instruments, education and other factors such as environmental and local visual impacts.

A. Solar heating cost

Compared to the energy prices for heat supplied by gas, fuel oil and electricity, solar thermal heating can be cost-effective under certain conditions ranging between £7 and £200 per GJ [2.5]. Solar heating costs vary considerably with weather conditions, the complexity of solar thermal installation, the application of solar thermal system for water heating only or for combined hot water preparation and space heating, and other factors such as the costs of labour and materials [2.1, 2.5, 2.7].

B. Financial incentives

Financial incentive is used to encourage energy customers to utilise renewable energy sources to meet heat demands, and aims to fill the cost gaps between the renewable energy sources and conventional energy technologies used for heating. The incentive schemes could be categorised into financial and fiscal [2.5, 2.8]. Financial incentive is direct financial support funded from government budgets, which includes capital grant (subsidy), operating grant and soft loan. Fiscal incentive includes tax credits, reductions and accelerated depreciation, based on investment cost or energy production.

In many countries, capital subsidies for solar hot water have become common strategies. More than 20 countries provide capital grants, Value Added Tax (VAT) exemptions or tax credits for solar water heating investments including Austria, Germany, Greece, Japan, the Netherlands, Spain, the United Kingdom and the United States. Capital grant or tax credit is typically 20-40% of a system's cost. The United States provides a 30% federal tax credit, in addition to many State-level rebates. Some companies also offer capital subsidies such as ESKOM in South Africa [2.9].

C. Regulatory instruments

Governments could intervene in the market by means of regulation, which forces the deployment of renewable energy heating by directly requiring the development of technologies. The regulatory instruments could be categorised into building regulations and standards [2.5].

Mandates for solar hot water in constructions have maintained a growing trend at both national and local levels [2.5, 2.9]. Israel, for a long period of 30 years, was the only country with a national-level mandate. Spain required owners of all new and renovated buildings to provide 30-70% of domestic hot water demand by solar thermal energy. India's national energy conservation codes require at least 20% of water heating capacity from solar for residential buildings, hotels and hospitals with central hot water systems. Hawaii became the first US state to mandate solar hot water in new single-family houses in

2009. Cities working on solar hot water policies, including Rome in Italy, would require 30-50% of hot water energy from solar for new buildings.

D. Education

Education to promote renewable energy heating aims to raise public awareness through information campaigns and training programmes. It may take the form of technical assistance, financial advice, labelling of appliances and information distribution. For example, Canada's Office of Energy Efficiency has provided the free-downloadable, web-based RETScreen tool and numerous free publications on energy efficiency and renewable energy [2.5]. Training programmes may be established in schools, universities or among professional groups, such as the Certificated Solar Heat Installer and Planner run by experts within the Austrian solar industry [2.5].

E. Other factors such as environmental and local visual impacts

The concerns around saving energy and reducing carbon emission could also drive the fast-growing solar thermal market. Solar thermal requires no fossil fuels, thus producing little environmental pollution during its manufacturing, operation and decommissioning. Carbon emission from solar thermal energy is, therefore, small. If the external costs of energy technologies (e.g., environmental taxes and carbon emission charges) were taken into account, solar thermal energy could be cost-competitive with most heating technologies [2.5].

Solar thermal markets could also be driven by local visual impact. Recent solar systems are placed onto building roofs, and are more integrated into roof systems and building envelopes.

2.1.3 Existing barriers to the diffusion of solar thermal market

Although solar thermal has a broad market prospect, there are still various barriers to its diffusion, which can be grouped into three categories, i.e., technical barriers, economic barriers and other barriers including legal, educational and behavioural barriers.

A. Technical barriers

Over decades of development, many technical barriers have been identified, such as the nonexistence of a universal certification approach to specify the standards for production and utilisation, high heat losses at night, insufficient information on technical capabilities and lack of trained and competent installers. Recent problems focused on the availability of space for installation of solar thermal collectors, thermal storage with high energy density, availability of appropriate materials for mass productions of collectors, integration of solar equipment as part of the building's fabric and protection of solar collectors from freezing in cold weather [2.1, 2.6]. Another barrier relating to the utilisation of solar energy is that the solar radiation reaching the Earth is intermittent, weather-dependent, highly dispersed, and unequally distributed over the surface of the Earth in that most of the energy is between 30^{o}N and 30^{o}S [2.1, 2.10].

B. Economic barriers

Several economic barriers have impacted on the desire for increased utilisation of solar thermal in developing countries, including lack of public awareness, lack of energy policies, low levels of income, lack of subsidies, short-term investing syndrome and lack of institutional support. For developed countries, the principal economic barriers are capital cost, poor regulation of promotion and poor public perceptions [2.1]. Solar heating cost is another significant economic barrier; although it is cheaper than the electricity price in Denmark and roughly the electricity price in Austria, Germany, Italy, the Netherlands and Japan, it is more expensive than the heat from natural gas in urban areas [2.11]. Finally, customers, especially the less wealthy, may only consider investments with immediate returns, since the benefits due to low running costs may not always offset the large capital expense [2.1].

C. Other barriers such as legal, educational and behavioural barriers

The largest barrier in this category is that property developers and building owners have little incentive to invest in energy-saving equipment in new constructions and rental markets. This is because the returns on investments will directly flow to the actual occupants rather than to them [2.1]. Another

barrier existing in collective dwellings or multi-storey buildings is that the installation of a single device may become technically complex, and will require permits from a majority of co-owners [2.1]. The diversity of local requirements is another barrier as solar systems need to be considered in terms of their compatibility with existing community aesthetic standards and architectural requirements [2.1, 2.12]. Finally, some barriers relate to behaviour including reluctance to manage a complex system, solar intermittence leading to low comfort levels for either space or water heating, and changes in habits [2.1].

2.2 Technical background of solar water heating systems

2.2.1 Working principle

A solar water heating system, as shown in Fig. 2-4 [2.13], consists of a discrete collector, which is designed to maximise solar absorption and reduce heat losses. The solar collector could be either a black-painted flat-plate absorber bonded to copper piping and covered with a transparent glass (flat-plate collector) or copper tubing surrounded with evacuated and selectively-coated glass tubes (evacuated-tube collector). When solar radiation passes through the transparent glass or evacuated tubes and impinges on the collector surface of high absorption, a large part of the energy is absorbed by the collector and then transferred to the fluid to be transported in the pipes. The heat transfer fluid, usually a mixture of water and antifreeze fluid, is either pumped (active system) or driven by natural convection (passive system) through the collector to a coil heat exchanger at the bottom of a cylinder tank (indirect system), where the heat it carried is further transported to the service water for storage or direct use. The tank contains an auxiliary heater, e.g., electric immersion heater or conventional boiler, for winter use and is insulated with polyurethane for hot water storing [2.14 ~ 2.15].

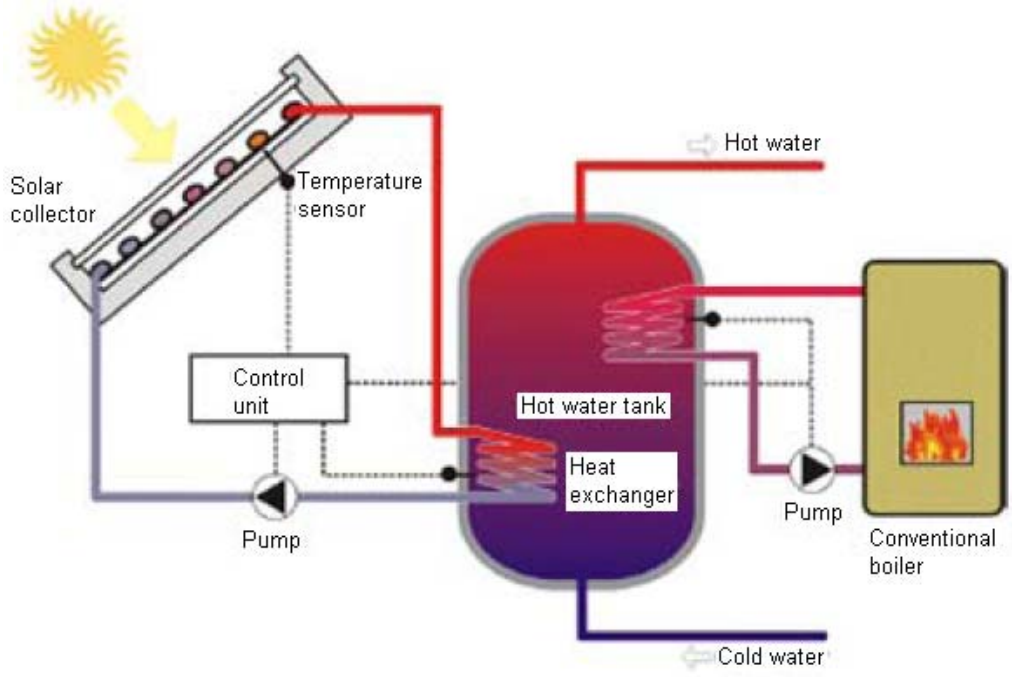

Fig. 2-4. Schematic of a conventional solar water heating system [2.13].

2.2.2 Classifications

A. Passive and active systems

Based on whether or not they require pumps to function, solar water heating systems could be grouped into two basic configurations, namely passive and active systems, as shown in Fig. 2-5 (a) and (b) [2.16].

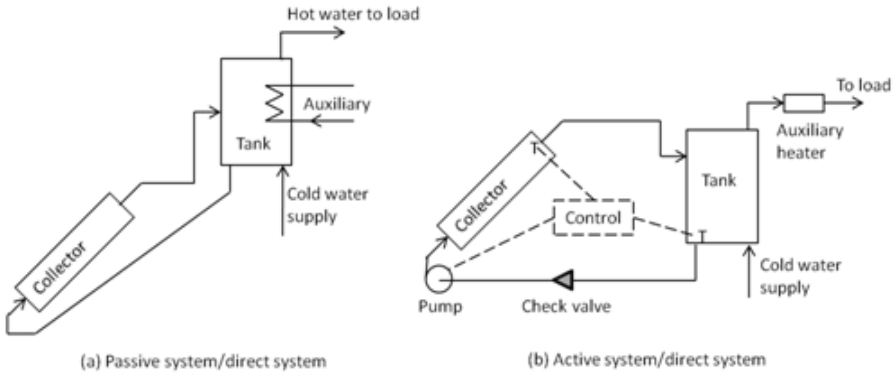

Fig. 2-5. Schematic of the passive and active solar water heating systems [2.16].

Passive systems transfer heat from the collector to the tank located above the collector by natural circulation, which could supply hot water at a temperature of 60^{o}C, and are the most commonly used solar water heaters for domestic applications [2.17]. **Active systems** use the electric pump, controller and valve

to circulate water through the collector. This category of solar system uses electrical energy to accomplish the transfer of thermal energy by running the pump. A differential thermostat is normally used to control the circulation of the water, when the temperature of the water at the top header is higher than the temperature at the bottom of the tank by a sufficient margin. A check valve may be required to prevent reverse water circulation [2.16].

Compared to the passive system, the efficiency of the active solar water heating system is one crucial advantage and is usually between 35 and 80% [2.18] over the passive system in the range of 30-50% [2.17]. Another advantage is that the collector in the active system does not need to be as close to the tank. Therefore, the active system can be used for high-rise buildings. The main drawbacks of the active system are its complicated nature which is dependent on electricity and the requirement for experienced personnel to operate it, which will lead to a much higher running cost than for the passive system.

B. Direct and indirect systems

Based on whether or not they require a heat exchanger, solar water heating systems could be categorised into direct (Fig. 2-5 [2.16] above) and indirect systems (Fig. 2-6 [2.16]).

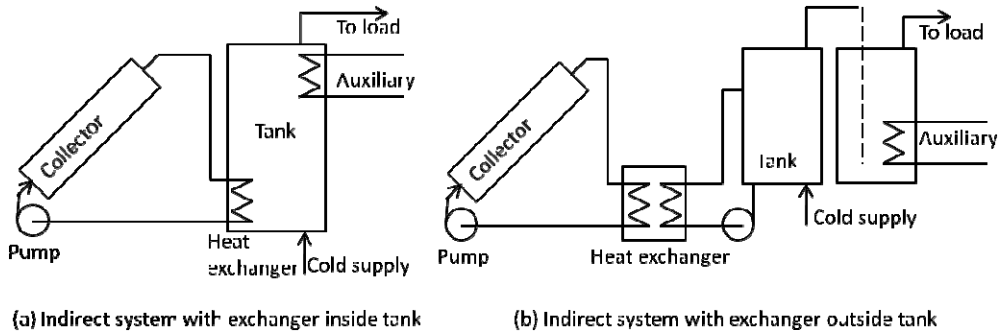

Fig. 2-6. Schematic of the indirect solar system with the exchanger inside or outside the tank [2.16].

In a **direct system**, the service water is directly circulated between the water tank and the collector, while for an **indirect system**, a heat transfer fluid,

usually antifreeze, distilled water or an organic fluid, is circulated through the solar collector. A heat exchanger is employed to affect the heat transfer from the collector to the service water in the tank. The heat exchanger could be used inside or outside the hot water tank as shown in Fig. 2-6 (a) and (b).

The indirect system in most situations performs better than the direct one, which is less climate-selective and more suitable for use in regions that experience cold temperatures.

C. Solar systems in different solar collector configurations

Solar collectors can have many variations according to their operating temperature. Fig. 2-7 summarises most of the possibilities [2.13]. Unglazed panels and flat-plate water and air collectors are categorised into the low temperature solar collectors. Evacuated-tube, line-focus, and point-focus collectors are classified as high temperature solar collectors.

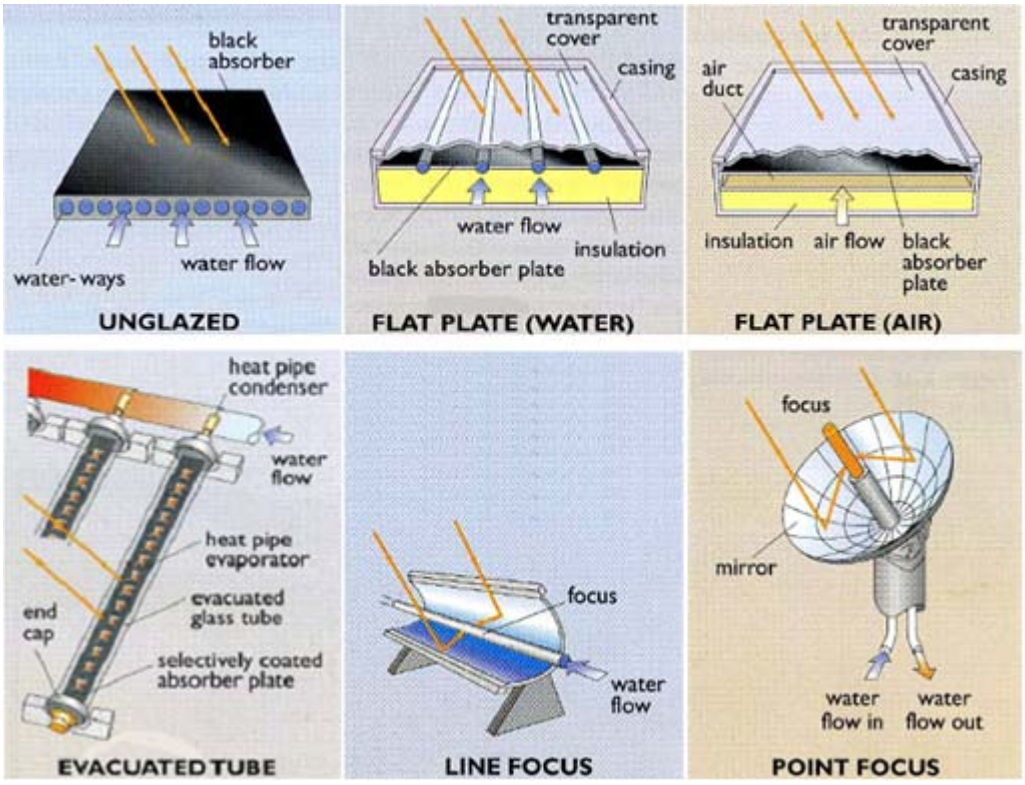

Fig. 2-7. Classification of solar collectors [2.13].

Unglazed panel is most suitable for swimming pool heating. It is only necessary for the water temperature to rise by a few degrees above ambient air temperature.

Flat-plate water collector is the mainstay of domestic solar water heating worldwide. It is usually single glazing but may have an extra second glazing. The panel usually has a black surface or selective coating that has both high optical absorption and low emission to cut heat loss. An absorber plate has high thermal conductivity to be capable of transferring the collected energy to the water with a minimum temperature drop.

Flat-plate air collector is not as popular as a water collector and is mainly used for space heating. An application of this collector is in combination with a photovoltaic panel to produce both heat and electricity.

Evacuated-tube collector consists of a set of modular tubes, where convective heat losses are minimised by virtue of the vacuum in the tubes. The absorber plate is a metal strip in the centre of each tube, and a heat pipe is used to carry the collected energy to the water which circulates along a header at the top of the pipe array.

Line-focus collector could concentrate the sunlight onto a pipe running down the centre of a trough that could be pivoted to track the Sun up and down or east to west. It is mainly used for generating steam for electricity plants. A line-focus collector can be orientated with its axis in either a horizontal or vertical plane.

Point-focus collector is also used for steam generation or driving a Stirling engine, but needs to track the Sun in two dimensions.

Flat-plate solar water heating systems have been used worldwide owing to their structural simplicity and the low cost of the flat-plate collector. However, evacuated-tube collector with heat pipes array is growing in popularity, as it has many advantages over the flat-plate collector. The main features of the

evacuated-tube and flat-plate collectors are compared in the following Table 2-1 [2.13, 2.19].

Table 2-1. Comparison of the evacuated-tube and flat-plate collectors [2.13, 2.19].

	Evacuated-tube collector	**Flat-plate collector**
Heat production	Rapid – vacuum prevents heat losses	Slow
Heat losses during daytime	Negligible	High
Influence of the incidence angle of the sun rays	Maximum solar absorption throughout the day – cylindrical shape	Maximum solar absorption at noon – flat shape
Cold weather operation	Satisfactory performance – vaporising/condensing processes within the heat pipes	Limiting effect – direct heat transfer processes, risk of freezing
Maximum operating temperature range	Above 95^{o}C	Up to 80^{o}C
Cost-effective	Advanced technology at competitive price	Old technology at higher price
Hot water availability	For a greater number of days throughout the year – high efficiency	For a lesser number of days throughout the year
Position of the collector on the roof	Assembled onto the surface of the roof	Preassembled flush with the roof – lifting may be required

2.2.3 Mathematical analysis

The performance of the solar water heating system will be influenced by the existence of the solar collector, heat exchanger or water tank, which will be separately described as:

A. Energy balance of solar collector

For any solar thermal system, the overall energy balance of the solar collector at a steady state is shown in Fig. 2-8 and could be expressed as [2.20]:

$$Q_u = Q_i - Q_l \tag{2-1}$$

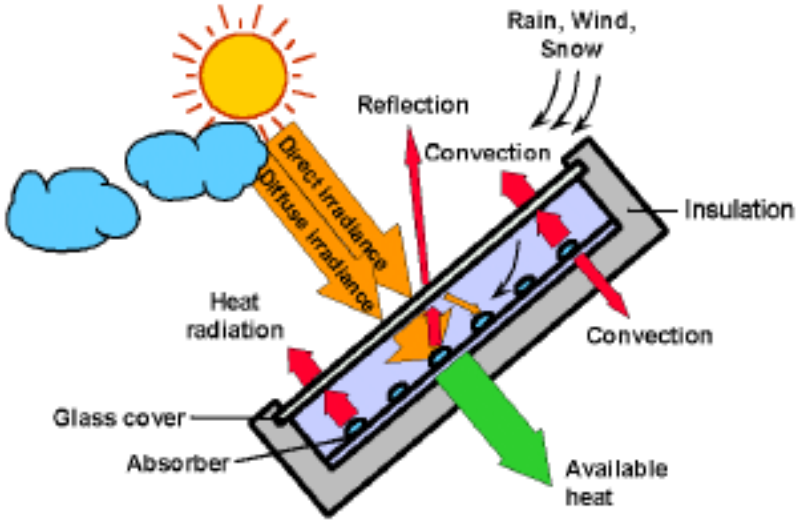

Fig. 2-8. Energy balance of a solar collector [2.20].

The energy absorbed by the solar collector depends on the optical properties of the collector cover and absorber plate and can be estimated as [2.20]:

$$Q_i = A_c I \tau \alpha \tag{2-2}$$

Part of Q_i will be released to the ambient. In the case of a flat-plate collector, the heat is normally assumed to release through the top, back and sides of the collector [2.20] as expressed in Eq. (2-3).

$$\begin{aligned} Q_l &= Q_{l,top} + Q_{l,back} + Q_{l,edge} \\ &= A_c U_{l,top}(T_c - T_a) + A_c U_{l,back}(T_c - T_a) + A_c U_{l,edge}(T_c - T_a) \\ &= A_c\left(U_{l,top} + U_{l,back} + U_{l,edge}\right)(T_c - T_a) \\ &= A_c U_l (T_c - T_a) \end{aligned} \tag{2-3}$$

$$U_{l,edge} = \frac{\lambda_{edge}}{\delta_{edge}} \frac{A_{edge}}{A_c} \tag{2-4}$$

It should be noted that $U_{l,top}$ is a function of the number and properties of the glass cover as well as the ambient temperature, and $U_{l,back}$ is a function of the thickness and thermal conductivity of the insulation.

Thus, the useful energy delivered by the collector in an area of A_c could be expressed as:

$$Q_u = A_c\big(I\tau\alpha - U_l(T_c - T_a)\big) \tag{2-5}$$

However, it is difficult to measure the mean plate temperature T_c. Therefore, Eq. (2-5) could be reformulated to calculate the useful energy delivered by the collector (Q_u) using the collector inlet fluid temperature (T_{fi}) by employing a collector heat removal factor (F_R) as in Eq. (2-6). The F_R is defined as the ratio of the heat delivered to the working fluid to the heat in the condition that the unified temperature of the collector plate equals the inlet fluid temperature. Since useful energy output is given by Eq. (2-7), F_R could be expressed as in Eq. (2-8). Eq. (2-6) is also known as the Hottel-Whillier-Bliss (HWB) Equation [2.20].

$$Q_u = A_c F_R \left(I\tau\alpha - U_l\big(T_{fi} - T_a\big)\right) \tag{2-6}$$

$$Q_u = C_p\dot{m}\big(T_{fo} - T_{fi}\big) \tag{2-7}$$

$$F_R = \frac{C_p\dot{m}(T_{fo}-T_{fi})}{A_c\big(I\tau\alpha-U_l(T_{fi}-T_a)\big)} \tag{2-8}$$

The collector efficiency (η) is the ratio of the useful energy delivered by the collector to the incident solar radiation on the collector during a specified period, which could be written as [2.20]:

$$\eta = \frac{\int Q_u dt}{A_c \int \mathrm{I} dt} \tag{2-9}$$

As the solar collector could be characterised using a number of design parameters, Eq. (2-9) could be simplified as:

$$\eta = \frac{Q_u}{A_c \mathrm{I}} = \frac{I\tau\alpha-U_l(T_c-T_a)}{I} = \tau\alpha - U_l\frac{T_c-T_a}{I} = F_R\tau\alpha - F_R U_l\frac{T_{fi}-T_a}{I} \tag{2-10}$$

It should be addressed that the variation of the collector efficiency with the operating temperature may be linear or nonlinear depending upon the characteristics of the collector. These can be represented as:

$$\eta = \eta_0 - U_l \frac{T_c - T_a}{I}$$, for a linear relationship (2-11)

$$\eta = \eta_0 - U_{l1} \frac{T_c - T_a}{I} - U_{l2} \frac{(T_c - T_a)^2}{I}$$, for a nonlinear relationship (2-12)

The variations of the efficiency with the combined factor of $(T_c-T_a)/I$ for typical solar collectors including unglazed panels, glazed black absorbers, glazed selective absorbers and evacuated tubes are presented in Fig. 2-9 [2.13]. It is found that the efficiencies for all the collector configurations fall with the rise of the mean plate temperature and the decrease of the ambient temperature and solar radiation. The evacuated tubes are found to have stable efficiency in the range of 55-70%, while the efficiency of the unglazed panels drops considerably from 90% to 0 at low $(T_c-T_a)/I$.

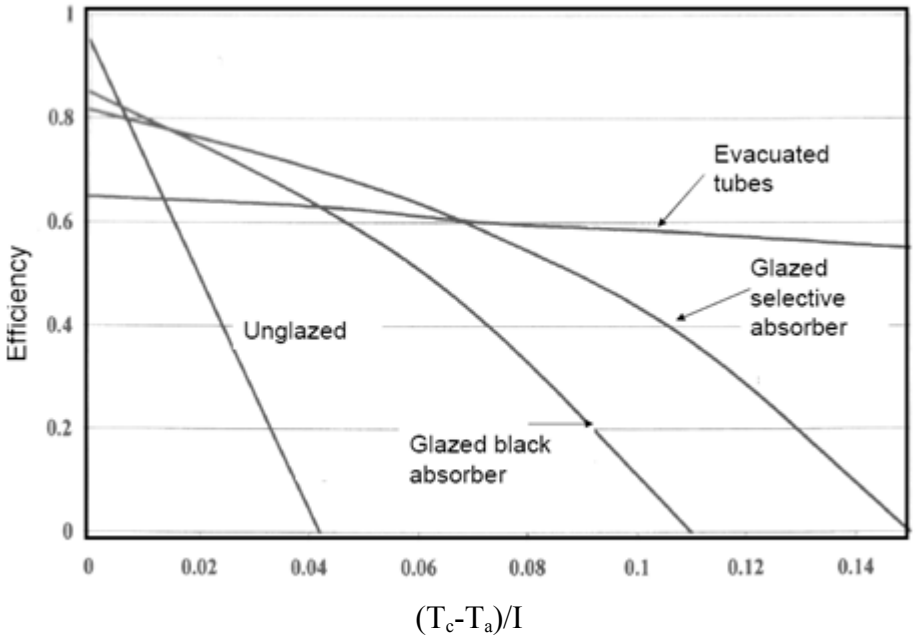

Fig. 2-9. Variations of the efficiency with the combined factor of $(T_c-T_a)/I$ for typical solar collectors [2.13].

B. Reduction of the useful energy delivered from the solar collector to the tank due to the employment of heat exchanger

When a heat exchanger is fitted between the solar collector and storage point, the performance of the solar system will be affected by the effectiveness of the heat exchanger (ε). As shown in Fig. 2-10, ε is defined as the ratio of the actual heat exchange rate to the maximum possible heat exchange rate [2.13]:

$$Q_u = \varepsilon\left(C_p\dot{m}\right)_{min}\left(T_{fo} - T_{si}\right) \tag{2-13}$$

Whereby, $(C_p\dot{m})_{min}$ is the minimum of $C_{pc}\dot{m}_c$ and $C_{ps}\dot{m}_s$.

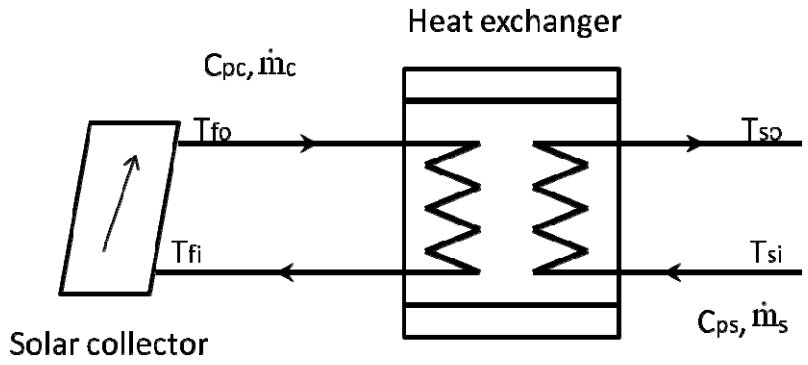

Fig. 2-10. Energy balance of the heat exchanger and its associated design parameters.

According to the Eq. (2-6) and Eq. (2-7) in the solar collector analysis, the relationship between the useful energy (Q_u) and the collector outlet fluid temperature (T_{fo}) could be established as:

$$Q_u = A_c F_R\left(I\tau\alpha - U_l\left(T_{fo} - \frac{Q_u}{C_{pc}\dot{m}_c} - T_a\right)\right) \tag{2-14}$$

Then T_{si} from Eq. (2-13) will substitute T_{fo} in Eq. (2-14). Thus, the useful energy delivered to the tank could be expressed by using an exchanger heat removal factor (F_R').

$$Q_u = A_c F_R{}'\left(I\tau\alpha - U_l(T_{si} - T_a)\right) \tag{2-15}$$

$$F_R{}' = \frac{F_R}{\frac{A_c F_R U_l}{C_{pc}\dot{m}_c}\left(\frac{C_{pc}\dot{m}_c}{\varepsilon(C_p\dot{m})_{min}}-1\right)+1} \quad (2\text{-}16)$$

This indicates the reduction in heat output due to the existence of the heat exchanger. In other words, the ratio of F_R/F_R' represents the increase in the collector area required by the system with a heat exchanger, in order to achieve the same energy output as the system without the exchanger.

C. Energy balance of water storage

Considering the water in the tank is fully mixed with a unified temperature, the internal energy change rate of the tank could be expressed as [2.21]:

$$C_{ptk} m_{tk} \frac{dT_{tk}}{dt} = Q_u - Q_L - Q_{l,tk} \quad (2\text{-}17)$$

Q_L is the heat load that is determined from the applications of the solar systems.

For space heating, $Q_L = UA_L(T_r - T_a)$ (2-18)

For water heating, $Q_L = C_p \dot{m}_w (T_r - T_w)$ (2-19)

$Q_{l,tk}$ is the heat loss from the tank, which is written as:

$$Q_{l,tk} = UA_{tk}(T_{tk} - T_a) \quad (2\text{-}20)$$

It should be noted that the heat losses from the water pipelines of the distribution system can also be added.

If the water in the tank is not fully mixed, i.e., stratified (in the case of a passive system), the tank could be modelled by dividing the water into layers and establishing energy balance equations for each layer [2.21].

As a result, the tank water temperature for a solar system having the collector, tank and load can be estimated by integrating Eq. (2-17) as:

$$T_{tk}{}^{+} = T_{tk} + \frac{dt}{C_{ptk}m_{tk}}\left(Q_u - Q_L - Q_{l,tk}\right) \quad (2\text{-}21)$$

For an initial value of T_{tk}, the water temperature at the end of dt can be calculated by using Eq. (2-21).

Thus, the entire day's useful energy, tank water temperature, load demand and contribution of the solar energy in meeting that demand can be obtained from various design parameters, e.g., collector area, tank capacity and time when auxiliary energy is needed [2.22].

2.3 Demonstration buildings for applications of solar water heating systems

Since the 1960s, flat-plate collectors supported by metal frames have been mounted on the flat rooftops of buildings as shown in Fig. 2-11 [2.23]. In recent years, roof-mounted solar collectors have been widely installed in single-family houses or multi-family buildings across different countries with different climates from cold to temperate, such as The Netherlands, Germany and Switzerland. Fig. 2-12 [2.24] illustrates a 23 m^2 roof-mounted solar collector in the configuration of evacuated tubes to support the central heating system for domestic hot water in Germany, which helped reduce the heating consumption by 90% compared to the conventionally constructed buildings. However, both flat-plate and evacuated-tube installations occupy a large roof space, leading to deterioration of the building's aesthetic view.

Fig. 2-11. 760 m^2 roof-mounted flat-plate collectors at the Brandaris Building, The Netherlands in 1968 [2.23].

Fig. 2-12. 23 m^2 roof-mounted evacuated tubes at the ISIS Demonstration Building, Germany in 2002 [2.24].

In order to improve the architectural appearance of the building, a roof-integrated solar water heating system has been proposed, which replaces the finishing layer of the roof insulation as shown in Fig. 2-13 [2.25]. However, this system has proven to be less efficient than the roof-mounted solar system owing to the fixed tilt angle of the collector, particularly during cold weather.

Fig. 2-13. 8.4 m^2 roof-integrated flat-plate collectors at the House W, Czech Republic in 2003 [2.25].

For both roof-mounted and roof-integrated solar water heating systems, the water will be transported over a long distance from the exterior building roof to the interior tank, and then flow back to the outside. This method will either consume a large amount of electricity to run a pump (active system) or result in low solar conversion efficiency by virtue of the natural circulation (passive system). This will lead to increased system electrical usage and operating costs, high heat loss during transportation and reduction of the building's aesthetic quality. Most importantly, freezing problems may occur, particularly for multi-storey buildings with a large number of occupants.

In order to solve the problems mentioned above, building balcony/façade integrated solar water heaters have been brought into use in many practical projects as shown in Fig. 2-14 [2.26] and Fig. 2-15 [2.27]. This category of system could shorten the water piping distance, improve the occupants' living conditions, reduce the construction costs and enhance the building's appearance, owing to the joint use of the building and solar system components or replacement of the conventional building wall by the solar system [2.28].

Fig. 2-14. 17 m^2 façade-integrated flat-plate collectors at the Plus Energy House, Austria in 2001 [2.26].

Fig. 2-15. 6 m^2 balcony-integrated evacuated-tube collectors at the Sunny Woods, Switzerland in 2001 [2.27].

Although a building balcony/façade integrated solar system is preferred over a roof-mounted or roof-integrated solar water heating system, it still has long pipelines transporting water between the exterior building wall and interior storage, which will ultimately affect the capability of heat transfer and lower the efficiency of solar conversion. In addition, this solar system still faces the problem of freezing during cold weather conditions, which is considered to be the biggest problem among the existing solar systems.

2.4 Basic concept of loop heat pipe (LHP)

Loop heat pipe (LHP) [2.29 ~ 2.30], as shown in Fig. 2-16 [2.31], is a two-phase (liquid/vapour) heat transfer device allowing a high thermal flux to be transported over a distance of up to several tens of metres in a horizontal or vertical position owing to its capillary or gravitational structure. LHP has a

separate evaporator and condenser, thus eliminating an entrainment effect occurring in between. LHP can operate under different gravitational regimes, regardless of whether the evaporator is above or below the condenser.

The working principle of the LHP device could be described as: The heat transfer fluid in the wick absorbs the heat added to the evaporator and vaporises via the vapour line to the condenser. Within the condenser, the vapour will be condensed to the liquid of the same temperature and return to the compensation chamber through the liquid line. The liquid will then be accumulated and stored in the compensation chamber and further saturate the wick.

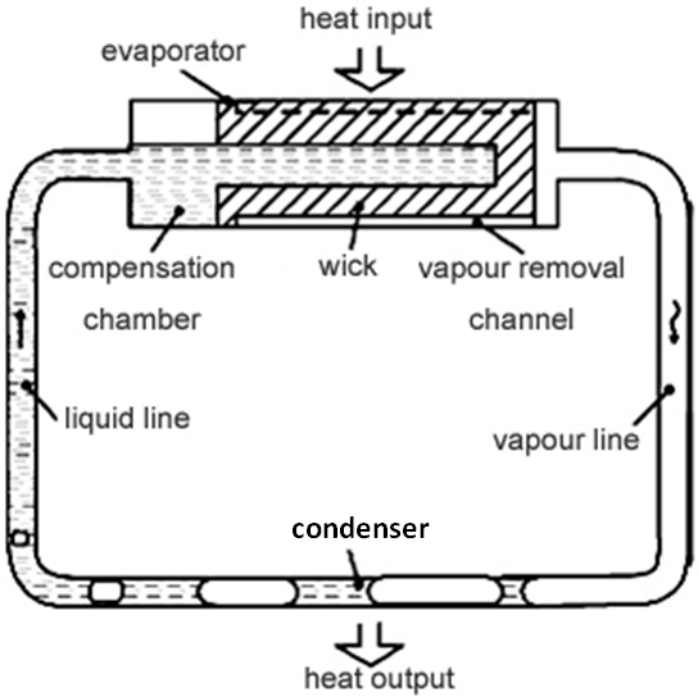

Fig. 2-16. Schematic of a conventional loop heat pipe (LHP) device [2.31].

LHP could be classified based on the varieties of designs and functions as shown in Table 2-2 [2.32].

Table 2-2. Classifications of the LHP devices [2.32].

Classifications of the LHP devices			
LHP design	**Evaporator shape**	**Evaporator design**	**Condenser design**
• Conventional (diode) • Reversible • Flexible • Ramified	• Cylindrical • Flat disk-shaped • Flat rectangular	• One butt-end compensation chamber • Two butt-end compensation chambers • Coaxial	• Pipe-in-pipe • Flat coil • Collector
Number of evaporators and condensers	**Temperature range**	**Operating temperature control**	
• One • Two and more	• Cryogenic • Low-temperature • High-temperature	• Without active control • With active control	

According to Reay and Kew [2.30], three elements of the LHP device, i.e., heat transfer fluid, wick and container, should be examined during its design.

In terms of the **heat transfer fluid**, three aspects should be considered, including the compatibility with the materials of the wick and container, vapour temperature range and a ratio of the pressure difference to the temperature difference between the evaporator and compensation chamber [2.32 ~ 2.34].

The **wick** in a porous structure is usually located in the evaporator [2.35]. It produces the capillary force to drive the liquid back to the evaporator and ensures the heat transfer liquid is evenly distributed over the evaporator surface. Sintered powder and mesh screen are the most common categories of wicks. Compared with mesh screen, a sintered metal wick has better control of the porosity and pore size, thus leading to higher heat dissipation of 50 W/cm^2 than the mesh of 10 W/cm^2 [2.36 ~ 2.37]. However, when applying these two wick categories to the same size containers, mesh could achieve better power handling capability owing to bigger vapour space and smaller wick thickness [2.38]. This makes it an attractive option over sintered powder, particularly for application in the heat pipes.

The **container** is an envelope to isolate the heat transfer fluid from the outside environment once sealed and vacuumed [2.30], which should be leak-proof, easy to fabricate and have high thermal conductance to ensure minimum temperature drop between the evaporator and condenser. Three commonly used container materials are copper, aluminium and stainless steel owing to their high thermal conductivity properties and possibilities of reliable seal and shape change [2.30]. In recent advances, other materials such as magnesium [2.39] and titanium [2.40] have become alternatives for container materials.

2.5 Researches of the LHP technology

2.5.1 Overview of the LHP technology

Since the first LHP was invented in 1974 in the Former Soviet Union [2.32], extensive studies on its practical applications and demonstration tests have been conducted, particularly in the late 1980s [2.41]. At present with the LHP devices successfully employed in many fields of applications, e.g., cooling of electronics and thermoregulation of spacecraft [2.32], LHP technology continues to be a crucial area of research. Numerous theoretical models covering various aspects of the LHP have been developed, which have proven to be useful in predicting LHP performance through the validations of tests, including operating limits and thermal performance characteristics.

A book written by Peterson [2.35] illustrated the performance limit approach for the heat pipe in the steady-state condition. This approach started with the calculation of the capillary limit, which could be determined iteratively as a function of the operating temperature. Other limits, i.e., viscous, sonic, entrainment and boiling, can also be calculated depending upon the operating temperature. Thus, the maximum power handling capability of the heat pipe at a certain orientation and operating temperature can be decided. Peterson [2.35] also analysed the heat pipe's heat transfer processes in the steady-state condition by using thermal resistances calculating method. This method presented a network from which various resistances around the heat pipe, e.g., radial resistances of the pipe wall and saturated wick at the evaporator, could

be obtained to calculate the overall temperature gradient between the evaporator and condenser.

In order to simplify the existing engineering models and reduce the required computing resources, Zuo and Faghri [2.42] developed a thermal network model to analyse the circulation of the working fluid in the heat pipe by using the thermodynamic cycle approach. This model can also be extended to the transient heat pipe analysis. Various components with different thermal resistances and dynamic responses could be found within the network as shown in Fig. 2-17 below, which will be represented in a simplified form through first order and linear differential equations.

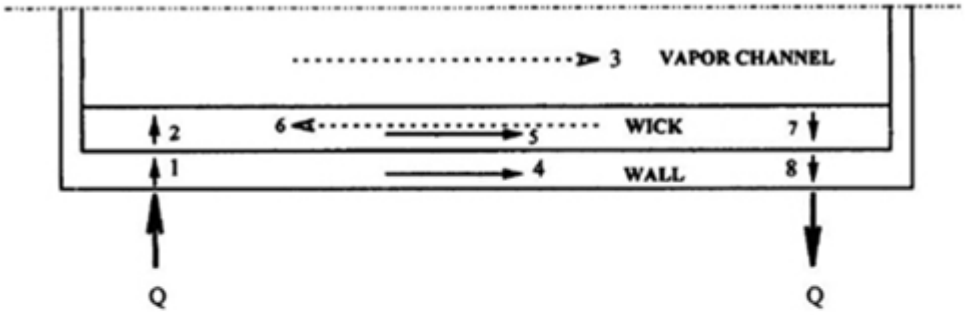

Process	Description
1	Radial heat conduction through the evaporator wall
2	Radial heat conduction through the evaporator liquid-wick
3	Vapor flow (heat convection)
4	Axial heat conduction through the adiabatic section wall
5	Axial heat conduction through the adiabatic section liquid-wick
6	Liquid flow (heat convection)
7	Radial heat conduction through the condenser liquid-wick
8	Radial heat conduction through the condenser wall

Fig. 2-17. Development of the thermal network model of the heat pipes by using thermodynamic cycle approach [2.42].

Kaya and Hoang [2.41] modelled the performance of a loop heat pipe based on steady-state energy balance equations at each component of the loop. Taking into account the heat exchange between the LHP components and surroundings, both convection and radiation environments were modelled. The loop operating temperature was found to be a function of the applied power at the given loop condition. The mathematical model was validated by experiments using two different LHP designs at different sink temperatures and elevations.

Comparison of the calculation and experimental results showed an agreement within 3%.

Bai et al. [2.43] established a mathematical model for the start-up process of a loop heat pipe based on the node network method. In this method, the LHP was divided into several nodes, and these nodes could be grouped into two types, namely the wall and fluid nodes. The governing equations including mass, momentum and energy were established for each node. A parametric analysis on the start-up characteristic of the LHP was conducted, which found that the LHP start-up performance could be improved from the development of a number of the operating conditions including large start-up heat input, low leak of heat from the evaporator to the compensation chamber and active cooling in the compensation chamber.

Pauken and Rodriguez [2.44] modelled and tested a loop heat pipe with two different working fluids, i.e., ammonia and propylene. Compared to ammonia, propylene had a lower freezing point and relatively better thermal property. The performance of the LHP with ammonia was characterised by a series of tests with heat inputs of 20 to 800 W placed on the evaporator, and the LHP filled with propylene was tested with heat inputs of 20 to 200 W to the evaporator. The constant conductance performance of the LHP was 170 W/K with ammonia and 44 W/K with propylene. Steady-state performance data of the LHP were used to validate a node network model of the device. The evaporator temperature was found to be functional of the heat input. Comparison between the observed and predicated data of the evaporator temperature indicated that the average difference was 0.85^{o}C with ammonia and 1^{o}C with propylene.

Hoang et al. [2.45] mentioned that the heat transfer characteristic of a loop heat pipe was difficult to predict, owing to the complicated nature of the thermal interaction between the LHP and environment. The overall thermal conductance varied not only with the power input, ambient and sink temperatures, but also the system's initial condition and previous operational history. Hence, the analytical modelling of the LHP often yielded inaccurate

results when compared with the actual data. They stated that the loops always adjusted themselves to reach steady state eventually, no matter how the operating conditions changed. They also indicated that in order to ensure a successful start up without exceeding the temperature limits, a starter heater or thermoelectric cooler could be used.

Riehl [2.46] tested a loop heat pipe system operating with acetone as the working fluid. Tests were carried out for the LHP at the positions of horizontal and the capillary evaporator above and below the condenser. Experimental results indicated that the system could present reliable performance in all situations under power levels as low as 1 W, and high operating temperatures could be achieved with the evaporator above the condenser.

Zan et al. [2.47] established an experimental formula for a sintered nickel powder wick. Wick structures with different porosity ranging from 65 to 80% were fabricated by a cold pressing sintering process, and parameters including porosity, pore radius and permeability were measured. The results showed that an optimal combination of the wick structure parameters existed, through which the performance of the LHP would achieve optimisation. The maximum heat transfer capacity was up to 500 W, and the thermal resistance was 0.12 K/W at the allowable working temperature of 80^{o}C.

Riehl and Dutra [2.48] presented the development of an experimental LHP. This LHP was built and tested with acetone as the working fluid, designed to handle up to 70 W of power and using a capillary evaporator to reduce its effective length. The experimental results illustrated an excellent thermal management capability of the proposed LHP for the limits to its design and operation, especially when considering the use of a less hazardous working fluid and particular geometric characteristic of the LHP.

Vlassov and Riehl [2.49] explored LHP modelling by developing a relatively precise condenser sub-model from the solutions of the conjugate equations of energy, momentum and mass balances, and only describing a few transient nodes within the evaporator and compensation chamber. Experimental LHP

consisted of a cylindrical stainless steel evaporator with an integral compensation chamber, where the wick was of micro-pore polyethylene. The condenser was an aluminium plate with acetone as the working fluid. The testing conditions were reproduced in the mathematical model, and its parameters were adjusted using the measured temperatures. It was concluded that the model was able to predict the LHP transient behaviour within 3-4^{o}C of accuracy.

A more comprehensive dynamic model was published by Launay et al. [2.50], who proposed a transient model to predict the thermal and hydrodynamic behaviour of a standard LHP. The model of the loop was divided into four sub-systems, i.e., the fluid in the compensation chamber, the evaporator, the condenser and the transport lines, where transient mass, energy or momentum conservation equations would be developed. The comparison of the modelling and experimental results for a transient test allowed validation of the established model to be made, and the maximum difference between the predicted and measured temperatures along the LHP was less than 3.5^{o}C with a liquid temperature variation of 28^{o}C.

Kaya et al [2.51] developed one model for the numerical simulation of the transient LHP operation including start-up phase, based on one-dimensional and time-dependent conservation equations for heat and fluid flow. During the model setup, some key parameters were either difficult or impossible to predict such as the incipient superheat at start up, and some parameters may be experimentally correlated including the external and internal heat transfer coefficients. These required parameters and experimentally-fitted values were used but controlled to a minimum number. The mathematical model simulated reasonably well with the transient response of the tested LHP unit. The start-up transients were also successfully reproduced at high powers. For the start-up simulations at low powers, the heat leak across the wick could be determined by fitting the experimental data to the modelling.

Huang et al. [2.52] classified the start-up phenomenon of a loop heat pipe into four modes (Fig. 2-18), i.e., failure, oscillation, overshoot and normal, based on

three experimentally-determined heat inputs, i.e., minimum, critical and overshoot. In the failure mode, the temperature at the evaporator continued to rise, but could not reach a steady state. In the oscillation start-up mode, the temperature of the evaporator increased owing to the continued heat input and evaporation of the fluid. The decrease of the temperature was caused by the condensation of the fluid in the condenser and return of the sub-cooled liquid to the compensation chamber. In the overshoot mode, oscillation only occurred at the beginning of the operation, and a steady state could be reached afterwards. For the normal mode, a smooth start up could be achieved due to a high heat input, indicating a stable temperature rise of the evaporator in the start up.

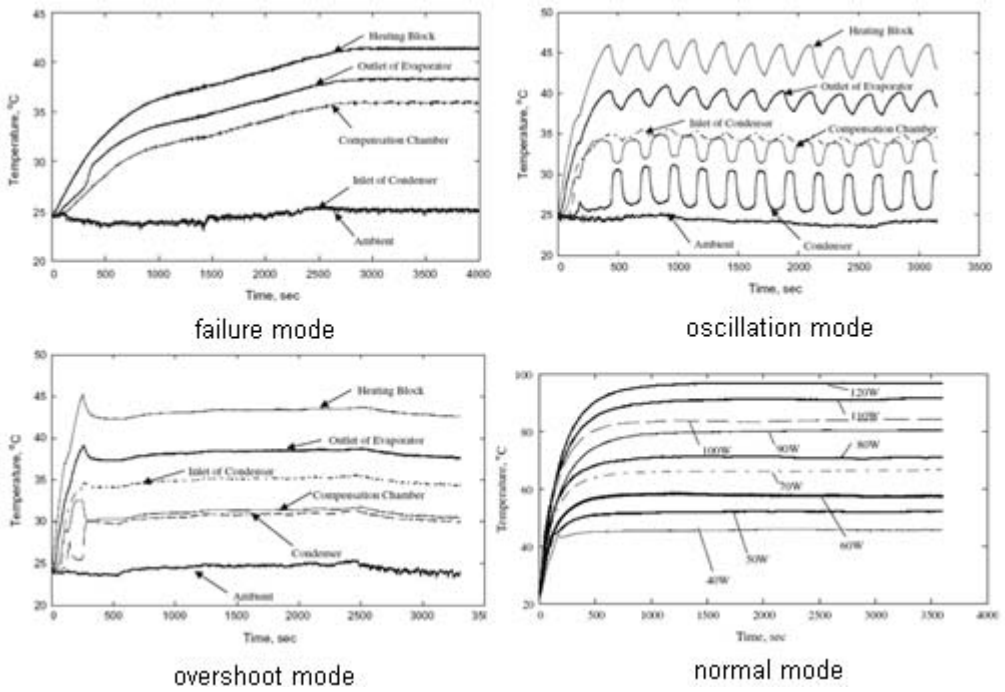

Fig. 2-18. Start-up modes of a loop heat pipe device [2.52].

The start-up characteristics of the LHP under low powers were studied by Wang et al. [2.53] through a series of experiments. It was found that the LHP can start up unfailingly under heat power as low as 6 W. They also testified that the start-up performance of the LHP could be improved, as the heat leak across the wick was reduced with the increase of the thickness of the sintered capillary interlayer.

2.5.2 Analysis of the review works

Works related to the LHP technology were found to be substantial, and the above case-to-case statements could be further analysed from the two aspects of performance characteristic and research methodology.

A. Analysis of the review works in terms of performance characteristic

In terms of the performance characteristic of the LHP, the research works can fall into the categories of steady-state and transient conditions. The operating limits and heat transfer performance of the LHP under steady-state conditions have already been widely researched by the development of the numerical models and validation of the experimental tests. A few research works have been conducted to study the transient behaviour of the LHP device, since the complex heat and mass transfer processes were involved in the operation of the LHP system.

Operating limits (heat transport capacity) is one of the most significant performance characteristics of the LHP. The procedure of solving the operating limits was given by Peterson [2.35], Zan et al. [2.47] and Riehl and Dutra [2.48]. As to the steady-state performance of the LHP, two methods were illustrated including pressure [2.41, 2.44] and thermal resistance [2.35, 2.42, 2.45] equations. Hoang et al. [2.45], Vlassov and Riehl [2.49] and Launay et al. [2.50] reproduced the main features of the transient LHP operation without the start-up phase. This is because the start up of a loop heat pipe is a complex dynamic process, and includes the redistribution and circulation of the heat transfer fluid in the loop accompanied by many phase change phenomena such as evaporation and condensation, before each component of the system reaches a steady state. The investigation of the start-up characteristic of the LHP was mainly through experimental methods [2.43, 2.52 ~ 2.53]. However, recent research works witnessed that it could be reproduced by an experimentally-correlated analysis [2.51].

B. Analysis of the review works in terms of research methodology

In terms of the research methodology used, the research works can be classified into theoretical analysis and computer modelling, and experimental study.

(a) Theoretical analysis and computer modelling

Many theoretical works have been carried out to study the performance of the LHP and its associated heat and mass transfer processes. These works could be divided into the following two groups:

(1) Analytical models to address the heat transfer and thermal resistance balances across different parts of the LHP [2.35, 2.41 ~ 2.42, 2.44 ~ 2.45, 2.47];
(2) Transient energy models to simulate the dynamic characteristics of the LHP [2.43, 2.49 ~ 2.51].

In summary, the established theoretical models are sufficient to reveal the complex nature of the LHP technology, optimise the system's configuration, suggest the favoured operating condition and predict its performance.

(b) Experimental study

The aims of the experimental study could be outlined as:

(1) To identify the real performance of the LHP under the specified operating condition;
(2) To examine the reliability and accuracy of the established computer model;
(3) To establish the correlation between the theoretical analysis and practical application.

Thus, the experimental or combined modelling and experimental works include:

(1) Operating temperature and its relevance to various operational parameters [2.46, 2.52];

(2) Power handling characteristics of the LHP [2.47 ~ 2.48, 2.53];
(3) Comparison between the modelling results and experimental data [2.44 ~ 2.45, 2.50];
(4) Validation and accuracy/error analysis of the computer model [2.41, 2.49, 2.51].

In summary, the experimental or combined modelling and experimental works are significant and have been found to be in agreement with most theoretical results. These works also provide feasible approaches to manage the theoretical findings with regards to practical applications.

2.5.3 Applications of LHP technology in solar water heating systems

LHP is suitable for use in building solar hot water system, owing to its unique features such as highly effective thermal conductance and flexible design embodiment and installation [2.54]. Zhuang [2.55] developed a loop heat pipe for variable installations of solar water heating systems as shown in Fig. 2-19, which could increase its capability of heat transfer in a small inclination angle to horizon or in a horizontal position.

Fig. 2-19. Loop heat pipe for solar water heater developed by Zhuang [2.55].

New Energy Centre (NEC) in National Taiwan University [2.56] developed a new solar water heater, which employed a loop heat pipe system attached to the back of a thermosiphon tube and used to transfer the heat from the tube to the water tank as shown in Fig. 2-20. This system with efficiency of 50.3% could be directly mounted on the rooftop of a building due to its structural integrity. However, this installation will occupy a large roof space of the building, thus detracting from the aesthetics of the building.

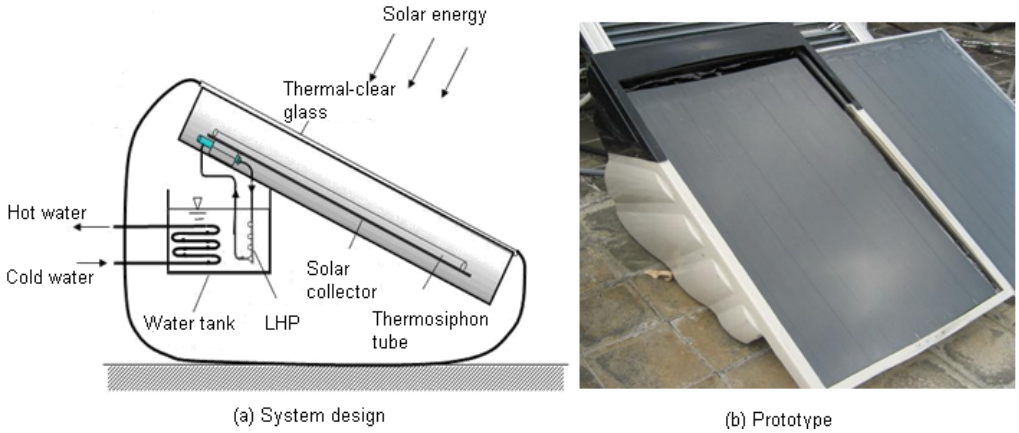

Fig. 2-20. LHP solar water heating system developed by NEC [2.56].

2.5.4 Conclusive remarks of the review works

In summary, the research works on LHP technology are substantial and focus on revealing the nature of the energy transfer occurring in the LHP, identifying the favoured system configuration and its associated components, optimising the structural/geometrical parameters of the system, suggesting the appropriate operating condition and building the bridge between theoretical analysis and experimental study. All these efforts contribute to a target of creating an energy-efficient, cost-effective and structure-optimal LHP system.

2.6 Opportunities for further work

Although significant works have been conducted by now, there are still obvious opportunities to develop this technology.

A. Developing new, economically feasible and energy-efficient solar systems employing LHP technology

A loop heat pipe system is particularly suitable for applications in solar thermal systems owing to its advanced features. However, current applications of LHP are mainly in the areas of outer space thermoregulation and electronic cooling. Hence, the opportunity to develop new solar systems employing LHP technology to replace conventional solar water heaters still remains open. This will create a new research area for the development of economically feasible and energy-efficient solar systems. The advantages of the systems still require

further validation through theoretical and experimental studies. As well as this, solar systems in different configurations are still open to exploration.

B. Optimising the structural/geometrical parameters of the solar system configurations to enhance the energy performance

Existing solar systems are technically and commercially mature and have no obvious chance to improve their performance. However, there are still opportunities for solar systems employing the LHP technology. The low cost, flexible LHP with built-in capillary would be a favourite choice to replace the conventional parallel-laid heat pipe, and its performance improvement through the optimal study of the structural/geometrical parameters is still in the research stage. The main challenge is to find a method of overcoming the difficulties remaining in the existing solar systems, e.g., winter freezing, long-pipe water running and low efficiency.

2.7 Summary

A critical review into the R&D and practical applications of the solar water heating system and loop heat pipe (LHP) technology has been carried out. The results of this research help understand the current status of the economic and technical developments, identify the barriers remaining to the existing solar systems, develop the potential research areas to improve the performance of the solar systems, establish the associated strategic plans related to the design and installation of the LHP and promote the solar thermal global market.

Solar thermal is the technology converting solar energy to usable heat for applications in water, space heating and cooling, electricity, fuels and agricultural and industrial processes. Over the past few decades, the global solar thermal market has grown rapidly owing to the low cost of the solar systems under certain conditions, financial incentives, regulatory instruments, education and environmental and local visual impacts. However, there still exist various barriers to the promotion of solar thermal, which could be summarised into technical, economic and other (legal, cultural and behavioural) barriers.

The working principle of the solar water heating system was described, as well as its classifications into passive and active systems, direct and indirect systems or based on the configurations of the solar collectors. The mathematical analytical equations for the determination of the heat output and system efficiency were presented for the solar system with a collector, heat exchanger or tank.

The practical applications of the solar water heaters in a building's roofs and envelopes were illustrated. The building balcony/façade integrated solar systems overcame the barriers of the conventional roof-mounted and roof-integrated solar water heaters and presented with advanced features, e.g., the improved architectural appearance and reduced construction cost of the building. However, the winter freezing and long water piping problems still limited the prevalence of this system, which could potentially be solved by employing LHP technology.

LHP was an efficient heat transfer device that could transport thermal energy for a long distance. It owned some advantages over the conventional heat pipe, e.g., gravity-unaffected and flexibility in its design and installation, which made it particularly suitable for applications in solar water heating systems. The three components of the LHP device, including the working fluid, wick and container, will influence the performance of the LHP.

The research works on the performance of LHP technology are substantial and could be summarised as focusing on revealing the nature of the energy transfer occurring in the LHP, identifying the favoured system configuration and its associated components, optimising the structural/geometrical parameters of the system, suggesting the appropriate operating condition and building the bridge between theoretical analysis and experimental study. All these efforts contribute to a target of creating an energy-efficient, cost-effective and structure-optimal LHP system.

Although significant works have been completed in solar thermal and LHP studies, there are still some opportunities existing for further development, e.g.,

developing new, economically feasible and energy-efficient solar systems employing LHP technology and optimising the structural/geometrical parameters of the solar system configurations to enhance their energy performance.

Chapter 3: Conceptual design of the façade-based solar LHP water heating system

3.0 Overview

In this chapter, the novel solar façade water heating system employing the LHP technology will be conceptually designed, based on a typical 3-member family flat in Beijing, China. This system is expected to be low cost, highly efficient, façade integrated and aesthetically appealing and have the potential to provide an alternative to the existing roof-mounted or conventional wall-hung solar water heating system.

The proposed solar façade LHP system, comprising the outdoor and indoor parts via the connection of transport lines, is initially described with the working principle. The prefabricated outdoor module could convert the solar energy to thermal energy in the form of low-temperature vapour. The vapour will be transported indoors through the transport line and condensed within the heat exchanger by releasing the heat to the service water. The heated water will then be stored in the tank for usage.

The geometrical size, material and quantity of the system's components, i.e., thermal-clear glass covers, wicked heat absorbing pipes, vapour/liquid headers, vapour/liquid transport lines, flat-plate heat exchanger, backboard, storage tank, pump and water pipelines, will be separately designed.

This work is the basis of the entire research project, whereby optimisations/modifications to the characteristic parameters of the system's components could be made through theoretical and experimental investigations in the following chapters.

3.1 System description and working principle

The proposed system is shown schematically in Fig. 3-1. The system can be clearly divided into two elements, i.e., outdoor and indoor. The outdoor part is a modular pack which receives the solar irradiation and converts it into heat energy in the form of low-temperature vapour. The indoor part consists of a

number of components including flat-plate heat exchanger, hot water tank, circulating pump and water piping connections, and is designed to generate hot water via condensation of the heat pipe vapour and store that water in the tank.

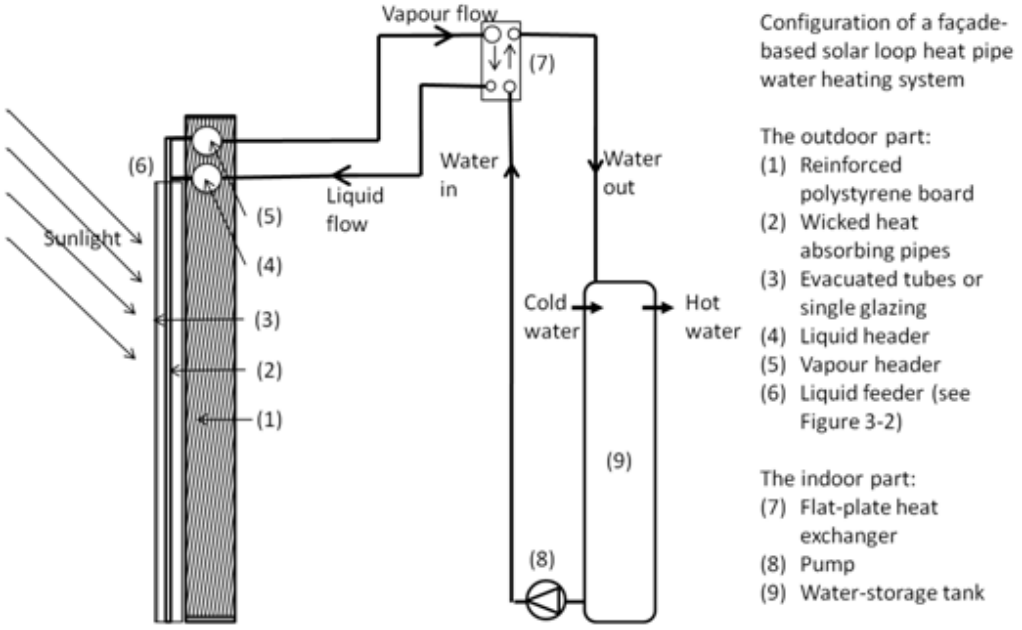

Fig. 3-1. Schematic of the novel façade-based solar LHP water heating system.

The outdoor part is a multi-layer façade structure comprising (1) a lightweight reinforced polystyrene board; (2) parallel-laid vertical heat absorbing pipes with internal capillary wicks, which evenly distribute the working fluid around the inner pipe walls via the wicks (meshes or sintered metal powders), and convert the heat transfer fluid into vapour upon receiving the solar irradiation striking the pipes; and (3) thermal-clear single glazing or double-walled evacuated tubes, which could allow transmission of the solar radiation into the module and prevent excessive thermal loss from the absorber surface to the ambient. On the upper part of the module, two headers, i.e., liquid and vapour ones, are also embedded into the façade board, feeding the liquid into the capillary pipes and receiving the vapour generated from the pipes. As shown in Fig. 3-2, the liquid feeder is an end-blocked cylinder with round-distributed mini-holes on the bottom connection to the wicked pipes, which would allow the liquid to be dipped into the wick voids equally. The speed of liquid feeding can be controlled by adjusting the height level of the liquid within the header, in order to achieve a balance between the liquid

evaporation and supply. The whole part of the unit could be made as a prefabricated panel, which could either replace the building's existing wall or hang on the exterior wall acting as a decoration layer.

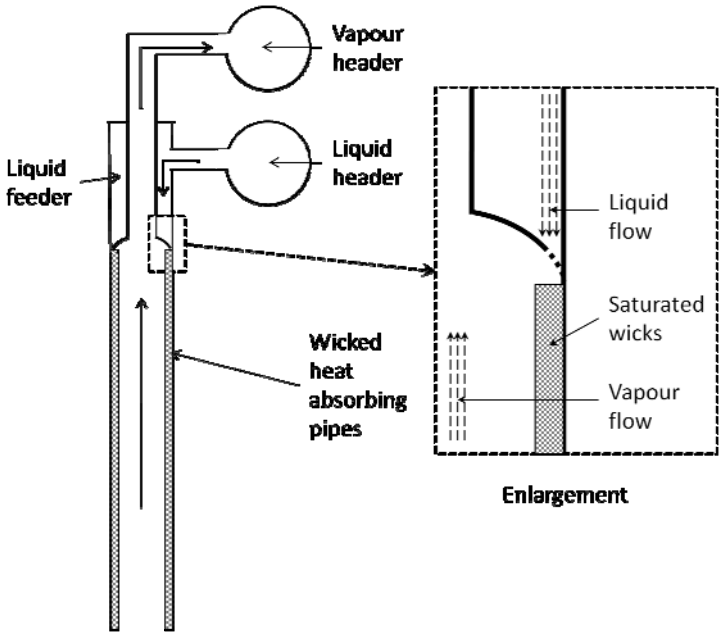

Fig. 3-2. Schematic of the connection of the vapour/liquid headers and heat absorbing pipe via the liquid feeder.

The indoor part comprises a well-insulated vapour transport line delivering the heat from the outdoor vapour header to the indoor exchanger owing to the vapour buoyancy, and a wall-hung flat-plate heat exchanger where the vapour is condensed to a liquid of the same temperature. The condensation heat is transferred to the cold water flowing across the exchanger channels adjacent to the vapour channels. At the outlet of the heat exchanger, a steam trap is assembled to stop the penetration of vapour through the pipe. Thus, only the condensed liquid can flow across and enter the liquid header via a liquid transport line, owing to the gravity caused by the height difference between the exchanger and liquid header.

This solar façade removes the need to transport water for a long distance, i.e., water circulation between the inside and outside of the building. Instead, the water, raised by a pump, simply circulates around the exchanger channels to obtain heat from the vapour and returns back into the water tank, beside the

exchanger via the water pipelines. The heated water will then be delivered to the outlet points when needed.

This innovative design allows the combination of solar water heating and LHP technologies and the integration of the heat absorbing pipes into the building wall, thus realising a building-integrated, cost-effective, highly-efficient and visually-pleasing solar heating system.

The **working principle** of the façade-based solar LHP water heating system could be described thus: When the solar energy strikes the south-facing collector surface across the high-solar-transmittance glass cover (evacuated tubes or single glazing), the received solar heat converts the heat transfer fluid adhered on the pipe wicks (mesh screen or sintered powder) into vapour. The vapour will flow upwards along the inner space of the pipes, enter the top-level vapour header and further transfer to the wall-hung flat-plate exchanger inside the building via the well-insulated vapour line, owing to the buoyancy effect of vapour. Within the exchanger, the vapour will be condensed into a liquid of the same temperature. The condensed liquid will flow across a steam trap assembled at the exchanger outlet and enter the liquid header via a liquid line, owing to the gravity effect caused by the height difference between the exchanger and liquid header. This liquid will then be evenly distributed to the capillary pipes through the dedicated liquid feeder fitted at the upper part of each wicked pipe.

Meanwhile, the released heat from the vapour condensation within the vapour channels of the exchanger will be transferred to the cold water flowing across the exchanger channels in the water cycle, which is raised by a pump from the bottom of the cylinder tank. The heated water will then be pumped back into the tank via the water pipelines and delivered to outlet points when needed.

It should be addressed that the heat transfer fluid of the LHP, which is separated from the service water by the exchanger plates, could be a mixture of water and glycol (antifreeze) or distilled water to protect against freezing. Therefore, it has no effect on the quality of water for living purposes and

causes no harm to users. It should be noted that the distilled water will not freeze at a subzero temperature in winter when solar radiation is unavailable, since the vacuum of the LHP can create a freezing point as low as -42^{o}C which is much lower than the winter air temperature [3.1].

3.2 Conceptual design

3.2.1 Selection of a sample block of flats

The project aims to develop a façade-based solar LHP water heating system, particularly suitable for a style of Chinese flats. For this reason, a 5-floor building containing 3-bedroom flats in Beijing (China) was selected to explore the potential layout of the proposed system. In order to obtain the maximum absorption of the solar radiation, the solar façade LHP systems were integrated with the south-facing balcony walls of the flats as shown in Fig. 3-3.

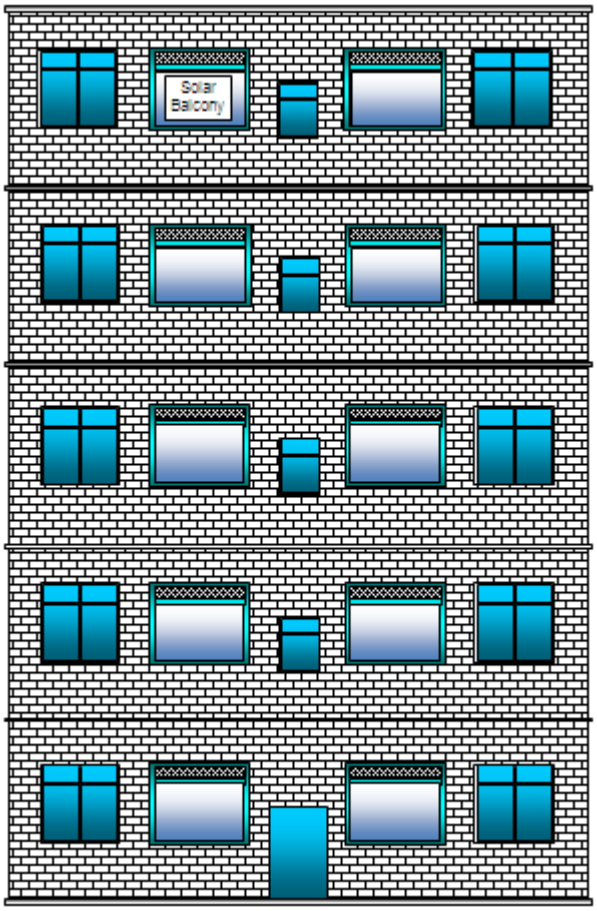

Fig. 3-3. Front view of a sample block of flats for applications of the façade-based solar LHP water heating systems.

The general layout of the solar system in a typical flat was shown schematically in Fig. 3-4. In order to avoid inconvenience to the occupants caused from the utilisation of the solar system, the heat exchanger and hot water tank were positioned inside the bathroom of the flat, and the vapour/liquid lines connecting the outdoor heat absorbing pipes and indoor wall-hung flat-plate heat exchanger were pre-embedded into the concrete or brick walls or lifted up to hang on the walls.

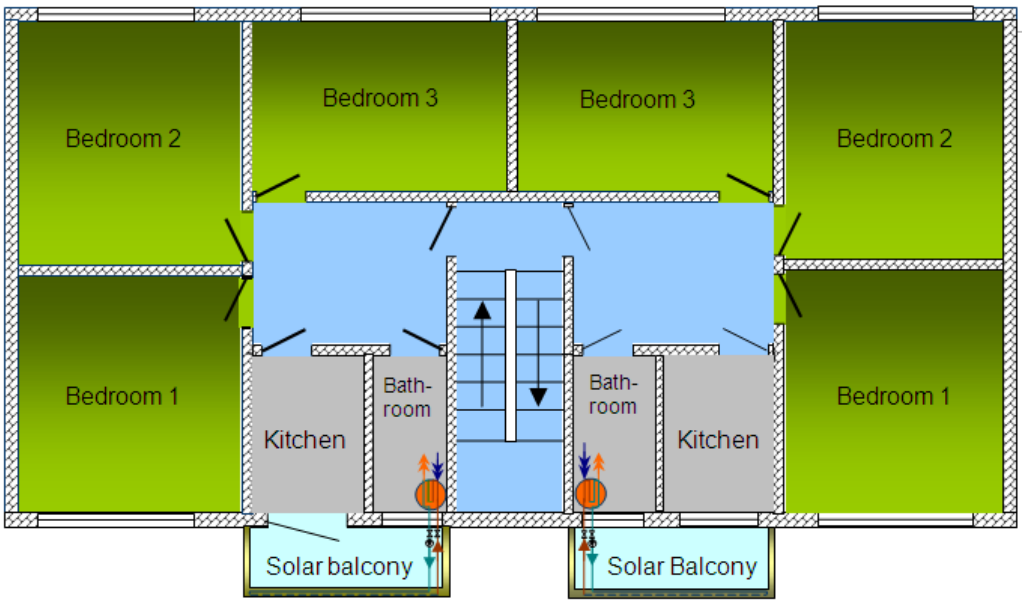

Fig. 3-4. Layout of the novel façade-based solar LHP water heating system in a typical flat.

3.2.2 Design principle of the system components

The components of the façade-based solar LHP water heating system, i.e., LHP, glass cover, backboard and water cycle, will be separately designed as follows.

1. LHP – wicked heat absorbing pipes (evaporator), headers, transport lines and heat exchanger (condenser)

(1) Wicked heat absorbing pipes

In order to design the components of the solar façade LHP system, the collector area should be initially determined from Table 3-1 [3.2] where each family member will require an evacuated-tube collector area of 1-1.2 m^2. Thus, the geometrical size and number of the heat absorbing pipes could be estimated in accordance to the collector area.

Table 3-1. Design size of the main components of the solar thermal system [3.2].

Components	**Dimensions**
Flat-plate collector	1.25-1.5 m^2 per person
Evacuated-tube collector	1-1.2 m^2 per person
Hot water tank	40-70 litres per m^2 collector surface
Heat exchanger	0.15-0.2 m^2 surface area per m^2 collector surface

For the material of the wicked heat absorbing pipes, the optical and thermal properties of the material should be considered, e.g., solar absorptivity, emissivity and thermal conductivity. Three commonly used materials are copper, aluminium and stainless steel owing to their high thermal conductance and ability to shape.

As to the wick, mesh screen and sintered powder are the two most popular types. The size of the wick should coordinate with the inner diameter and length of the heat absorbing pipes.

(2) Headers and transport lines

The diameter and length of the vapour/liquid headers and transport lines could be determined from the thermodynamic properties of the working fluid (primarily in the vapour phase) and the size of the wicked heat absorbing pipes. In addition, the length of the transport lines is also affected by the distance of the heat transfer fluid travelling between the interior and exterior of the building. When choosing the appropriate material of these two components, the capability of thermal conduction should be considered to reduce the temperature drop between the evaporator and condenser.

(3) Heat exchanger

The surface area of the flat-plate heat exchanger for the heat transfer from the condensing working fluid (vapour) to the service water could be theoretically sized according to Table 3-1 above, which will decide the length, width and height of the exchanger channels and number of exchanger plates. The

appropriate exchanger model could be selected from the SWEP Company, which is a professional heat exchanger manufacturer, with its associated size, material and working pressure.

2. Glass cover – evacuated tubes or single glazing

At present, evacuated tubes are the favoured glass cover in solar thermal systems. This is because the vacuum in the space between the two layers of glass tubes minimises the heat losses from the heat absorbing pipes to the surroundings, thus leading to a stable solar absorption of the system and protecting the inside capillary pipes. Single glazing could be selected as an alternative to the evacuated tubes, since it has similar optical and thermal properties to the evacuated tubes.

(1) Evacuated tubes

The geometrical size and number of tubes are related to the size and number of the heat absorbing pipes. Based on this, the evacuated tubes could be chosen from the market products with the specific outer/inner diameters and lengths. The tubes could be made of borosilicate which has high solar transmittance and U-value.

(2) Single glazing

The single glazing plate should cover the overall area of the solar collector. Thus, the length and height of the plate are decided from the size and number of the wicked heat absorbing pipes and the position of the vapour/liquid headers relative to the pipes. The plate can also be selected from a list of market products with specific geometrical, optical and thermal properties.

3. Backboard

The backboard should be large enough to fit over the heat absorbing pipes and headers, in order to realise the integration of the solar system's components to the building. However, its size is limited by the design and construction of the building wall. Many lightweight materials with low thermal conductance, such as expanded polystyrene and rigid polyurethane foams, are potential materials for the backboard.

4. Water cycle – water tank, electric pump and water pipelines

(1) Water tank

From Table 3-1 above, the tank can be primarily sized in its capacity where 40-70 litres correspond to 1 m^2 of the collector surface area. The tank model could be selected from the market according to the specific capacity. It should be mentioned that the tank of the specific size should be able to fit into the bathroom of the flat for hot water storage.

(2) Electric pump

The electric pump for the water circulation between the flat-plate heat exchanger and storage could be selected from the market products, based on the resistance losses (pressure head) occurring in the straight water pipelines and local fittings assembled in the water cycle system, and the volume rate of water flowing across the pump. In addition, the diameters of the inlet/outlet of the pump can be in accordance with the diameters of the water pipelines to simplify the construction procedure and save on the construction time.

(3) Water pipelines

The function of the water pipelines is to form the water cycle system by connecting the flat-plate exchanger, pump and tank. Hence, the length of the water piping is the distance the water needs to flow in the water cycle system. Its diameter is principally in relation to the water flow rate controlled by the pump.

3.3 Summary

This chapter introduced a novel façade-based solar LHP water heating system, which has the potential to overcome the difficulties associated with existing solar water heaters, thus creating a façade integrated, low cost, highly efficient and aesthetically appealing solar heating structure. This work is the basis of the whole research project, which raised the questions to be solved in the following chapters.

The proposed solar system could be divided into outdoor and indoor parts, which were connected via the transport lines. The outdoor part, consisting of the glass cover, wicked heat absorbing pipes and headers, was capable of absorbing solar energy and vaporising the heat transfer fluid. The indoor part was composed of the heat exchanger, tank, electric pump and water piping, which could transfer the absorbed heat to the service water through the condensation of the evaporated heat transfer fluid.

Based on a 3-member family flat in Beijing, China, the components of the system were initially designed from three aspects of size, quantity and material or selected from the market product catalogue. It should be addressed that the preliminary design of the system components could receive further optimisation through theoretical modelling and experimental testing in the following chapters.

Chapter 4: Operating limits of the façade-based solar LHP water heating system

4.0 Overview

In Chapter 3, the façade-based solar LHP water heating system was conceptually designed, based on a typical 3-member flat in Beijing, China. In accordance with the design parameters of the proposed system components, Chapter 4 will investigate the heat transfer performance of the LHP system by developing an analytical model.

In this chapter, six limits to the system's operation, i.e., capillary, entrainment, viscous, boiling, sonic and filled liquid mass, will be determined. Relations between the limits and several associated parameters, i.e., heat transfer fluid temperature, heat pipe diameter, wick type and height difference between the absorbing pipes array and exchanger, will be established through comprehensive analysis. The simulation results indicated that, under the fixed diameter of the mesh-screen wicked heat absorbing pipe of 16 mm, temperature of the heat transfer fluid of 60^{o}C and exchanger-to-pipes height difference of 1.5 m, the LHP device could achieve the heat transfer (capillary) limit of 2,362 W/m^2. This figure was higher than the maximum required heat transfer of 855 W/m^2, meaning that the LHP device could operate normally without restriction from the system structure.

This research will help determine the most appropriate material, geometrical size and quantity for the proposed system components and predict the steady-state performance of these components.

4.1 Characteristic parameters of the system components

Based on the solar system for practical application in the sample block of flats described in Chapter 3, the area of the solar collector was estimated at 3.48 m^2, and the geometrical, optical and thermal parameters of the main components of the proposed solar system are summarised from Table 4-1 to Table 4-3. These figures represent the design size of the solar system and input parameters of the theoretical model.

Table 4-1. Characteristic parameters of the wicked heat absorbing pipes.

Absorbers – copper (with coating of nickel)			
Emissivity	0.1	Absorptivity	0.98
Heat absorbing pipes – copper			
Number	55	Diameter (m)	0.013-0.019
Length (m)	1.5	Thermal conductivity (W/(m·K))	383.8
Two-layer mesh-screen wicks – copper			
Length (m)	1.5	Total thickness (m)	$7.5*10^{-4}$
Number of pores	9,158	Diameter of pores (m)	$3.86*10^{-5}$
Sintered-powder wicks – copper			
Length (m)	1.5	Total thickness (m)	$7.5*10^{-4}$
Porosity	0.64	Diameter of powder particles (m)	$4.47*10^{-5}$

Table 4-2. Geometrical parameters of the vapour/liquid headers and lines.

Vapour/liquid headers – copper			
Length (m)	3.73	Diameter (m)	0.08
Vapour/liquid lines – copper			
Length (m)	5	Diameter (m)	0.05

Table 4-3. Characteristic parameters of the flat-plate heat exchanger.

Flat-plate heat exchanger – SWEP model: B10T Stainless Steel Condenser			
Length (m)	0.119	Plate thickness (m)	$3*10^{-4}$
Height (m)	0.289	Number of plates	50
Inner width of one channel (m)	$1.94*10^{-3}$	Plate thermal conductivity (W/(m·K))	16.3

4.2 Mathematical analysis and computer model setup

The heat transport capacity of the LHP system is governed by six different limits, namely capillary, entrainment, viscous, boiling, sonic and filled liquid mass, which will be indicated as follows.

4.2.1 Capillary limit

Capillary limit is a parameter indicating the capability of the heat pipe wick in carrying liquid flow for heat transfer [4.1]. The larger the liquid volume carried with the wick, the higher the heat transport capacity the heat pipe would have.

In operation, capillary force, together with the gravity, will be greater than or equal to the flow resistances from the liquid and vapour. This could be expressed as:

$$\Delta P_{CL} + \Delta P_g \geq \Delta P_v + \Delta P_l \quad (4\text{-}1)$$

By solving the above equation, the capillary limit for heat pipe heat transfer relating to capillary pressure can be obtained.

The four items in the Eq. (4-1), ΔP_{CL}, ΔP_g, ΔP_v and ΔP_l, could be separately addressed below.

1. Capillary pressure

The capillary pressure ΔP_{CL} could be expressed as [4.1 ~ 4.2]:

$$\Delta P_{CL} = \frac{4\sigma}{D_w} \cos\theta \quad (4\text{-}2)$$

Where, D_w is the effective pore diameter of the wick and can be expressed as [4.2 ~ 4.3]:

For mesh-screen wick, $D_w = \frac{1}{N_{ms}}$ (4-3)

For sintered-powder wick, $D_w = 0.42 D_{sp}$ (4-4)

2. Gravitational pressure

ΔP_g is the gravitational pressure caused by the height difference between the top heat exchanger and bottom heat pipes array and could be expressed as [4.2]:

$$\Delta P_g = \rho_l g \left(\frac{H_{he}}{2} + H_{he-hp} + \frac{L_{hp}}{2}\right) \sin\Phi \quad (4\text{-}5)$$

3. Vapour pressure drop

Vapour pressure drop ΔP_v comprises four parts, i.e., vapour pressure drop in the heat absorbing pipes, vapour header, vapour line and heat exchanger, which could be written as follows:

$$\Delta P_v = \Delta P_{vhp} + \Delta P_{vvh} + \Delta P_{vvl} + \Delta P_{vhe} \tag{4-6}$$

The four items in the above equation can be calculated separately as below.

(1) Vapour pressure drop in heat absorbing pipes

For a single pipe, the vapour pressure drop can be expressed as [4.2, 4.4]:

$$\Delta P_{vhp} = \left(\frac{C_{hp}(f_{vhp}Re_{vhp})\mu_v}{2\pi\left(\frac{D_{hp}-2\delta_w}{2}\right)^4 \rho_v h_{fg}} \right) L_{hp} \left(\frac{Q_{CL}}{N_{hp}}\right) \tag{4-7}$$

Where, f_{vhp} and C_{hp} are the characteristic parameters of the pipe and could be determined as follows.

If $Re_{vhp} \leq 2{,}300$ and $M_{vhp} \leq 0.2$, $f_{vhp}Re_{vhp} = 16, C_{hp} = 1$ (4-8)

If $Re_{vhp} \leq 2{,}300$ and $M_{vhp} > 0.2$,

$$f_{vhp}Re_{vhp} = 16, C_{hp} = \left(1 + \left(\frac{\gamma-1}{2}\right) {M_{vhp}}^2\right)^{0.5} \tag{4-9}$$

If $Re_{vhp} > 2{,}300$ and $M_{vhp} \leq 0.2$, $f_{vhp}Re_{vhp} = 0.038, C_{hp} = {Re_{vhp}}^{0.75}$ (4-10)

If $Re_{vhp} > 2{,}300$ and $M_{vhp} > 0.2$,

$$f_{vhp}Re_{vhp} = 0.038, C_{hp} = \left(1 + \left(\frac{\gamma-1}{2}\right) {M_{vhp}}^2\right)^{0.5} {Re_{vhp}}^{0.75} \tag{4-11}$$

Of which, Re_{vhp} and M_{vhp} could be written as [4.5]:

$$Re_{vhp} = \frac{2}{\pi\left(\frac{D_{hp}-2\delta_w}{2}\right)\mu_v h_{fg}} \frac{Q_{CL}}{N_{hp}} \tag{4-12}$$

$$M_{vhp} = \frac{1}{\pi\left(\frac{D_{hp}-2\delta_w}{2}\right)^2 \rho_v h_{fg} (R_v T \gamma)^{0.5}} \frac{Q_{CL}}{N_{hp}} \tag{4-13}$$

γ is the ratio of specific heat and can be expressed as [4.6]:

$$\gamma = \frac{C_p}{C_v} \tag{4-14}$$

It should be noted that C_p and C_v are relatively constant within a moderate temperature range. Therefore, γ is regarded as constant and 1.28 for water vapour.

Since the absorbing pipes are arranged in parallel and each pipe is filled with the same amount of liquid mass, vapour pressure of a single pipe could represent the whole section pressure loss.

(2) Vapour pressure drop in vapour header/vapour line

The vapour pressure drop in the vapour header could be expressed as [4.1 ~ 4.2]:

$$\Delta P_{vvh} = \left(\frac{C_{vh}(f_{vvh} Re_{vvh}) \mu_v}{2\pi\left(\frac{D_{vh}}{2}\right)^4 \rho_v h_{fg}} \right) L_{vh} Q_{CL} \tag{4-15}$$

C_{vh} and ($f_{vvh}Re_{vvh}$) can be calculated using equations from Eq. (4-8) to Eq. (4-14).

The vapour pressure drop in the vapour line could be expressed by Eq. (4-15) similarly.

(3) Vapour pressure drop in heat exchanger

The vapour pressure drop in a single vapour channel of the condenser could be expressed as [4.1 ~ 4.2]:

$$\Delta P_{vhe} = \left(\frac{C_{he}(f_{vhe}Re_{vhe})\mu_v}{2\pi\left(\frac{D_{he}-2\delta_{lf}}{2}\right)^4 \rho_v h_{fg}} \right) \frac{H_{he}}{2} \left(\frac{Q_{CL}}{N_{he}/2-1} \right) \quad (4\text{-}16)$$

C_{he} and $(f_{vhe}Re_{vhe})$ can also be obtained from Eq. (4-8) to Eq. (4-14). δ_{lf} is the thickness of the liquid film on the surface of the heat exchanger plate, which can be expressed as [4.7]:

$$\delta_{lf} = \frac{0.93(v_l\mu_l)^{2/3}}{\sigma_l{}^{1/6}(\rho_l g)^{0.5}} \quad (4\text{-}17)$$

Since the vapour channels are in parallel and the same amount of vapour passes through each channel, the total vapour pressure drop could be represented by what happened in a single channel.

4. Liquid pressure drop

Similarly, liquid pressure drop ΔP_l comprises four parts, i.e., liquid pressure drop in the heat exchanger, liquid line, liquid header and absorbing pipes, which could be calculated using the following equation [4.2 ~ 4.3]:

$$\Delta P_l = \Delta P_{lhe} + \Delta P_{lll} + \Delta P_{llh} + \Delta P_{lhp} \quad (4\text{-}18)$$

The four items in the Eq. (4-18) are calculated separately as below.

(1) Liquid pressure drop in heat exchanger

Liquid pressure loss in a single channel of heat exchanger could be calculated by using the following equation:

$$\Delta P_{lhe} = \left(\frac{8\mu_l}{\pi\left(\frac{\delta_{lf}}{2}\right)^4 h_{fg}\rho_l} \right) \frac{H_{he}}{2} \left(\frac{Q_{CL}}{N_{he}/2-1} \right) \quad (4\text{-}19)$$

Similar to the vapour pressure, the liquid pressure drop in a single channel could represent the total liquid pressure drop within the heat exchanger.

(2) Liquid pressure drop in liquid line/liquid header

Liquid pressure losses in the liquid transport line ΔP_{lll} and liquid header ΔP_{llh} can also be expressed by the same form of equation as Eq. (4-19).

(3) Liquid pressure drop in heat absorbing pipes

The liquid pressure drop in one wicked absorbing pipe is caused by viscosity of water and wick and could be expressed as follow:

$$\Delta P_{lhp} = \left(\frac{\mu_l}{K\pi\left(\frac{\delta_w}{2}\right)^2 h_{fg}\rho_l} \right) L_w \left(\frac{Q_{CL}}{N_{hp}} \right) \tag{4-20}$$

Where, K is the permeability relating to different structures of wick, i.e., mesh screen and sintered powder, which is shown below.

For the mesh-screen wick, the permeability K can be expressed as:

$$K = \frac{{D_{ms}}^2 {\varphi_{ms}}^3}{122(1-\varphi_{ms})^2} \tag{4-21}$$

Where, φ_{ms} is the porosity of mesh-screen wick and can be expressed as:

$$\varphi_{ms} = 1 - \frac{1.05\pi N_{ms} D_{ms}}{4} \tag{4-22}$$

For the sintered-powder wick,

$$K = \frac{{D_{sp}}^2 {\varphi_{sp}}^3}{150\left(1-\varphi_{sp}\right)^2} \tag{4-23}$$

The total liquid pressure drop in the pipes is taken from the pressure drop in a single pipe, since the heat absorbing pipes are arranged in parallel and the same amount of liquid exists in each pipe.

4.2.2 Entrainment limit

Entrainment could result in the carrying over of liquid droplets with the vapour flow and could cause the reduction of heat transfer. In this case, owing to the separation of the liquid and vapour flows during transportation, an entrainment effect only occurs at the wicked absorbing pipes (evaporator) and heat exchanger (condenser). This would largely reduce the flow resistance of the system and provide the potentially enhanced system heat output, a unique merit possessed by the loop heat pipe over the conventional heat pipe [4.1, 4.3]. The entrainment limit in wicked heat absorbing pipes can be expressed as:

$$Q_{EL,hp} = \pi \left(\frac{D_{hp}-2\delta_w}{2}\right)^2 h_{fg} N_{hp} z \left(\frac{\sigma_v \rho_v}{D_w}\right)^{0.5} \quad (4\text{-}24)$$

The same equation will be applied to the case for the heat exchanger. The only difference is that the structural parameters of the heat absorbing pipes should be substituted by the corresponding parameters of the heat exchanger channels.

The smaller one of $Q_{EL,hp}$ and $Q_{EL,he}$ would represent the entrainment limit of the system as follows:

$$Q_{EL} = \left(Q_{EL,hp}, Q_{EL,he}\right)_{min} \quad (4\text{-}25)$$

4.2.3 Viscous limit

As the vapour viscosity is far less than the liquid viscosity, the limit due to the viscous effect would primarily occur at vapour phase flow. This limit reflects the difficulty of vapour flow when carrying a certain level of heat [4.2 ~ 4.3]. Viscous effects would apply to different parts of the system including the heat absorbing pipes, vapour adiabatic section such as vapour header and vapour line, and heat exchanger. The viscous limit for the absorbing pipes could be calculated using the following equation:

$$Q_{VL,hp} = \pi \left(\frac{D_{hp}-2\delta_w}{2}\right)^4 \frac{h_{fg} P_v \rho_v N_{hp} z}{16 \mu_v L_{hp}} \quad (4\text{-}26)$$

This equation will be applied to other parts of the system. The only difference is that D_{hp} and L_{hp} should be replaced by the characteristic parameters in relation to these parts of the system. A minimum of the above items would represent the viscous limit of the whole system, which could be written as:

$$Q_{VL} = \left(Q_{VL,hp}, Q_{VL,vh}, Q_{VL,vl}, Q_{VL,he}\right)_{min} \tag{4-27}$$

4.2.4 Boiling limit

Boiling limit represents the extremely high temperature operating conditions at which the liquid within a certain area of the wick (or wall) is dried out, and the wicked heat absorbing pipes and heat exchanger stop working. The boiling limit for the absorbing pipes could be expressed as follows [4.2 ~ 4.3]:

$$Q_{BL,hp} = \frac{2\pi L_{hp}\lambda_w T N_{hp} z}{h_{fg}\rho_v \ln\left(\frac{D_{hp}}{D_{hp}-2\delta_w}\right)}\left(\frac{2\sigma_v}{r_b} - \Delta P_{CL,max}\right) \tag{4-28}$$

It should be noted that λ_w is the effective thermal conductivity of the wick, as the particles of wick are in contact but not tightly packed [4.1].

The same equation could be used to calculate the boiling limit for the heat exchanger. The equivalent diameter of the exchanger channel and thickness of the liquid film adhered on the exchanger plate should be used to replace D_{hp} and δ_w.

The smaller in the $Q_{BL,hp}$ and $Q_{BL,he}$ would represent the boiling limit of the loop heat pipe system as shown below:

$$Q_{BL} = \left(Q_{BL,hp}, Q_{BL,he}\right)_{min} \tag{4-29}$$

4.2.5 Sonic limit

If a heat pipe generates an extremely high vapour speed, e.g., as high as sonic or supersonic level, the heat pipe would be choked which would limit its further heat take-up. This limitation is called the sonic limit, which may happen

at the places where vapour exists. For this application, the limitation may occur at the absorbing pipes, adiabatic section including vapour header and vapour line, and heat exchanger. The sonic limit for the absorbing pipes could be expressed as follows [4.2 ~ 4.3]:

$$Q_{SL,hp} = \pi \left(\frac{D_{hp}-2\delta_w}{2}\right)^2 \rho_v h_{fg} N_{hp} z \left(\frac{R_v T \gamma}{2(\gamma+1)}\right)^{0.5} \quad (4\text{-}30)$$

The sonic limit for other parts of the system could be calculated in a similar way, but the associated parameters should be used to replace D_{hp} and δ_w in Eq. (4-30).

The minimum of the above items related to different parts of the system would represent the sonic limit of the whole system, and this could be expressed as follows:

$$Q_{SL} = \left(Q_{SL,hp}, Q_{SL,vh}, Q_{SL,vl}, Q_{SL,he}\right)_{min} \quad (4\text{-}31)$$

4.2.6 Filled liquid mass limit

The heat transport capacity of the loop heat pipe system is also governed by filled liquid mass, which, owing to the influence of gravity, is a term used to describe the limitation of the mass of the working fluid charged into the system. The liquid mass limit for the wicked absorbing pipes could be expressed as [4.1, 4.8]:

$$Q_{FL,hp} = \left(\frac{m}{xL_w}\right)^3 \frac{g h_{fg}}{3\pi^2 \mu_l \rho_l {D_w}^2 {N_{hp}}^2} \quad (4\text{-}32)$$

This equation can also be utilised in other liquid parts of the system, i.e., heat exchanger, liquid line and liquid header. In that case, L_w and D_w should be replaced by the characteristic parameters associated with these parts. The minimum of the above items would represent the liquid mass limit of the whole system as shown below:

$$Q_{FL} = \left(Q_{FL,hp}, Q_{FL,lh}, Q_{FL,ll}, Q_{FL,he}\right)_{min} \quad (4\text{-}33)$$

4.2.7 Algorithm for the computer model setup

The six operating limits were calculated, and the smallest of these limits was identified as the governing limit of the loop heat pipe system. The algorithm for the modelling setup in the FORTRAN 95 program is indicated as follows:

1. Given the LHP system structure, the data relating to the system configuration could be obtained.
2. Assuming the operating temperature of the loop heat pipe system, the thermal property of the heat transfer fluid could be obtained.
3. Running an iteration to work out capillary limit (Q_{CL}):
   (1) Assuming an initial value of Q_{CL};
   (2) Capillary pressure ΔP_{CL} can be obtained using Eq. (4-2) to Eq. (4-4);
   (3) Gravitational pressure ΔP_g can be obtained using Eq. (4-5);
   (4) Vapour pressure drop ΔP_v can be obtained using Eq. (4-6) to Eq. (4-17);
   (5) Liquid pressure drop ΔP_l can be obtained using Eq. (4-18) to Eq. (4-23);
   (6) If $((\Delta P_{CL}+\Delta P_g)–(\Delta P_v+\Delta P_l))/(\Delta P_{CL}+\Delta P_g) < -0.5\%$ (error allowance), then decrease Q_{CL} by 10 and return to step (2) for recalculation;
   (7) If $((\Delta P_{CL}+\Delta P_g)–(\Delta P_v+\Delta P_l))/(\Delta P_{CL}+\Delta P_g) > 0.5\%$ (error allowance), then increase Q_{CL} by 10 and return to step (2) for recalculation;
   (8) If $-0.5\% \leq ((\Delta P_{CL}+\Delta P_g)–(\Delta P_v+\Delta P_l))/(\Delta P_{CL}+\Delta P_g) \leq 0.5\%$, heat balance of the whole system is achieved, and real value of Q_{CL} can be obtained.
4. Calculating the entrainment limits in relation to the wicked heat absorbing pipes and heat exchanger and taking the smaller one as the entrainment limit of the system (by Eq. (4-24) and Eq. (4-25)).
5. Calculating the viscous limits in relation to different parts of the system and taking the smallest one as the viscous limit of the whole system (by Eq. (4-26) and Eq. (4-27)).

6. Calculating the boiling limits in relation to the wicked heat absorbing pipes and heat exchanger and taking the smaller one as the boiling limit of the whole system (by Eq. (4-28) and Eq. (4-29)).
7. Calculating the sonic limits relating to different parts of the system and taking the smallest one as the sonic limit of the whole system (by Eq. (4-30) and Eq. (4-31)).
8. Calculating the filled liquid mass limits for different parts of the system and taking the smallest one as the limit for the whole system (by Eq. (4-32) and Eq. (4-33)).
9. Taking the minimum of the above six limits as the governing limit of the whole system.
10. Program stops.

4.3 Analytical results and discussions

The results obtained from running the above analytical model will be used to analyse the relationship between the limits and a number of heat pipe operational parameters, i.e., temperature of heat transfer fluid, inner diameter of heat absorbing pipe, wick type and height difference between the absorber and condenser. When the heat transfer fluid temperature is controlled at 60^{o}C, the wick is made of mesh screen, the inner diameter of heat pipe is 16 mm, and the height difference between the condenser and absorber is 1.5 m, the limit of heat transport capacity is 2,362 W/m^2 (limited by capillary). This figure is larger than the maximum solar radiation received in the south-orientated façade in Beijing, i.e., 855 W/m^2 [4.9]. This means that the system could perform effectively in operation with no constraints imposed by system configuration.

4.3.1 The impact of the heat transfer fluid temperature

In the case of the mesh-screen wicked heat absorbing pipes with diameters of 16 mm and an exchanger-to-pipes height difference of 1.5 m, analysis is carried out using the above analytical model to investigate the heat transfer capacity (operating limits) of the loop heat pipe under different temperatures of heat transfer fluid across the loop. This develops a profile showing the variations of six limits with heat transfer fluid temperatures as in Table 4-4.

Table 4-4. Variations of the six limits against the heat transfer fluid temperatures.

Fluid temp. (^oC)	**Capillary limit (W/m^2)**	**Entrainment limit (kW/m^2)**	**Sonic limit (kW/m^2)**	**Boiling limit (kW/m^2)**	**Viscous limit (MW/m^2)**	**Filled liquid mass limit (GW/m^2)**
30	1,426	3.6	8.2	2,222	0.02	17.16
40	1,778	4.5	13.8	1,367	0.36	19.55
50	2,025	6.1	26.4	742	1.25	22.87
60	2,362	7.2	39.2	518	2.61	25.34
70	2,613	8.8	60.5	347	6.44	28.57
80	2,941	9.9	81.9	264	11.71	31.33
90	3,219	12	126	175	27.06	34.89

From Table 4-4, it is found that the capillary, entrainment, sonic, viscous and filled liquid mass limits increase with the temperature increasing; however, the boiling limit presents a downward trend when the temperature goes up. The capillary limit is the governing limit of the whole system as it is the minimum of the six limits.

The variation of capillary limit with the temperature of heat transfer fluid is also presented in Fig. 4-1. Higher temperature leads to a higher rate of liquid evaporation, and thus the heat transport capacity of the system increases. The heat transfer fluid temperature of 60^oC enables 2,362 W/m^2 of the governing limit, higher than the maximum heat transfer required from Beijing weather conditions.

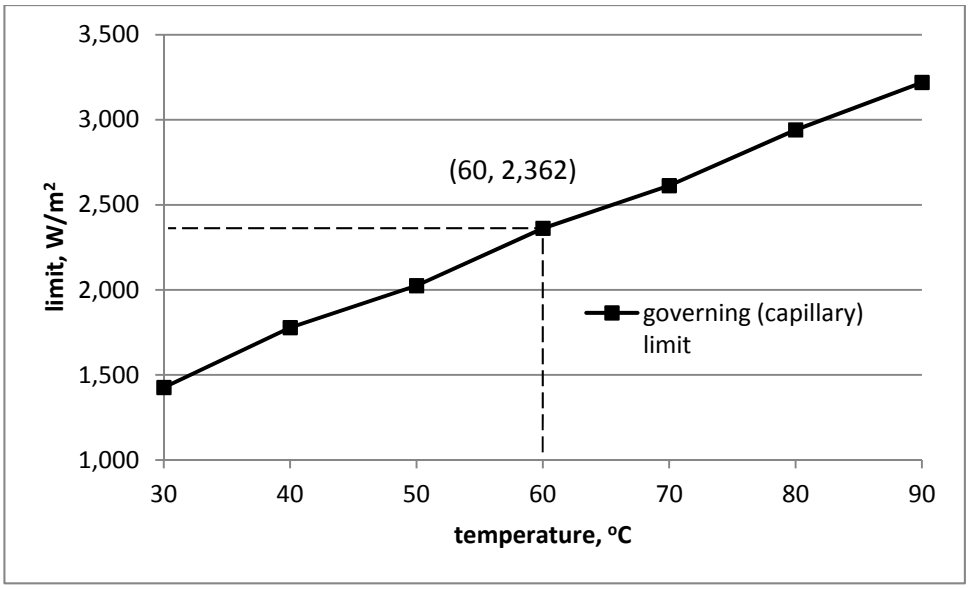

Fig. 4-1. Variation of the capillary limit with the heat transfer fluid temperature.

The entrainment limit occurs in the wicked heat pipes. An increasing temperature would lead to an increased vapour flow rate, which would cause lower shear force between the vapour and liquid layers. Therefore, the entrainment limit would be higher.

Increasing temperatures would cause a higher circulation rate of vapour flow across the loop system. As a result, the sonic limit of the system would be higher.

Heat transfer in heat absorbing pipes dominates the boiling limit. With the temperature increasing, the vapour evaporation rate would be increased. This would cause a danger of dry-out of the heat pipe wall, and, as a result, the boiling limit would drop.

Viscous limit occurs in the vapour transport line. It is dependent upon Reynolds number, which relates to the thermodynamic properties of working fluid. When the temperature is raised, Reynolds number grows; therefore, the viscous limit would be higher.

4.3.2 The impact of the heat absorbing pipe diameter

Fixing the heat transfer fluid temperature at 60^{o}C, choosing mesh screen as the wick and keeping the exchanger-to-pipes height difference at 1.5 m, the variations of the limits against the pipe inner diameters are investigated, and the results are presented in Table 4-5.

Table 4-5. Variations of the six limits against the heat absorbing pipe diameters.

Pipe diameter (m)	**Capillary limit (W/m^2)**	**Entrainment limit (kW/m^2)**	**Sonic limit (kW/m^2)**	**Boiling limit (kW/m^2)**	**Viscous limit (MW/m^2)**	**Filled liquid mass limit (GW/m^2)**
0.013	1,901	4.8	39.2	416	1.34	25.31
0.014	2,056	5.6	39.2	450	1.87	25.32
0.015	2,210	6.4	39.2	484	2.54	25.33
0.016	2,362	7.2	39.2	518	2.61	25.34
0.017	2,516	8.1	39.2	552	2.61	25.35
0.018	2,669	9.1	39.2	586	2.61	25.36
0.019	2,822	10.1	39.2	621	2.61	25.37

From Table 4-5, it is found that the capillary, entrainment, boiling and filled liquid mass limits increase with the diameter increasing. However, the viscous limit increases first and then remains static. The sonic limit is maintained constantly. The governing limit is the capillary limit, which is the minimum of the six limits.

Variation of the governing limit (capillary) against pipe diameter is shown in Fig. 4-2. A linear relation between the capillary and diameter is found. A larger diameter leads to a higher capillary-governed heat transfer owing to the increased space for vapour transportation. The suggested heat pipe diameter is 16 mm with the achieved heat transfer capacity of 2,362 W/m^2.

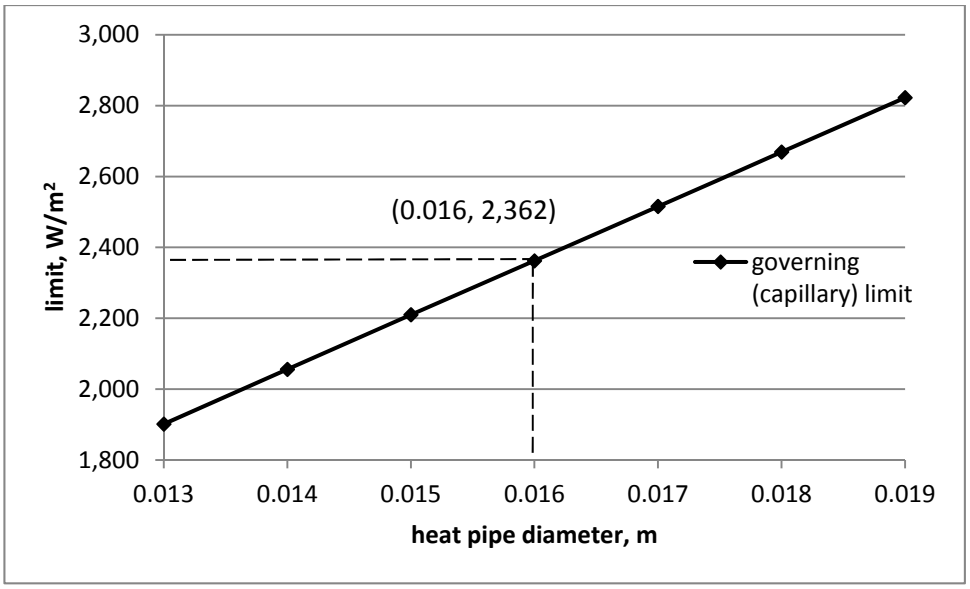

Fig. 4-2. Variation of the capillary limit with the heat absorbing pipe diameter.

The larger the heat pipe diameter, the lower the speed of vapour flow across the loop, which reduces the force between the vapour and liquid inside the heat absorbing pipes. Therefore, the entrainment limit is increasing.

The sonic limit occurs in the heat exchanger, which is not related to the diameter of the pipe. This explains the stability of the sonic limit against the heat pipe diameter.

Increasing the heat pipe diameter would enable a lower speed of vapour flowing in the loop, which would tend to generate a higher boiling limitation.

The viscous limit for the wicked pipes is the smallest item in comparison with the other parts of the system. Increasing the heat pipe diameter leads to increased Reynolds number, and hence the system's viscous limit would be higher. When the heat pipe diameter increases to 0.016 m, the viscous limit for the heat exchanger represents the viscous limitation of the whole system, which is not related to the heat pipe diameter.

Increasing the heat pipe diameter would also allow more vapour to be generated and thus more liquid to be filled into the pipe. This will allow an increased filled liquid limitation.

4.3.3 The impact of the wick structure

Keeping the heat pipe diameter and exchanger-to-pipes height difference the same and fixing the heat transfer fluid temperature at 60^{o}C, the impact of the wick structure on the heat transport capacity (operating limits) is investigated using the previously addressed analytical model. Two types of wicks, i.e., (copper) mesh screen and sintered powder, are considered. From Table 4-6, the results indicate that mesh screen achieves a higher heat transport capacity and hence is the preferred choice over the sintered powder. For both wicks, capillary is the governing limit to heat transfer, and the values are dependent upon the structures of the wicks. The other limits, namely entrainment, viscous, sonic, boiling and filled liquid mass, remain the same for both wick structures. This phenomenon could be explained by the definition of each limit: capillary is the term indicating the wick's capability for dragging and lifting up liquid, while the other limits are not directly related to the structure of the wick.

Table 4-6. Comparison of the limits between the mesh-screen and sintered-powder wicks.

Wick types	**Capillary limit (W/m^2)**	**Entrainment limit (kW/m^2)**	**Sonic limit (kW/m^2)**	**Boiling limit (kW/m^2)**	**Viscous limit (MW/m^2)**	**Filled liquid mass limit (GW/m^2)**
Mesh screen	2,362	7.2	39.2	518	2.61	25.34
Sintered powder	1,665	7.2	39.2	518	2.61	25.34

4.3.4 The impact of the exchanger-to-pipes height difference

For the loop heat pipe system with the mesh-screen wick, absorbing pipe diameter of 16 mm and heat transfer fluid temperature of 60^{o}C, the impact of the exchanger-to-pipes height difference on the heat transport capacity (operating limits) is investigated using the above analytical model, and the results are presented in Table 4-7.

Table 4-7. Variations of the six limits with the height difference between the heat absorbing pipes and exchanger.

Height difference (m)	**Capillary limit (W/m^2)**	**Entrainment limit (kW/m^2)**	**Sonic limit (kW/m^2)**	**Boiling limit (kW/m^2)**	**Viscous limit (MW/m^2)**	**Filled liquid mass limit (GW/m^2)**
1.2	2,088	7.2	39.2	518	2.61	25.34
1.3	2,180	7.2	39.2	518	2.61	25.34
1.4	2,272	7.2	39.2	518	2.61	25.34
1.5	2,362	7.2	39.2	518	2.61	25.34
1.6	2,454	7.2	39.2	518	2.61	25.34
1.7	2,546	7.2	39.2	518	2.61	25.34
1.8	2,637	7.2	39.2	518	2.61	25.34

Table 4-7 indicates that the capillary is the governing limit which increases with the increasing of the exchanger-to-pipes height difference, whereas the other limits remain unchanged.

Variation of the capillary limit as the governing limit of the system against exchanger-to-pipes height difference is presented in Fig. 4-3. A linear relation is found, and the rising height difference leads to an increase of heat transfer capacity owing to the effect of gravity. A higher height difference leads to a higher gravitational force, which enhances the capability of the system in transporting liquid flow and thus increases the heat flux of the system. The appropriate height difference between the absorber and heat exchanger would be 1.5 m with an achieved heat transport capacity of 2,362 W/m^2. Height difference has no impact on the other five limits, and thus discussion into their interrelations could be omitted.

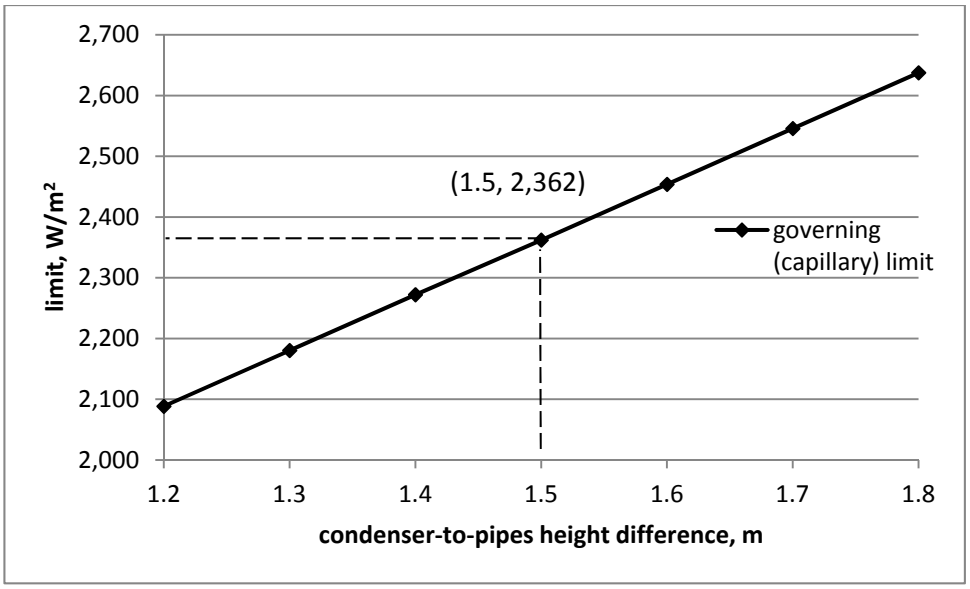

Fig. 4-3. Variation of the capillary limit with the height difference between the heat absorbing pipes and exchanger.

4.4 Summary

In this chapter, an analytical model for the novel solar LHP system was developed to investigate its heat transport capacity (operating limits). The results of the investigation work will help identify the appropriate material and size of the system components and predict the heat transfer performance of the initially designed system. The optimised system structure will be further analysed in its dynamic performance.

Six potential limits for the operation of the LHP, i.e., capillary, entrainment, sonic, boiling, viscous and filled liquid mass, were considered. The capillary limit is the original limit analysed to determine the temperature of the heat transfer fluid. The other five limits will be calculated in accordance with the capillary limit. The minimum of the six limits will be treated as the governing limit of the whole system, which will affect the operation of the system. An algorithm illustrated the process of model setup. Given the geometrical parameters of the LHP components, variations of the heat transport limits with several structural and operational system parameters, including temperature of heat transfer fluid, heat pipe diameter, wick structure and exchanger-to-pipes height difference, were investigated.

The results indicated that the capillary limit was the governing limit of the system heat transfer. Mesh-screen wick could achieve a higher heat transfer than sintered power and hence was a preferred choice for the system configuration. The system should be operated at a consistently high temperature, in order to achieve enhanced system performance. Similarly, the diameter of the absorbing pipe should be relatively large, and the exchanger-to-pipes height difference should be a large figure.

For a solar water heating application in Beijing requiring the maximum heat transfer of 855 W/m^2, the loop heat pipe system had sufficient capacity in transporting heat from the outside to the inside of the building. On condition that the absorbing pipes were fitted with mesh-screen wicks, their diameters were fixed to 16 mm, the temperature of heat transfer fluid was controlled at 60^oC, and the exchanger-to-pipes height difference was at 1.5 m, the system would achieve the heat transport capacity of 2,362 W/m^2 which was higher than the required heat transfer. This setting could be considered as the preferred system configuration and operating conditions, when it was applied to solar water heating systems in buildings in Beijing, China.

Chapter 5: Theoretical analysis and computer simulation of the dynamic performance of the façade-based solar LHP water heating system

5.0 Overview

Chapter 4 analysed six operating limits of the LHP device by setting up a mathematical model. As a logic extension of Chapter 4, Chapter 5 will investigate the dynamic performance of the loop heat pipe solar system by developing a computer model and conducting computer simulations.

In this chapter, an analytical model for the dynamic performance of the solar façade LHP system will be developed, taking into account the heat balances occurring in different parts of the proposed system, i.e., solar collector, heat pipes loop, heat exchanger and tank. To validate the analytical model, two previously published papers with theoretical and experimental data will be used to examine the accuracy of this model predication under the same weather and operating conditions with the same system structure. It was found that an agreement could be achieved between the results of the established modelling and previous works within a reasonable error limit. The differences may be due to the predications of the thermal conductance and internal heat transfer coefficients, and inaccuracy in the calculations of the heat exchange with the ambient by natural convection.

This research will help identify the behaviour of the solar system, indicate the preferred choice of the system configurations and predict the performance of the solar system over a long operating period.

5.1 Mathematical analysis of thermal processes and computer model setup

5.1.1 Thermo-fluid principle and mathematical equations

Heat transfer occurring in a solar LHP water heating system involves four processes, i.e., converting solar radiation into heat received by the solar collector $Q_{ab}(t)$, transporting the absorbed heat from the collector to the heat exchanger via evaporation and condensation of the heat transfer fluid in the heat pipes loop $Q_{loop}(t)$, transferring the heat from the exchanger to the passing

water $Q_{he}(t)$, and transporting the passing-water-carried-heat into the water tank. These processes are interconnected and time-relevant and will finally achieve a balance.

Assuming t represents a time point during the system's operation which, with the unit of seconds, starts from a reference point of 0 (referring to the time of sunrise), and dt stands for an infinitesimal increase of time t, the heat balance of the LHP system could be expressed as:

$$\int_t^{t+\Delta t} Q_{ab}(t)dt = \int_t^{t+\Delta t} Q_{loop}(t)dt = \int_t^{t+\Delta t} Q_{he}(t)dt = \int_t^{t+\Delta t} Q_{tk}dt \qquad (5\text{-}1)$$

Given a short time interval of Δt, e.g., time for the water to run a single circulation from leaving the tank, crossing the exchanger and back to the tank, Eq. (5-1) could be simplified as:

$$Q_{ab,ave}\Delta t = Q_{loop,ave}\Delta t = Q_{he,ave}\Delta t \qquad (5\text{-}2)$$

Assuming Q varies linearly during the short time interval,

$$Q_{ab,ave} = \frac{Q_{ab}(t)+Q_{ab}(t+\Delta t)}{2} \qquad (5\text{-}3)$$

$$Q_{loop,ave} = \frac{Q_{loop}(t)+Q_{loop}(t+\Delta t)}{2} \qquad (5\text{-}4)$$

$$Q_{he,ave} = \frac{Q_{he}(t)+Q_{he}(t+\Delta t)}{2} \qquad (5\text{-}5)$$

The three items in the Eq. (5-1), $Q_{ab}(t)$, $Q_{loop}(t)$ and $Q_{he}(t)$, could be separately illustrated as follows.

A. Conversion of the solar radiation into the absorbed heat

During operation, solar energy striking the collector enters the inner chambers of the pipes array across the glass cover (double-walled evacuated tubes or single-glazing plate) and is absorbed by the coated surface of the collector. Part

of the absorbed energy will be dissipated back to the ambient owing to the established temperature difference between the collector surface and surroundings, whilst the remaining energy will be absorbed by the heat pipe fluid and convert the fluid to vapour. This process is illustrated by Fig. 5-1 (a) for the heat absorbing pipes covered with evacuated tubes or (b) with single glazing, which could be expressed as:

$$Q_{ab}(t) = Q_{en}(t) - Q_{loss}(t) \tag{5-6}$$

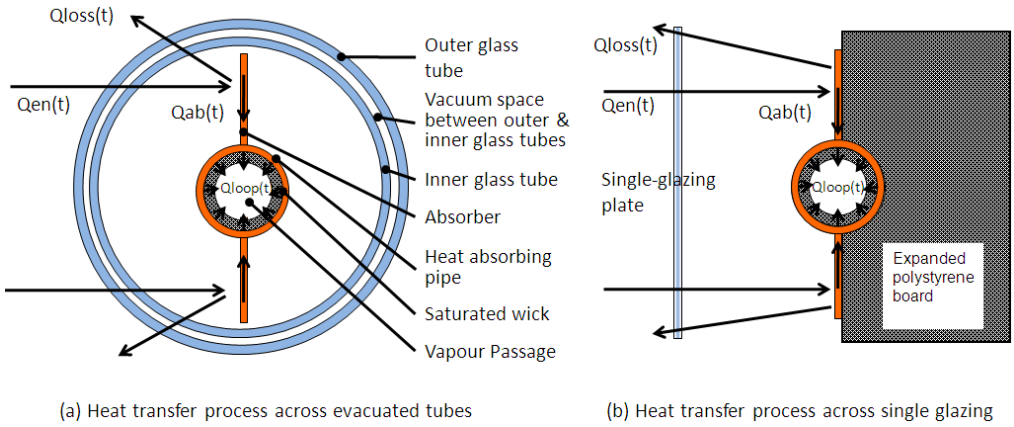

Fig. 5-1. Schematic of the heat transfer within the absorber surface across (a) evacuated tubes or (b) single glazing.

In accordance with the total collector area of A_c, the solar energy entering the inner chamber and being absorbed by the coated surface $Q_{en}(t)$ could be calculated from Eq. (5-7) for the LHP system with the evacuated tubes or Eq. (5-8) for the single glazing [5.1].

$$Q_{en}(t) = \tau_{go}\tau_{gi}\alpha_c A_c I(t) \tag{5-7}$$

$$Q_{en}(t) = \tau_g \alpha_c A_c I(t) \tag{5-8}$$

Whereby, I(t) is the instant solar radiation on the collector surface depending upon the time and geographical location of the site. In practical applications, the hour-based solar data at various geographical locations could be extracted from the EnergyPlus database [5.2]. For instant figures, the interpolation

approach could be applied. This method will lead to the resolution of the instant solar radiation based on the solar data at the hours prior to and after the referred time point.

It should also be mentioned that the transmittance of the glass cover τ_g varies with the incidence angle of the sunlight. In this case, a maximum value of the transmittance is employed.

Assuming the collector surface with the temperature of $T_c(t)$, the heat dispersion $Q_{loss}(t)$ from the absorbers to the ambient across the evacuated tubes could be expressed as [5.3]:

$$Q_{loss}(t) = Q_{loss}\big(T_c(t), T_{amb}(t)\big) = \frac{T_c(t)-T_{amb}(t)}{R_{c-gi}(t)+R_{gi}+R_{gi-go}(t)+R_{go}+R_{go-amb}(t)} \quad (5\text{-}9)$$

$$R_{c-gi}(t) = \frac{1}{h_{air}\left(\frac{A_c+A_{gi}N_g}{2}\right)} + \frac{\frac{1}{\varepsilon_c}+\frac{1}{\varepsilon_{gi}}-1}{\sigma\big(T_c(t)+T_{gi}(t)\big)\big(T_c(t)^2+T_{gi}(t)^2\big)}\frac{1}{A_c} \quad (5\text{-}10)$$

$$R_{gi} = \frac{\delta_{gi}}{\lambda_{gi}A_{gi}N_g} \quad (5\text{-}11)$$

$$R_{gi-go}(t) = \frac{\frac{1}{\varepsilon_{gi}}+\frac{1}{\varepsilon_{go}}-1}{\sigma\big(T_{gi}(t)+T_{go}(t)\big)\big(T_{gi}(t)^2+T_{go}(t)^2\big)}\frac{1}{A_{gi}N_g} \quad (5\text{-}12)$$

$$R_{go} = \frac{\delta_{go}}{\lambda_{go}A_{go}N_g} \quad (5\text{-}13)$$

$$R_{go-amb}(t) = \left(\frac{1}{h_{amb}} + \frac{1}{\sigma\varepsilon_{go}\big(T_{go}(t)+T_{amb}(t)\big)\big(T_{go}(t)^2+T_{amb}(t)^2\big)}\right)\frac{1}{A_{go}N_g} \quad (5\text{-}14)$$

Similarly, the heat dispersion from the absorbers to the ambient across a single layer of flat-plate glass cover could be expressed as:

$$Q_{loss}(t) = Q_{loss}\big(T_c(t), T_{amb}(t)\big) = \frac{T_c(t)-T_{amb}(t)}{R_{c-g}(t)+R_g+R_{g-amb}(t)+R_{sb}+R_{bb}} \quad (5\text{-}15)$$

$$R_{c-g}(t) = \frac{1}{h_{air}\left(\frac{A_c+A_g}{2}\right)} + \frac{\frac{1}{\varepsilon_c}+\frac{1}{\varepsilon_g}-1}{\sigma\left(T_c(t)+T_g(t)\right)\left(T_c(t)^2+T_g(t)^2\right)}\frac{1}{A_c} \quad (5\text{-}16)$$

$$R_g = \frac{\delta_g}{\lambda_g A_g} \quad (5\text{-}17)$$

$$R_{g-amb}(t) = \left(\frac{1}{h_{amb}} + \frac{1}{\sigma\varepsilon_g\left(T_g(t)+T_{amb}(t)\right)\left(T_g(t)^2+T_{amb}(t)^2\right)}\right)\frac{1}{A_g} \quad (5\text{-}18)$$

$$R_{sb} = \frac{\delta_{sb}}{\lambda_{sb} A_{sb}} \quad (5\text{-}19)$$

$$R_{bb} = \frac{\delta_{bb}}{\lambda_{bb} A_{bb}} \quad (5\text{-}20)$$

In terms of the ambient temperature, the hour-based figures could also be extracted from the EnergyPlus database [5.2]. For instant temperature, the interpolation approach is applied. This will lead to the resolution of the instant ambient temperature based on the temperature data at the hours prior to and after the referred time point.

B. Transportation of the absorbed heat from the solar collector to the heat exchanger

The absorbed heat $Q_{ab}(t)$ should be immediately taken away from the absorbers by using the heat pipes loop as indicated in Fig. 5-2. This could be achieved by liquid evaporation in the heat absorbing section and vapour condensation on the heat exchanger plate surface. This part of heat $Q_{loop}(t)$ could be written as [5.1, 5.3]:

$$Q_{loop}(t) = \frac{T_c(t)-T_{he}(t)}{R_{hp}+R_w(t)+R_v(t)+R_l(t)+R_{he}} \quad (5\text{-}21)$$

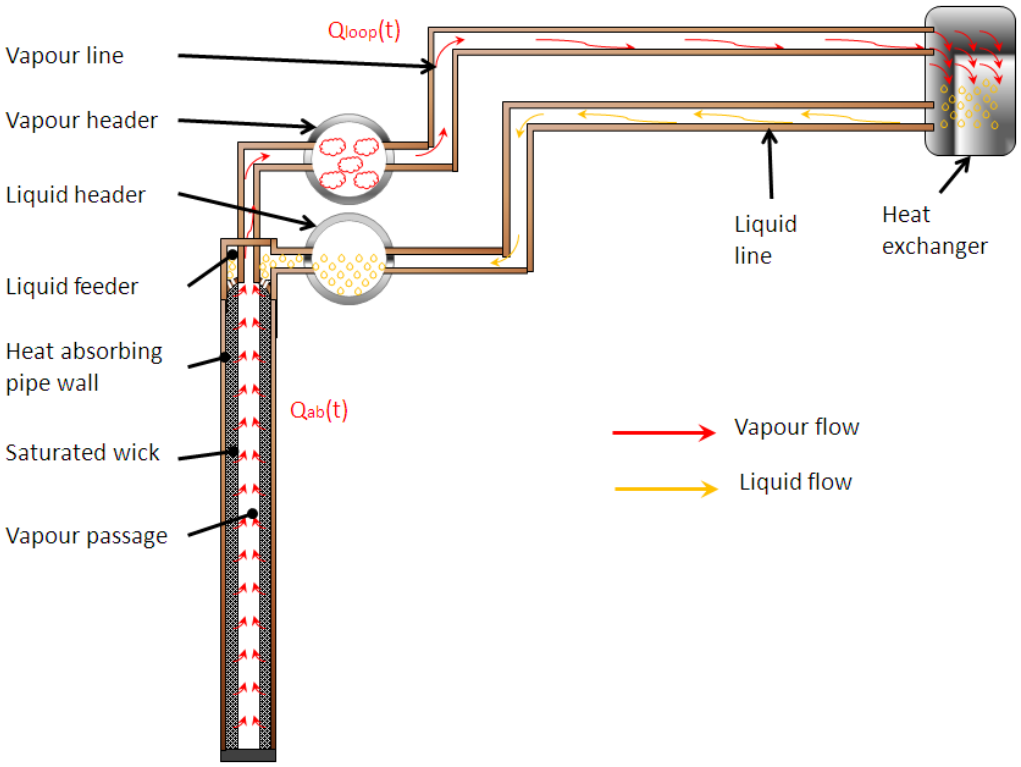

Fig. 5-2. Schematic of the heat transfer between the heat absorbing pipes and heat exchanger.

This process involves several thermal resistances, which are the factors impacting on the magnitude of the loop heat transfer and could be illustrated separately as follows [5.1, 5.4]:

1. Absorbing pipes wall resistance

$$R_{hp} = \frac{\ln\left(\frac{D_{hpo}}{D_{hpi}}\right)}{2\pi L_{hp}\lambda_{hp}N_{hp}} \tag{5-22}$$

2. Saturated wick resistance

$$R_w(t) = R_w\left(\lambda_w(t)\right) = \frac{\ln\left(\frac{D_{hpi}}{D_{hpi}-2\delta_w}\right)}{2\pi L_w\lambda_w(t)N_{hp}} \tag{5-23}$$

$\lambda_w(t)$ is the effective thermal conductivity of the wick depending upon the porosity of the wick and saturation property of the working fluid. For a two-layer mesh-screen wick [5.5],

$$\lambda_w(t) = \lambda_w\big(\lambda_l(t)\big) = \lambda_l(t)\frac{(\lambda_l(t)+\lambda_s)-(1-\varphi)(\lambda_l(t)-\lambda_s)}{(\lambda_l(t)+\lambda_s)+(1-\varphi)(\lambda_l(t)-\lambda_s)} \tag{5-24}$$

φ is the porosity of the mesh-screen wick, which can be expressed as [5.5]:

$$\varphi = 1 - \frac{1.05\pi N_w D_w}{4} \tag{5-25}$$

The thermal conductivity of the saturated water deposited within the voids of the mesh-screen wick is a temperature-related parameter and could be extracted from the Property Table of the Water/Steam [5.6] by using the interpolation approach. At a certain time point, there is a corresponding temperature that could result in a specific thermal conductivity of the water.

3. Vapour flow resistance

$$R_v(t) = R_{vhp}(t) + R_{vvh}(t) + R_{vvl}(t) + R_{vhe}(t) \tag{5-26}$$

(1) Vapour flow resistance in the heat absorbing pipes

$$R_{vhp}(t) = \frac{\Delta P_{vhp}(t) T_v(t)}{\rho_v(t)\dot{m}_v(t)h_{fg}(t)^2} \tag{5-27}$$

The vapour density $\rho_v(t)$ and latent heat $h_{fg}(t)$ are temperature-related parameters and thus functions of the operating time. Figures of $\rho_v(t)$ and $h_{fg}(t)$ could be extracted from the Property Table of the Water/Steam [5.6] by using the interpolation approach.

The vapour mass flow rate could be expressed as:

$$\dot{m}_v(t) = \dot{m}_v\left(Q_{ab}(t), h_{fg}(t)\right) = \frac{Q_{ab}(t)}{h_{fg}(t)} \tag{5-28}$$

In operation, the vapour will not fully occupy the loop space, and hence a parameter called vapour void fraction is defined [5.7]:

$$\varphi_{hp}(t) = \frac{t*\dot{m}_v(t)}{\pi N_{hp}\left(\frac{D_{hpi}-2\delta_w}{2}\right)^2 L_{hp}\rho_v(t)} \tag{5-29}$$

Since the heat absorbing pipes are arranged in parallel, there will be several parallel vapour flow streams each within an absorbing pipe. The pressure loss of the vapour is inversely proportional to the number of the absorbing pipes and expressed as:

$$\Delta P_{vhp}(t) = \Delta P_{vhp}\left(\dot{m}_v(t), \rho_v(t)\right) = \frac{\dot{m}_v(t)^2}{8\rho_v(t)\left(\frac{D_{hpi}-2\delta_w}{2}\right)^4 N_{hp}} \tag{5-30}$$

(2) Vapour flow resistance in vapour header/vapour line

$$R_{vvh}(t) = \frac{\Delta P_{vvh}(t)T_v(t)}{\rho_v(t)\dot{m}_v(t)h_{fg}(t)^2} \tag{5-31}$$

The vapour pressure drop along the vapour header $\Delta P_{vvh}(t)$ is expressed as:

$$\Delta P_{vvh}(t) = \Delta P_{vvh}\left(\mu_v(t), \dot{m}_v(t), \rho_v(t)\right) = \frac{8\mu_v(t)\dot{m}_v(t)L_{vh}}{\pi\rho_v(t)\left(\frac{D_{vh}}{2}\right)^4} \tag{5-32}$$

The vapour viscosity ($\mu_v(t)$) is also a temperature-related parameter and could be extracted from the Property Table of the Water/Steam [5.6] by using the interpolation approach. At a certain time point, there is a corresponding temperature in existence that could result in an associated vapour viscosity.

The flow resistance within the vapour line $R_{vvl}(t)$ could be similarly expressed as shown in Eq. (5-31) and Eq. (5-32).

(3) Vapour flow resistance in heat exchanger channels

$$R_{vhe}(t) = \frac{\Delta P_{vhe}(t) T_v(t)}{\rho_v(t) \dot{m}_v(t) h_{fg}(t)^2} \tag{5-33}$$

The pressure drop of the vapour flowing across the heat exchanger channels could be expressed as:

$$\Delta P_{vhe}(t) = \Delta P_{vhe}\big(\dot{m}_v(t), \rho_v(t)\big) = \frac{\dot{m}_v(t)^2}{2\pi^2 \rho_v(t) \left(\frac{D_{hei} - 2\delta_l}{2}\right)^4 \left(\frac{N_{he}}{2} - 1\right)} \tag{5-34}$$

4. Condensed liquid film thermal resistance

The liquid film will be evenly distributed across the exchanger plate surface at the heat transfer fluid side, and its associated flow resistance $R_l(t)$ is:

$$R_l(t) = R_l\big(\lambda_l(t)\big) = \frac{\ln\left(\frac{D_{hei}}{D_{hei} - 2\delta_l}\right)}{2\pi L_l \lambda_l(t) \left(\frac{N_{he}}{2} - 1\right)} \tag{5-35}$$

5. Heat exchanger wall resistance

$$R_{he} = \frac{\ln\left(\frac{D_{heo}}{D_{hei}}\right)}{2\pi L_{he} \lambda_{he} \left(\frac{N_{he}}{2} - 1\right)} \tag{5-36}$$

C. Transfer of the heat from the heat exchanger to the passing water

The heat transferred to the exchanger surface will be taken away by the passing water, leading to an increase in water temperature. For an inlet water temperature of $T_i(t)$, a temperature rise of $T_o(t)$-$T_i(t)$ will occur after the water passes across the exchanger as indicated in Fig. 5-3. The heat transfer between the exchanger surface and passing water could be expressed as [5.1, 5.3]:

$$Q_{he}(t) = A_{he} h_l(t) \big(T_{he}(t) - T_{ave}(t)\big) = C_p(t) \dot{m}_l \big(T_o(t) - T_i(t)\big) \tag{5-37}$$

$$T_{ave}(t) = \frac{T_o(t) + T_i(t)}{2} \tag{5-38}$$

It should be noted that other methods for the calculation of the temperature difference could be applied, such as log-average.

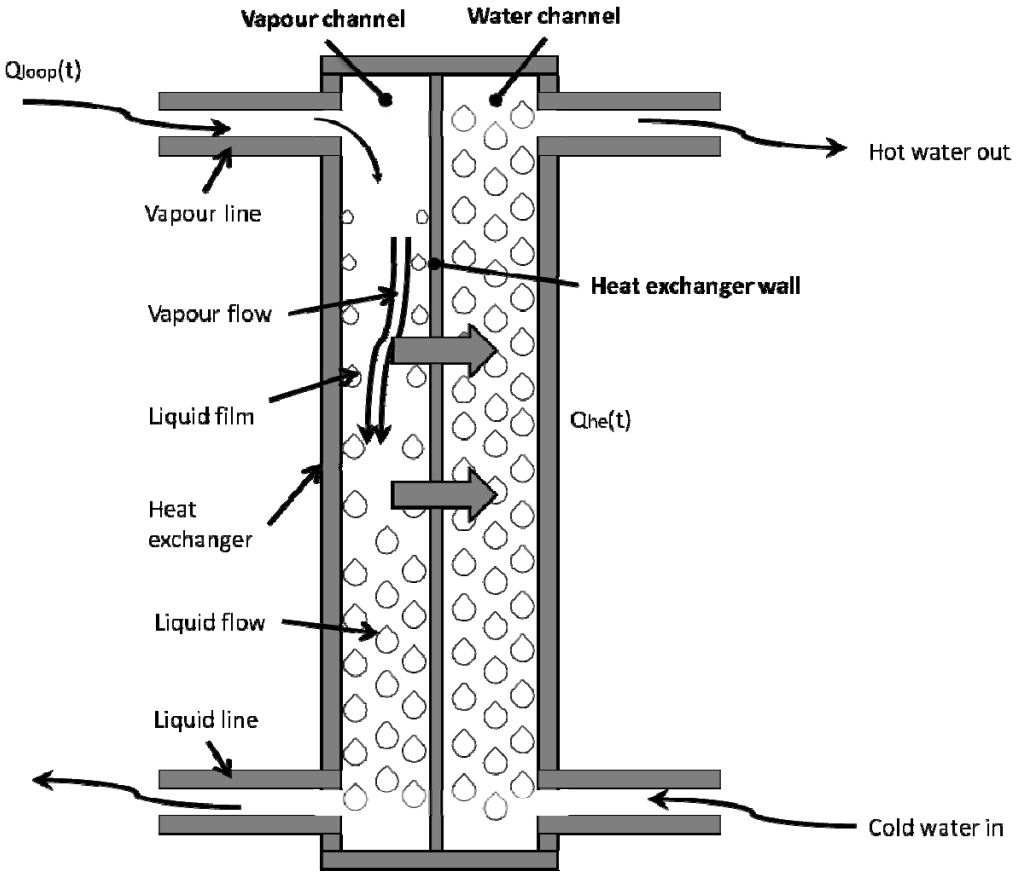

Fig. 5-3. Schematic of the heat transfer process from the heat exchanger wall to the passing water.

$h_l(t)$ is the water convective heat transfer coefficient. For the water flowing across a single heat exchanger channel [5.8],

$$h_l(t) = \frac{\lambda_l(t) Nu(t)}{D_{heo}} \tag{5-39}$$

Since the Reynolds number of the water flows across the exchanger channels widely below 2000, the flow could be treated as laminar. In this case, the Nusselt number could be written as [5.8]:

$$Nu(t) = 1.86 \left(\frac{D_{heo}}{L_{he}}\right)^{\frac{1}{3}} \left(\frac{\mu}{\mu_{he}}\right)^{0.14} Re(t)^{\frac{1}{3}} Pr(t)^{\frac{1}{3}} \tag{5-40}$$

Of which, Reynolds number Re(t) and Prandtl number Pr(t) could be expressed as follows [5.8]:

$$Re(t) = \frac{v_l D_{heo} \rho_l(t)}{\mu_l(t)} \tag{5-41}$$

$$Pr(t) = \frac{C_p(t)\mu_l(t)}{\lambda_l(t)} \tag{5-42}$$

$(\mu/\mu_{he})^{0.14}$ is a factor related to the exchanger plate temperature and could be treated as 1.05 at heating operating condition [5.8].

The water density $\rho_l(t)$, viscosity $\mu_l(t)$ and specific heat capacity $C_p(t)$ are also the temperature-related parameters and could be extracted from the Property Table of the Water/Steam [5.6] by using the interpolation approach. At a certain time point, there is a corresponding temperature in existence that could result in the determination of the values for the above water parameters.

It should be understood that when the water receives thermal energy from the Sun through the LHP system, it, in the meantime, also consumes a certain amount of electrical energy owing to the operation of the circulating pump. This electrical energy will be used to overcome the flow resistance across the water loop between the water storage and heat exchanger, i.e., frictional and local resistances, under an adequate water flow rate.

In this system, frictional resistance loss refers to pressure losses across the straight water pipelines between the heat exchanger and water tank and can be expressed as [5.9]:

$$H_f(t) = H_f\big(\zeta(t)\big) = \sum\left(\zeta(t)\frac{L_{wp}}{D_{wp}}\frac{{v_l}^2}{2g}\right) \tag{5-43}$$

$\zeta(t)$ is the frictional factor depending upon the Reynolds number of the flow and roughness degree of the pipes' inner surface, which can be obtained from a Moody Chart in Ref. [5.9].

Local resistance loss refers to pressure drops occurring at the local fittings assembled in the system, e.g., bends, elbows, joints and valves. The local resistance factor for each fitting could also be obtained from Ref. [5.9]. Hence, the total local resistance pressure loss can be expressed as:

$$H_l = \sum \left(\xi \frac{{v_l}^2}{2g} \right) \tag{5-44}$$

The power consumption occurring in the water cycle could be expressed as:

$$Q_{pump}(t) = \frac{\dot{m}_l g}{\eta_{pump}} \left(H_f(t) + H_l \right) \tag{5-45}$$

The Coefficient of Performance (COP) of the solar system is defined as the ratio of the received heat to the pump power [5.10].

$$COP(t) = \frac{Q_{he}(t)}{Q_{pump}(t)} \tag{5-46}$$

The solar conversion efficiency of the system could be expressed as the ratio of the system heat output to the effective solar energy.

$$\eta(t) = \frac{Q_{he}(t)}{Q_{en}(t)} \tag{5-47}$$

D. Heat transportation into the water tank

It is assumed that $\dot{m}_l$ represents the mass flow rate of the water crossing the heat exchanger; $T_i(t)$ and $T_o(t)$ represent the temperatures of the water at the inlet and outlet of the heat exchanger. At the start-up point, $T_i(t)$ is equal to the tap water temperature. During operation, the water is brought into the heat exchanger, takes the heat away from the heat pipes loop and undergoes a temperature rise of $T_o(t)$-$T_i(t)$ when leaving the heat exchanger. This water will

then be delivered to the tank and mixed with the main water body within the tank, resulting in a temperature of $T_{tk}(t)$. This heating process is illustrated in Fig. 5-4. It should be noted that the temperature of the tank water is taken as unified that the temperature stratification is neglected.

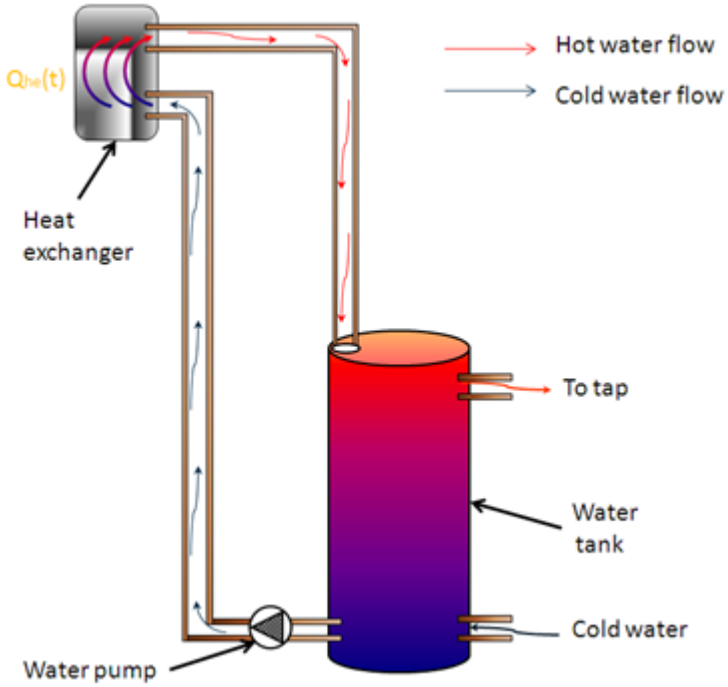

Fig. 5-4. Schematic of the water flow and heat transfer between the heat exchanger and tank.

The heat absorbed by the water flowing across the heat exchanger should be equal to the heat for raising the temperature of the tank water. This could be described as:

$$C_p(t)\dot{m}_l\big(T_o(t) - T_i(t)\big) = C_p(t)\rho_{tk}(t)V_{tk}\frac{dT_{tk}(t)}{dt} \tag{5-48}$$

The exchanger outlet water temperature $T_o(t)$ could be calculated from Eq. (5-37) and expressed in the following alternative way.

$$T_o(t) = \frac{Q_{he}(t)}{C_p(t)\dot{m}_l} + T_i(t) \tag{5-49}$$

Eq. (5-48) can be rewritten as:

$$\dot{m}_l\big(T_o(t) - T_i(t)\big)dt = \rho_{tk}(t)V_{tk}dT_{tk}(t) \quad (5\text{-}50)$$

During Δt time interval, a heat energy correlation could be expressed as:

$$\int_t^{t+\Delta t} \dot{m}_l\big(T_o(t) - T_i(t)\big)dt = \int_{T_{tk}(t)}^{T_{tk}(t+\Delta t)} \rho_{tk}(t)V_{tk}dT_{tk}(t) \quad (5\text{-}51)$$

In case of a small time interval, Eq. (5-51) could be simplified as:

$$\dot{m}_l \frac{\big(T_o(t+\Delta t) - T_i(t+\Delta t)\big) + \big(T_o(t) - T_i(t)\big)}{2}\Delta t = \rho_{tk}(t)V_{tk}\big(T_{tk}(t+\Delta t) - T_{tk}(t)\big) \quad (5\text{-}52)$$

The start tank water temperature T_{tk0} is equal to the initial exchanger inlet water temperature.

$$T_{tk0} = T_{i0} \quad (5\text{-}53)$$

The tank water temperature after Δt time could be calculated as follows:

$$T_{tk}(t+\Delta t) = \frac{\dot{m}_l \Delta t}{\rho_{tk}(t)V_{tk}} \frac{\big(T_o(t+\Delta t) - T_i(t+\Delta t)\big) + \big(T_o(t) - T_i(t)\big)}{2} + T_{tk}(t) \quad (5\text{-}54)$$

If the time interval Δt is the time needed for the water running through the short water loop, the tank water temperature at t+Δt, i.e., $T_{tk}(t+\Delta t)$, could be treated as the temperature of the water entering the heat exchanger at the next water run. Repeating the above process (from Eq. (5-48) to Eq. (5-54)) one run after another, the instant temperatures of the exchanger inlet and outlet water and tank water could be acquired.

5.1.2 Computer modelling setup

The above four heat transfer processes will eventually achieve a balance. The algorithm used for the model setup in the FORTRAN 95 program is indicated as follows:

1. Given the LHP system structure, the data relating to the system configuration could be obtained.
2. Assuming the flow rate of water across the pipelines, calculating the time interval Δt for the water to travel a single run across the water loop, and determining the number of water circulations across the loop during a single-day operation (8 hours from 09:00:00 to 17:00:00).
3. Taking the tap water temperature as the initial tank (exchanger inlet) water temperature T_{i0}.
4. Assuming a start heat pipe fluid temperature T_0.
5. Working out the values of the external parameters including solar radiation I(t) and ambient temperature $T_{amb}(t)$.
6. Carrying out the heat analysis of the solar system on the basis of (1) the starting time point 0 referring to 09:00:00; (2) Δt time interval being the time needed for one run of water flowing across the water loop; and (3) system operation ended at 17:00:00. In terms of a time point (t) belonging to the system's operating period of between 09:00:00 and 17:00:00, the following items have been considered:
   (1) Based on the given $T_i(t)$, the absorber surface temperature will be calculated, and heat balance occurring on the absorber will be analysed, leading to the determination of the glass surface temperature at the time point of t.
   (2) The heat balance of the heat pipes loop will be analysed using the Eq. (5-6) to Eq. (5-36), resulting in the determination of the absorber surface temperature as well as the heat gain of the loop heat pipes at the time point of t.
   (3) The heat balance within the exchanger will be analysed using the Eq. (5-37) to Eq. (5-42), resulting in the determination of the heat gain of the water passing across the heat exchanger $Q_{he}(t)$ at the time point of t.
   (4) The electrical energy consumed by pump $Q_{pump}(t)$ will be analysed using the Eq. (5-43) to Eq. (5-45).
   (5) The energy performance COP(t) and efficiency $\eta(t)$ of the system will be obtained by using the Eq. (5-46) and Eq. (5-47).

(6) The heat balance in the tank will be analysed using the Eq. (5-48) to Eq. (5-54), resulting in the determination of the tank water temperature $T_{tk}(t+\Delta t)$.

(7) Taking $T_{tk}(t+\Delta t)$ as the start tank (exchanger inlet) water temperature of the next water run and returning to step 5 to rerun the program to obtain $Q_{ab}(t+\Delta t)$ and $Q_{he}(t+\Delta t)$.

7. According to the Eq. (5-1) to Eq. (5-5),
   (1) If $(Q_{ab,ave}-Q_{he,ave})/Q_{ab,ave} > 0.5\%$ (error allowance), increasing T(t) by $0.1^{o}C$ and returning to step 5 for recalculation.
   (2) If $(Q_{ab,ave}-Q_{he,ave})/Q_{ab,ave} < -0.5\%$ (error allowance), decreasing T(t) by $0.1^{o}C$ and returning to step 5 for recalculation.
   (3) If $-0.5\% \leq (Q_{ab,ave}-Q_{he,ave})/Q_{ab,ave} \leq 0.5\%$, the whole system will be thought to have achieved a heat balance at the time slot between t and $t+\Delta t$, resulting in the determination of the heat pipe fluid temperature $T(t+\Delta t)$ and other associated thermal parameters.
8. Taking the simulation results of the current time run as the start of the next time run and returning to step 5 for re-simulation.
9. Program stops when the time runs out at the end of the day, i.e., 17:00:00, while the model iteration number matches to the water circulation number in a single-day (8-hour) operation.

5.2 Validation of the model using the published data

To validate the computer model, the data from two previously published papers will be brought into use and compared with the modelling results of the same setups.

5.2.1 Case 1

The start-up behaviour of a loop heat pipe is one of the key aspects in evaluating its performance. Under the support of the National Natural Science Foundation of China (Project No. 50676006) and the Innovation Foundation of BUAA for PhD Graduates, Bai et al. [5.11] investigated the performance of a typical LHP system by using a dedicated mathematic model and conducting experiments. A parametric analysis on the start-up characteristics of the LHP,

e.g., the start-up heat input, heat sink temperature and ambient temperature, was carried out to improve the performance of the LHP. The schematic of the testing LHP is shown in Fig. 5-5. The evaporator and compensation chamber (CC) of the loop were made of stainless steel excluding the nickel powder wick. Ammonia with high purity was charged into the LHP. The transport lines and condenser were also made of stainless steel smooth-walled tubes. The characteristic parameters of the LHP are summarised in Table 5-1.

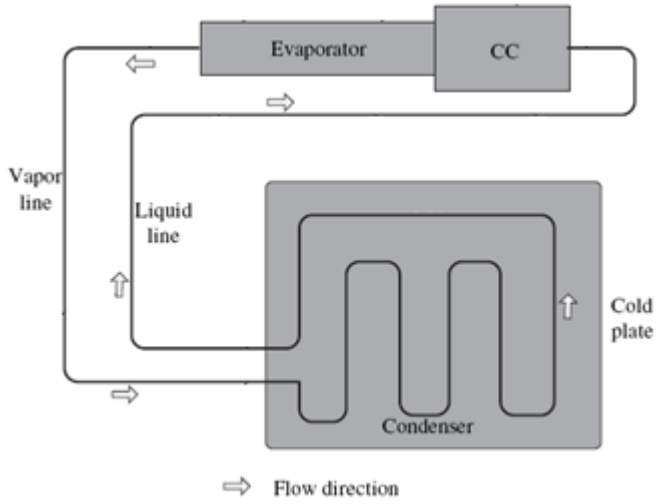

Fig. 5-5. Schematic of the testing loop heat pipe [5.11].

Table 5-1. Characteristic parameters of the LHP [5.11].

Evaporator					
Outer diameter (m)	0.02	Inner diameter (m)	0.016	Length (m)	0.15
Wick					
Outer diameter (m)	0.016	Inner diameter (m)	0.006	Length (m)	0.12
Maximum radius (m)	$1*10^{-6}$	Permeability (m^2)	$> 5*10^{-14}$		
Vapour line					
Outer diameter (m)	0.003	Inner diameter (m)	0.002	Length (m)	2
Condenser					
Outer diameter (m)	0.003	Inner diameter (m)	0.002	Length (m)	0.8
Liquid line					
Outer diameter (m)	0.003	Inner diameter (m)	0.002	Length (m)	2.6
Compensation chamber					
Volume (m^3)	$2.25*10^{-5}$				
Working fluid					
Mass (kg)	0.027				

Several characteristic temperatures along the loop, e.g., temperatures of the evaporator wall and condenser inlet, from the previous modelling and experiments are shown in Fig. 5-6 in the cases of different operating conditions for (a) the heat input of 10 W and ambient temperature of 23^{o}C and (b) the heat input of 5 W and ambient temperature of 18^{o}C.

Fig. 5-6 also presents the simulation results of this modelling after entering the same parameters as the testing structural/operating conditions described above. It was found that the temperatures of the evaporator wall (heat absorbing pipes wall) and condenser inlet (heat transfer fluid) increased over the system's operating period. Comparative analysis between the testing and modelling data from Ref. [5.11] and the results from this modelling indicated that an agreement could be achieved with a maximum error of 12.9%. This error may be caused by the predications of the thermal conductance and internal heat transfer coefficients, and inaccuracy in the calculations of the heat exchange with the ambient by natural convection. However, within a reasonable error limit (15%), this model could predict the performance of the LHP.

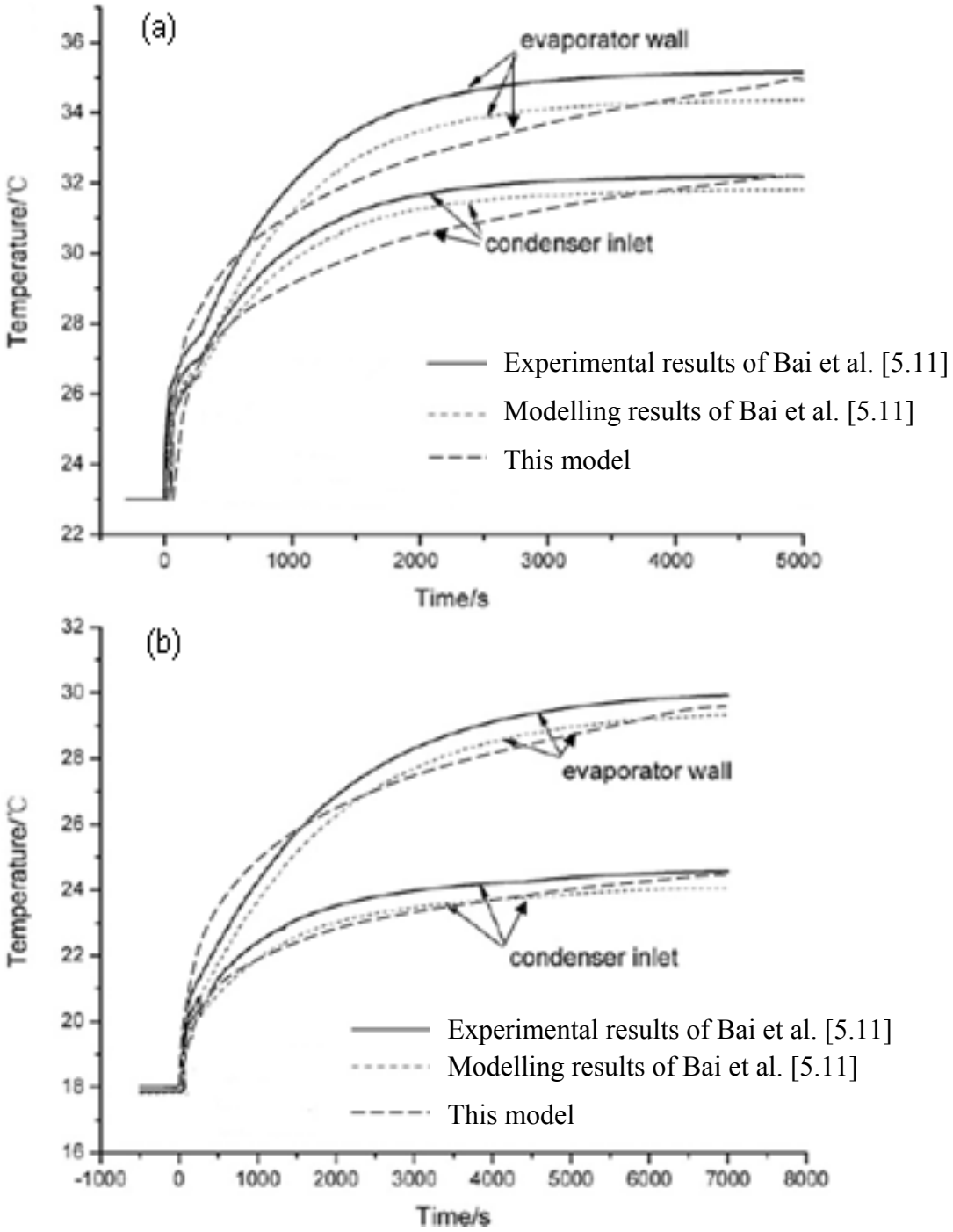

Fig. 5-6. Comparison of the testing and modelling data with the results of this modelling for the temperatures of the evaporator wall and condenser inlet of the LHP in the cases of (a) the heat input of 10 W and ambient temperature of 23^{o}C and (b) the heat input of 5 W and ambient temperature of 18^{o}C [5.11].

5.2.2 Case 2

Kaya et al. [5.12] developed a one-dimensional, time-dependent numerical model and carried out an experimental study to investigate the transient

performance of a loop heat pipe device. They stated that the model could satisfactorily simulate the overall dynamic behaviour of a loop heat pipe unit tested under ambient environment, and the start-up transient was successfully reproduced at high powers. They also mentioned that the experimental correlation remained an important component for accurate prediction of transient LHP operation. The LHP used was a stainless steel/ammonia unit with a sintered nickel wick. The main geometrical parameters of the LHP are summarised in Table 5-2.

Table 5-2. Geometrical parameters of the LHP [5.12].

Evaporator					
Outer diameter (m)	0.017	Inner diameter (m)	0.014	Length (m)	0.2
Wick					
Outer diameter (m)	0.014	Inner diameter (m)	0.006	Porosity	0.6
Effective radius (m)	$9*10^{-7}$	Permeability (m^2)	$2*10^{-14}$		
Vapour line					
Outer diameter (m)	0.003	Inner diameter (m)	0.002	Length (m)	0.5
Condenser					
Outer diameter (m)	0.023	Inner diameter (m)	0.02	Length (m)	0.26
Liquid line					
Outer diameter (m)	0.003	Inner diameter (m)	0.002	Length (m)	0.5
Compensation chamber					
Outer diameter (m)	0.024	Inner diameter (m)	0.021	Length (m)	0.115

The testing was conducted under a start-up power of 197.7 W, and the applied power gradually decreased to 9.9 W. Fig. 5-7 presents the time variations of the temperature of the compensation chamber wall from the testing measurement and modelling calculation in Ref. [5.12].

To enable validation of the established computer model, the input parameters, including the applied power, ambient temperature (24.7^{o}C), sink temperature (14.7^{o}C), geometrical parameters relating to the system configuration and properties of the working fluid, were adjusted to the same values indicated in Ref. [5.12]. The simulation results are also presented in Fig. 5-7.

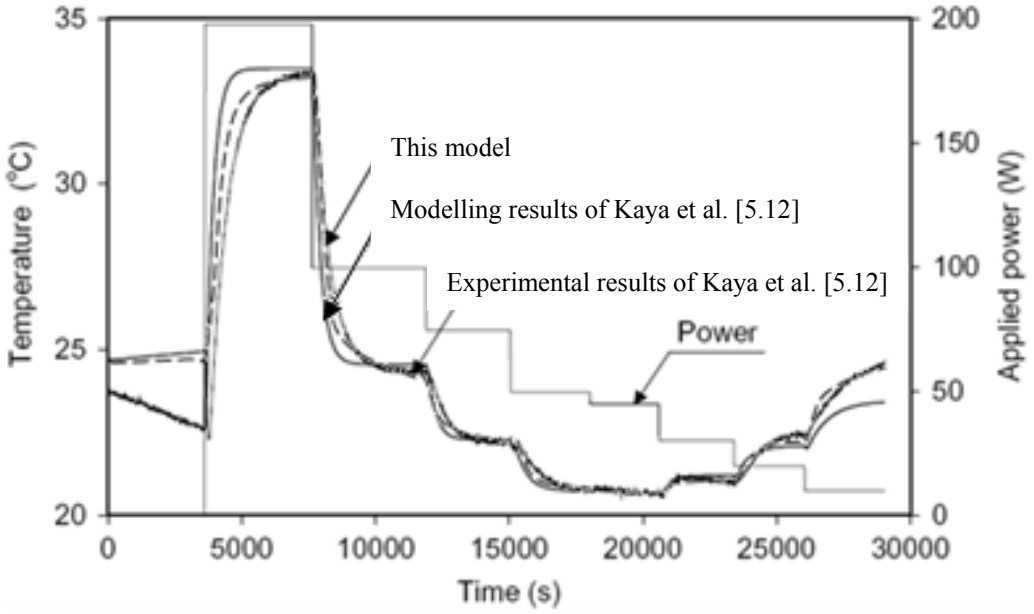

Fig. 5-7. Comparison of the testing and modelling data with the results of this modelling for the compensation chamber wall temperature [5.12].

From Fig. 5-7, it can be seen that an agreement on the temperature of the compensation chamber wall (liquid feeder wall) could be achieved, while the error values were limited to 8.7%. The reasons for the errors may be due to the predications of the thermal conductance and internal heat transfer coefficients, and inaccuracy in the calculations of the heat exchange with the ambient by natural convection. Nevertheless, the accuracy achieved by this model indicated that the model was able to predict the performance of the LHP device at its dynamic operational processes.

5.3 Summary

In this chapter, a computer model was developed to simulate the dynamic performance of the proposed solar LHP system on the basis of the heat balance mechanism. This implied that, at a certain time interval, the four processes of heat transfer in the LHP system, i.e. solar energy absorbed by the collector, heat energy transported across the loop heat pipe, heat energy transferred from the condensation section of the loop heat pipe to the passing water, and heat energy received by the tank water, were in the equalisation condition. The iteration process was activated by the trial-and-error method under the initial assumed parameters. This research will help examine the behaviour of the solar

system, suggest the preferred system components and predict the dynamic performance over the system's operating period.

In order to verify the analytical model, two groups of published measurement data were used, and the associated structural and operational parameters were input into the established computer model, thus generating two sets of modelling results. Comparison between the previous testing and modelling data and the results of this modelling indicated that adequate accuracies of 87.1% and 91.3% could be obtained for the two cases, when using this model to predict the performance of the LHP device. Errors may be caused by the predications of the thermal conductance and internal heat transfer coefficients, and inaccuracy in the calculations of the heat exchange with the ambient by natural convection.

Chapter 6: Experimental testing and model verification of the façade-based solar LHP water heating system

6.0 Overview

In Chapter 5, a computer model was developed to investigate the dynamic performance of the façade-based solar LHP water heating system. Following up the previous work, this chapter will address the establishment of the experimental rig and testing of the system performance using the rig. The experimental results will compare with the modelling results of the same setups. Errors between both will be analysed.

In this chapter, a prototype LHP solar water heating system will be constructed and tested at the SRB (Sustainable Research Building) Laboratory, University of Nottingham. The performance characteristics of the prototype, i.e., heat transfer fluid temperature, tank water temperature, solar efficiency and system COP, will be analysed. The model accuracy was inspected through comparison of the measurement data and modelling results with the average discrepancy of 7.2%, indicating that the model can achieve a reasonable accuracy in predicting the LHP system performance.

Two types of glass covers, namely evacuated tubes and single glazing, will be applied to the prototype, and each type will be tested on two different days (Case 1 to Case 4). For both cover configurations, it was found that the heat transfer fluid temperature rose dramatically in the start-up stage and maintained a gradual growth afterwards. The water temperature rose steadily throughout the day with an increase of 13.5^{o}C for the evacuated tube system and 10.0^{o}C for the single glazing system. For the evacuated tubes, the average testing solar efficiencies were 48.8% and 46.7% for the two cases with the COPs of 14.0 and 13.4, respectively. In terms of the single glazing plate, the testing efficiencies were 36.0% and 30.9% for the two cases with the COPs of 10.5 and 8.9 on average, respectively. Experimental results also indicated that the evacuated tube based system was the preferred configuration of the solar façade LHP system compared to the single glazing system.

This research work will help identify the real behaviour of the system, suggest the optimum operating condition, optimise the geometrical size of the system configuration, and approve/modify the computer model through accuracy/error analysis. The approved or modified model will be further applied to the long-term performance inspection and economic and environmental evaluations.

6.1 LHP system with evacuated tubes

6.1.1 Construction of the prototype system and its associated testing rig in the laboratory

A prototype LHP system with evacuated tubes was constructed at the SRB (Sustainable Research Building) Laboratory, University of Nottingham. The photograph of the prototype is shown in Fig. 6-1.

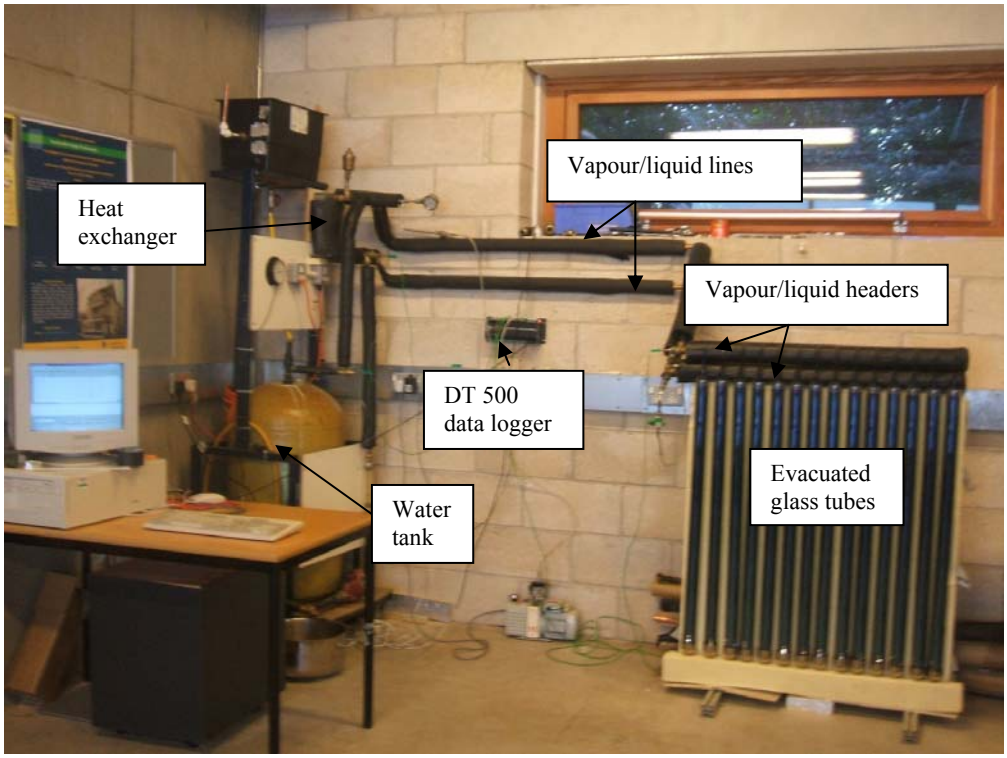

Fig. 6-1. Prototype and testing rig of a façade-based solar LHP water heating system with evacuated tubes.

From Fig. 6-1, it can be seen that the absorbing pipes covered with the double-walled, evacuated tubes were laid on a vertically-positioned reinforced polystyrene insulation board and connected to the vapour/liquid headers. The headers were linked to the heat exchanger located at the upper level of the

absorbing pipes using insulated connection pipes, thus forming a heat pipes loop. A total of 3.4 litres of distilled water was charged into the loop, and then evacuation was made against the loop until an absolute pressure of 0.1bar was achieved. The loop included vapour/liquid transport lines, each having a total length of 2.5 m incorporating a few bends, valves and a steam trap. The flat-plate heat exchanger, on the other side of its channels, connected to a water tank located at 1 m below the exchanger using a short pipe circuit incorporating the insulated pipelines, a pump, a water flow meter and several valves, thus forming the water circuit to allow the service water to circulate.

At the end of the vapour transport line and the inlet and outlet of the water pipes, K-type thermocouple probes (Fig. 6-2 [6.1 ~ 6.2]) were assembled to measure the temperatures of the fluids. A wire temperature sensor (Fig. 6-3 [6.2 ~ 6.3]) was used to measure the ambient temperature. A pressure gauge (Fig. 6-4 [6.4]) with accuracy of ±1.6% was also installed in the vapour transport line for the measurement of the heat pipe operating pressure. All these measurement sensors were linked to a DT500 data logger (Fig. 6-5 [6.5]) and a computer for data recording and analysis.

- Mineral insulated K thermocouples
- 150 mm & 250 mm length versions
- Temperature range: 0 ~ +1,100^{o}C
- Accuracy: ±0.2^{o}C
- Particularly suitable for high pressure, high vacuum or high vibration applications

Fig. 6-2. K-type thermocouple [6.1 ~ 6.2].

- K unscreened PVC thermocouple
- Temperature range: -10 ~ +105^{o}C
- Accuracy: ±0.2^{o}C

Fig. 6-3. Wire temperature sensor [6.2 ~ 6.3].

- Accuracy: ±1.6%
- Temperature range: -40 ~ +60°C
- Scale range: -1 ~ 0bar
- Suitable for all gaseous and liquid media

Fig. 6-4. Pressure gauge [6.4].

- Accuracy: ±1.5%
- 10-30 sensor channels, 7 digital channels
- Up to 1,390,000 data points

Fig. 6-5. DT500 data logger [6.5].

The ambient conditions were manually created and controlled in the laboratory space, such as the radiation of 816 W/m^2, which compared well with the maximum solar radiation of 855 W/m^2 in Beijing, China [6.6]. A solar simulator (halogen lamp) was erected in front of the collector with the preset figure of the radiation by a pyranometer (Fig. 6-6 [6.7]). Optimised water flow rate of 1.6 l/min was also adjusted through a dedicated flow meter (Fig. 6-7 [6.8]). A photograph of the prototype under the laboratory testing is shown in Fig. 6-8.

- First class solar radiation sensor
- Spectral range: 305 ~2,800 nm
- Sensitivity (nominal): 15 μV/(W·m^2)
- Temperature range: -40 ~ 80°C
- Range: 0 ~ 2,000 W/m^2

Fig. 6-6. Pyranometer [6.7].

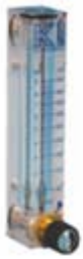

- Flow rate range: 0.8 ~ 9 l/min
- Maximum operating temperature: 65°C
- Accuracy: ±5%

Fig. 6-7. Water flow meter [6.8].

Fig. 6-8. Laboratory testing of the prototype LHP system with evacuated tubes.

A total of 14 evacuated borosilicate tubes were installed on 1 m^2 of gross absorbing area, and these were integrated with other system components, i.e., vapour/liquid headers and transport lines, heat exchanger, water tank and piping. The optical, geometrical and thermal parameters of the system components are given in Table 6-1 to Table 6-4.

Table 6-1. Specification of the evacuated glass tubes.

Evacuated tubes – borosilicate glass 3.3			
Transmittance	0.93	Length (m)	1
Emissivity	0.02	Outer diameter (m)	0.058
Thickness (m)	0.003	Inner diameter (m)	0.047
Number	14	Thermal conductivity (W/(m·K))	1.2

Table 6-2. Specification of the wicked heat absorbing pipes.

Absorbers – copper (with coating of nickel)			
Emissivity	0.1	Absorptivity	0.98
Heat absorbing pipes – copper			
Number	14	Outer diameter (m)	0.0162
Length (m)	1	Inner diameter (m)	0.0158
Thermal conductivity (W/(m·K))	383.8		
Two-layer mesh-screen wicks – copper			
Length (m)	1	Total thickness (m)	$7.5*10^{-4}$
Number of pores	9,158	Diameter of pores (m)	$3.86*10^{-5}$

Table 6-3. Specification of the vapour/liquid headers and transport lines.

Vapour/liquid headers – stainless steel			
Length (m)	0.982	Diameter (m)	0.04
Vapour/liquid lines – copper			
Length (m)	2.5	Diameter (m)	0.016

Table 6-4. Specification of the heat exchanger and tank with water pipes.

Flat-plate heat exchanger – SWEP model: B10T stainless steel			
Length (m)	0.119	Plate thickness (m)	$3*10^{-4}$
Height (m)	0.289	Number of plates	20
Inner width of one channel (m)	$1.94*10^{-3}$	Plate thermal conductivity (W/(m·K))	16.28
Water piping – copper			
Length (m)	3	Diameter (m)	0.016
Water tank			
Volume (m^3)	0.18		

In order to examine the reliability and repeatability of the system's performance, tests were carried out on two different days each for an operating period of 8 hours from 09:00:00 to 17:00:00, and the testing data were recorded every 5 seconds.

6.1.2 Comparative analysis of the testing and modelling results

For comparison between the modelling and experimental results, the model developed in Chapter 5 was adjusted to the same operational/geometrical conditions as for the experimental cases. Case 1 was carried out on 3rd

December 2009 under a stable ambient temperature of 16.8°C and an initial tap water temperature of 23.4°C. Case 2 was undertaken on 7th December 2009, when the ambient temperature was relatively constant at 18.5°C, and the initial tap water temperature was at 24.1°C. The trends of variation of the heat pipe fluid and water temperatures during the all-day operation of 8 hours from 09:00:00 to 17:00:00 are shown in Fig. 6-9 and Fig. 6-10. The efficiencies and COPs derived from the laboratory testing and simulation results are compared as in Fig. 6-11 and Fig. 6-12.

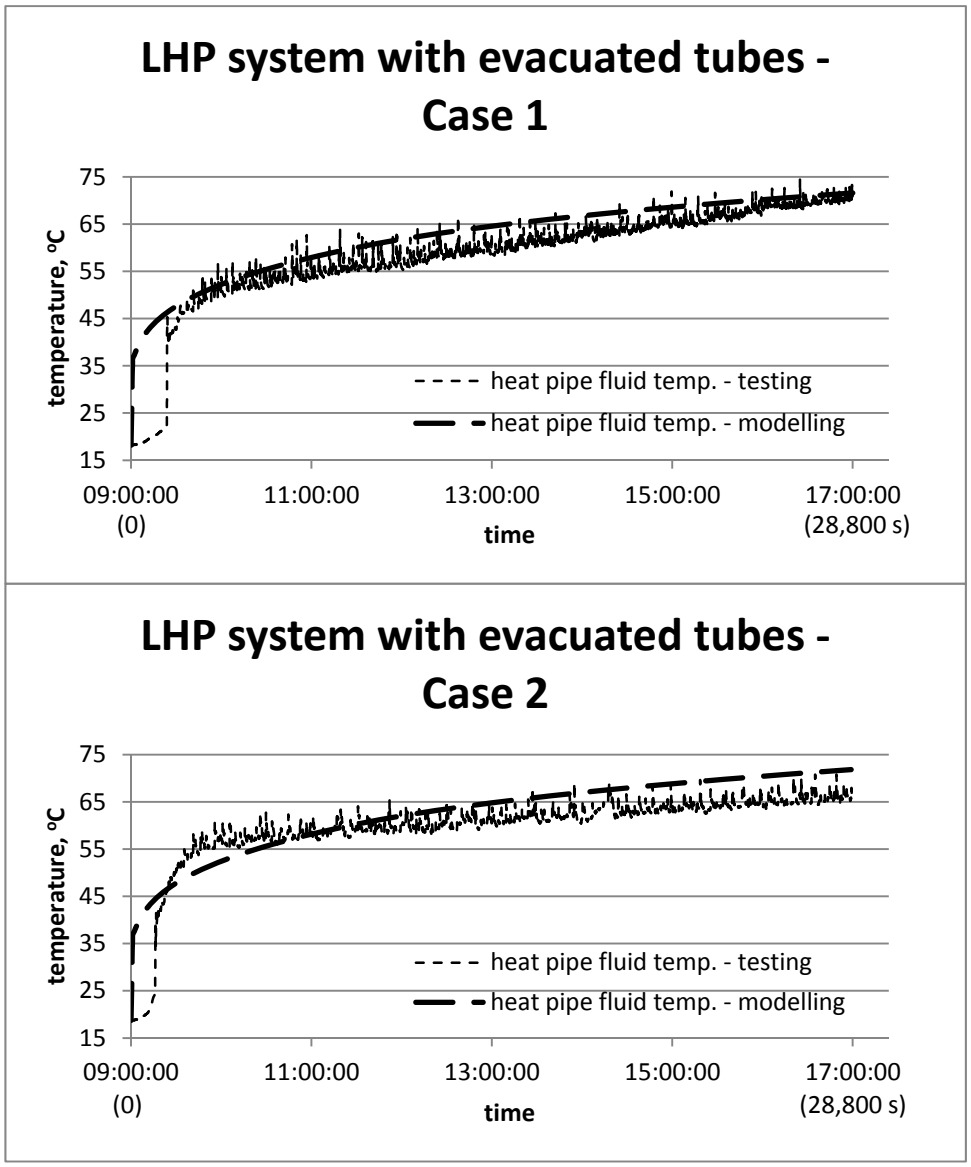

Fig. 6-9. Comparison of the testing and modelling heat transfer fluid temperatures for the LHP system with evacuated tubes.

Fig. 6-9 compared the modelling and testing results of the heat pipe fluid temperature, which showed an agreement with the average error of 7.2%. In terms of the two cases, the heat pipe fluid temperature presented a fast growth trend in the early operation and a close-to-linear increase afterwards. This phenomenon was caused by the requirement of building up temperature of the fluid within the loop heat pipe. At the start-up state, the temperature of the fluid within the heat pipe loop was not high enough to establish an effective heat transfer between the fluid and passing water. Under this circumstance, the heat absorbed by the absorbing pipes was largely trapped in the loop space that would cause the rapid increase of the fluid temperature. When the temperature of the fluid was raised by a certain level, the effective heat transfer between the heat pipe fluid and passing water was established. This would lead to a balance between the heat absorption of the absorbing pipes and dissipation from the heat pipe fluid to the passing water, and thus relatively steady variation of the heat pipe fluid temperature. As to the slow response of the volume of the heat transfer fluid in the heat absorbing pipes loop, the testing temperatures appeared to be in fluctuation.

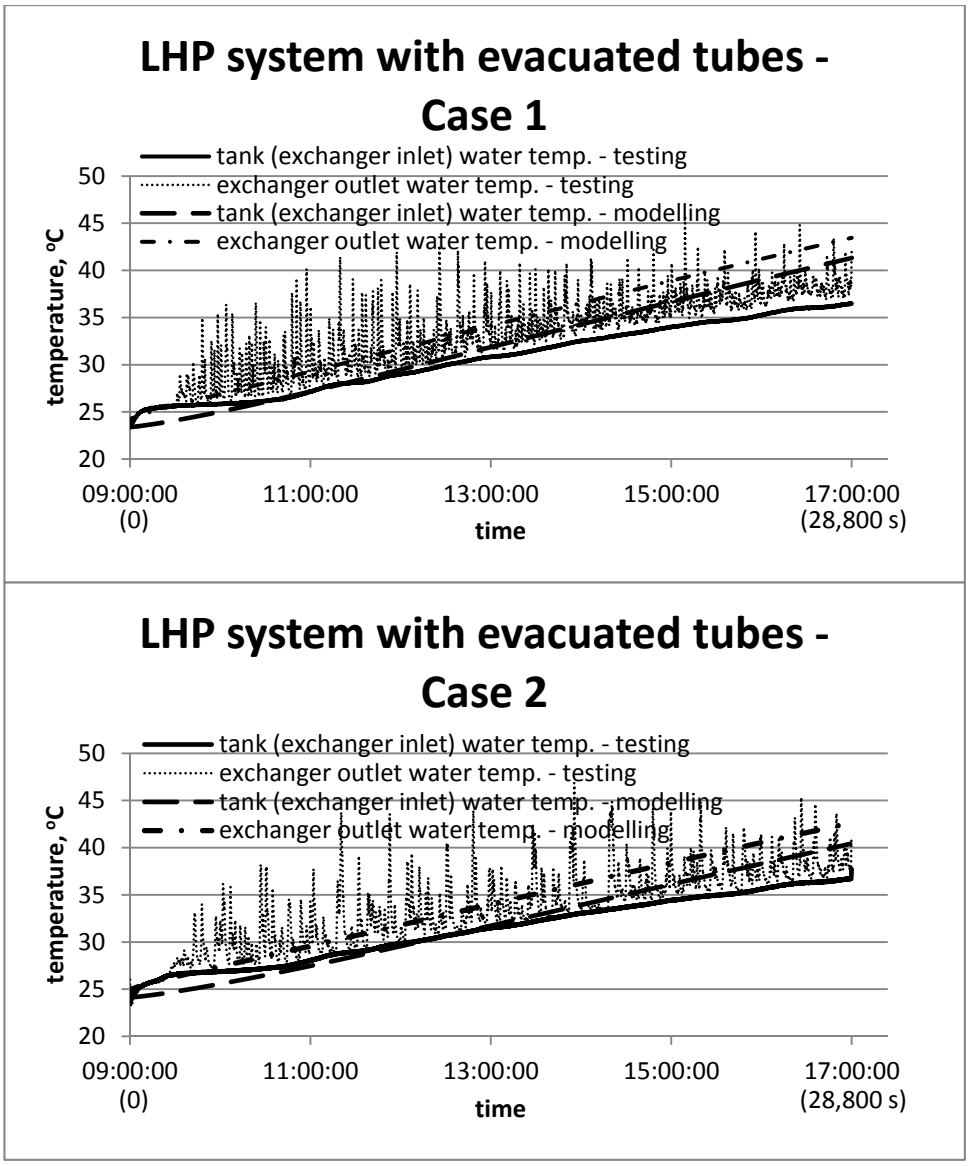

Fig. 6-10. Comparison of the testing and modelling water temperatures for the LHP system with evacuated tubes.

Fig. 6-10 presented the comparison of the modelling and testing results of the water temperatures in the tank and exchanger outlet. For the two cases, it was found that the modelling results were slightly higher than the testing results, especially in the later hours of operation during the day. Theoretically, the final temperatures of the water could reach 40^{o}C, but actual measurement values were about 3-5^{o}C lower. It can also be found that the water temperatures in the outlet of the exchanger were fluctuating owing to the slow response of the heat pipe working fluid volume.

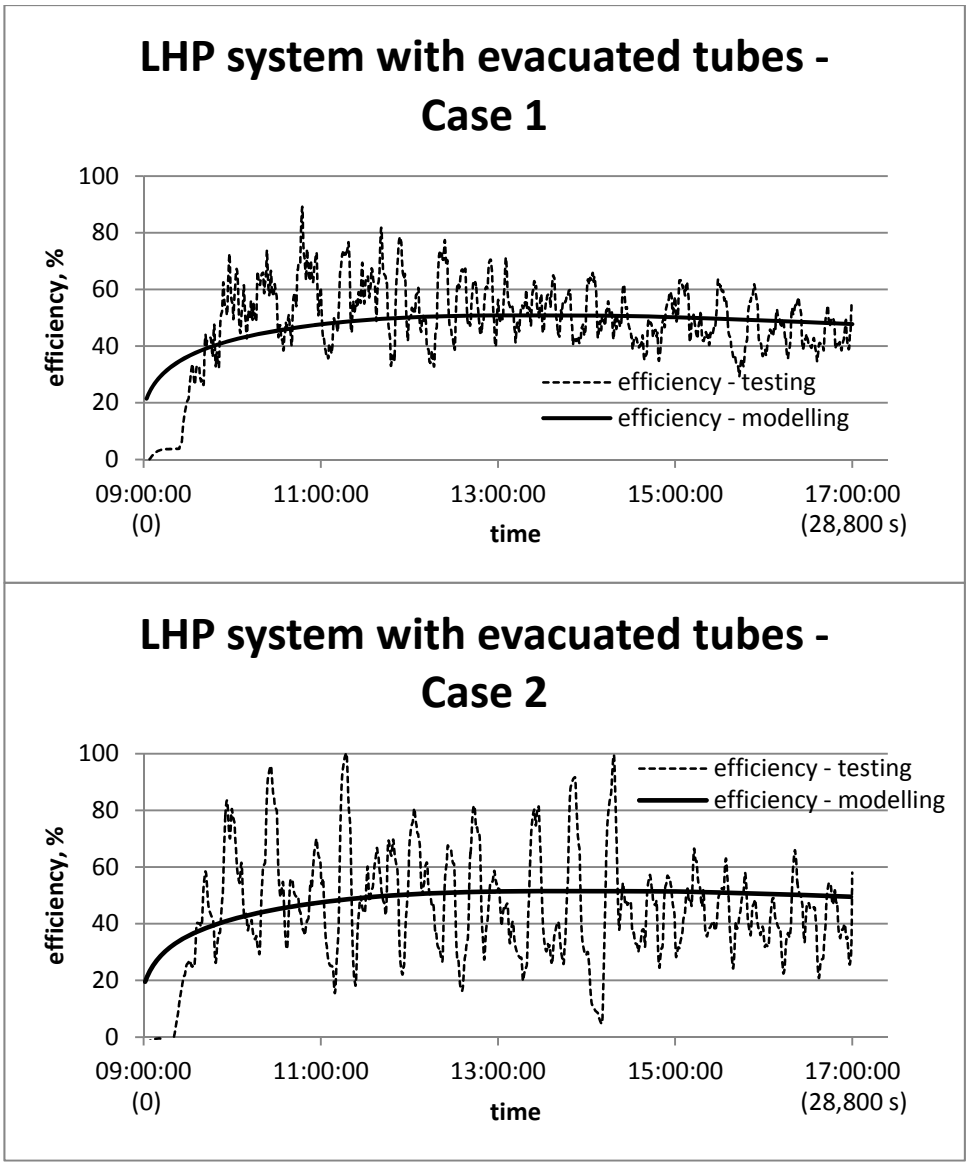

Fig. 6-11. Comparison of the testing and modelling efficiencies of the LHP system with evacuated tubes.

The testing and modelling results of the efficiency of the LHP system with evacuated tubes are shown in Fig. 6-11. The efficiencies were found to increase in the early operation and fall slightly afterwards over the whole day. The average testing and modelling values were 48.8% and 48.0% for Case 1 and 46.7% and 47.0% for Case 2, indicating that an agreement could be achieved between the experimental tests and theoretical simulations. It can also be found that the testing efficiencies were fluctuant owing to the slow response of the heat pipe fluid volume in the LHP system.

It should be noted that owing to the limitations of the laboratory conditions, it was unlikely to simulate the actual operation of the system under real weather conditions. However, the efficiency figures generated from the laboratory testing could be compared against those derived from the computer simulations, thus enabling analysis of the accuracy of the computer model and verification of the effectiveness of the system.

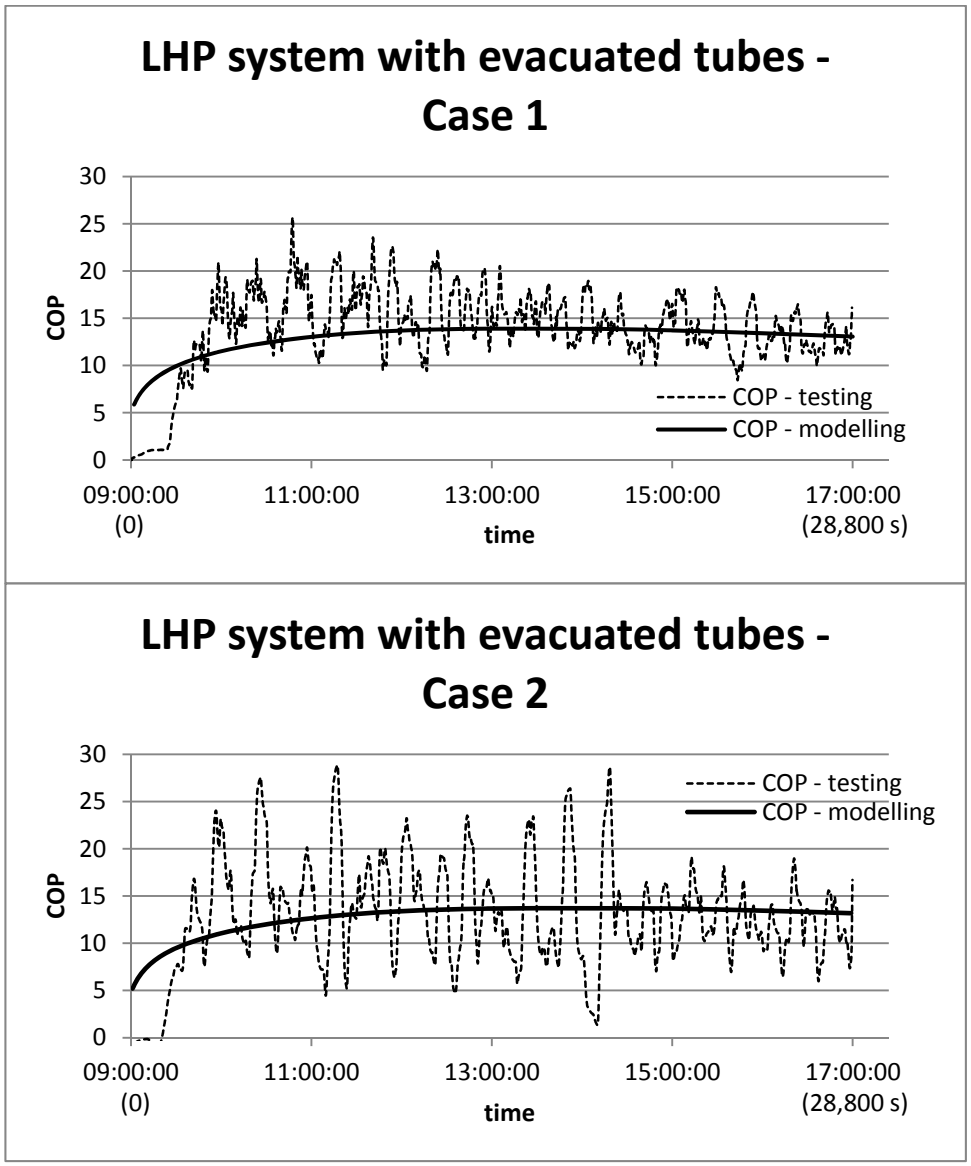

Fig. 6-12. Comparison of the testing and modelling COPs of the LHP system with evacuated tubes.

The testing and modelling COPs of the system operated on the two different days are presented in Fig. 6-12, which were significantly increased and then linearly reduced during the operating hours. The averaged COPs for testing and

modelling could be determined at 14.0 and 13.0 for Case 1 and 13.4 and 12.7 for Case 2, suggesting that the performance of the system could be predicted by the modelling within a reasonable error limit. The testing COPs were also found to fluctuate over the whole day, which could be explained from the slow response of the working fluid in the LHP.

It should be noted that the pump power input was measured once a day for 10 minutes using a portable power analyzer, which gave a relatively stable reading figure of around 20 W.

6.2 LHP system with single glazing

6.2.1 Construction of the prototype LHP system with single glazing

Retaining the same structure of LHP system and altering the double-walled tubes to a single glazing (as shown in Fig. 6-13), a modified solar system configuration, as detailed in Table 6-5, was developed for further laboratory testing and performance evaluation. The flat-plate glazing was fixed in front of the heat absorbing pipes at 20 mm distance, while the backside insulation remained the same.

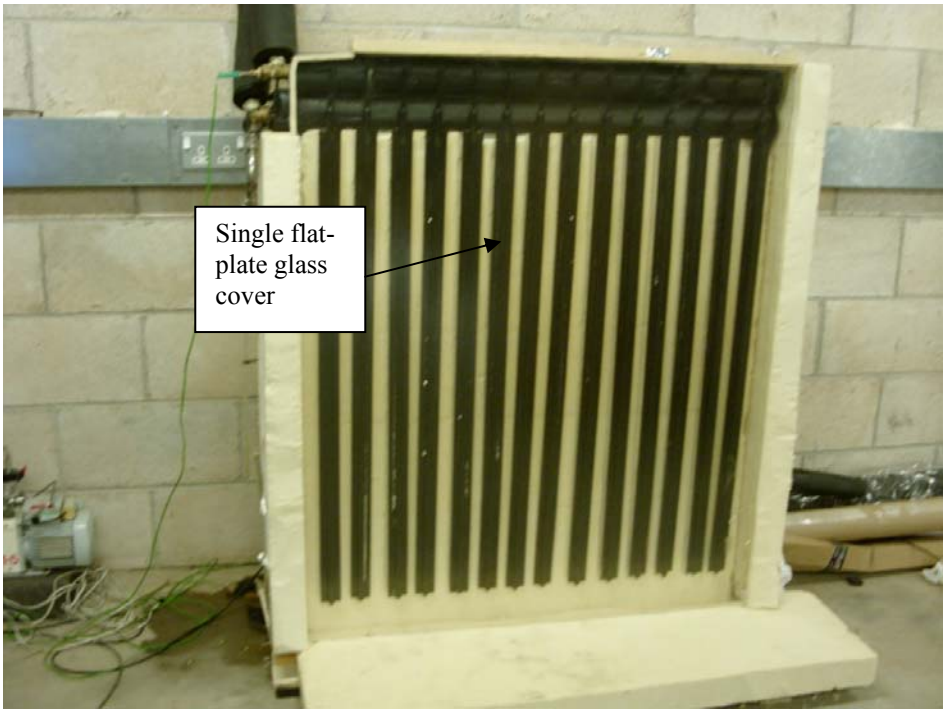

Fig. 6-13. Front view of the LHP system with single glazing.

Table 6-5. Specification of the single flat-plate glass.

Single flat-plate glass - Pilkington Sunplus™			
Transmittance	0.912	Length (m)	1
Emissivity	0.837	Height (m)	1.2
Thickness (m)	0.0032	Thermal conductivity (W/(m·K))	0.937

The laboratory testing was also carried out on two days each with an operating period of 8 hours from 09:00:00 to 17:00:00. The testing data were also recorded every 5 seconds and further analysed to verify the reliability and repeatability of the system's performance.

6.2.2 Comparative analysis of the testing and modelling results

Comparison was made between the modelling and experimental results for the LHP system with single glazing from Fig. 6-14 to Fig. 6-17. Case 3 was carried out on 26th January 2010 under the ambient temperature of 19.5^{o}C and the starting up water temperature of 24.8^{o}C. Case 4 was undertaken on 28th January 2010 under an ambient temperature of 19.8^{o}C and an initial tap water temperature of 27.1^{o}C.

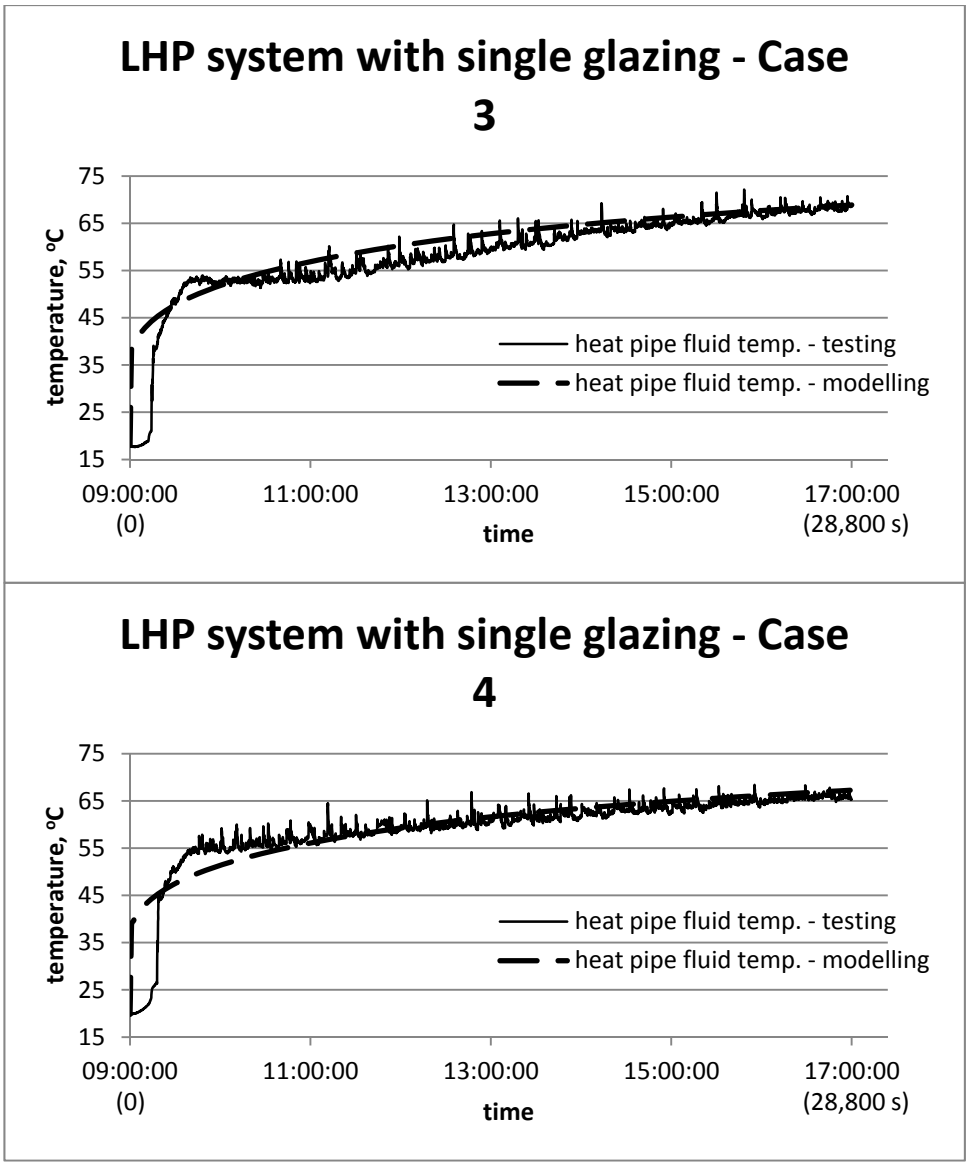

Fig. 6-14. Comparison of the testing and modelling heat pipe fluid temperatures for the LHP system with single flat-plate glass cover.

Fig. 6-14 presents the comparison of the modelling and testing results of the heat pipe fluid temperature for the LHP system with the single glazing. In the early operation of the two days, the temperature of the heat pipe fluid increased significantly. Afterwards, it steadily rose until the end of the operation. The testing temperatures of the heat pipe fluid showed a certain level of fluctuation due to the slow response of the heat pipe fluid in the LHP system.

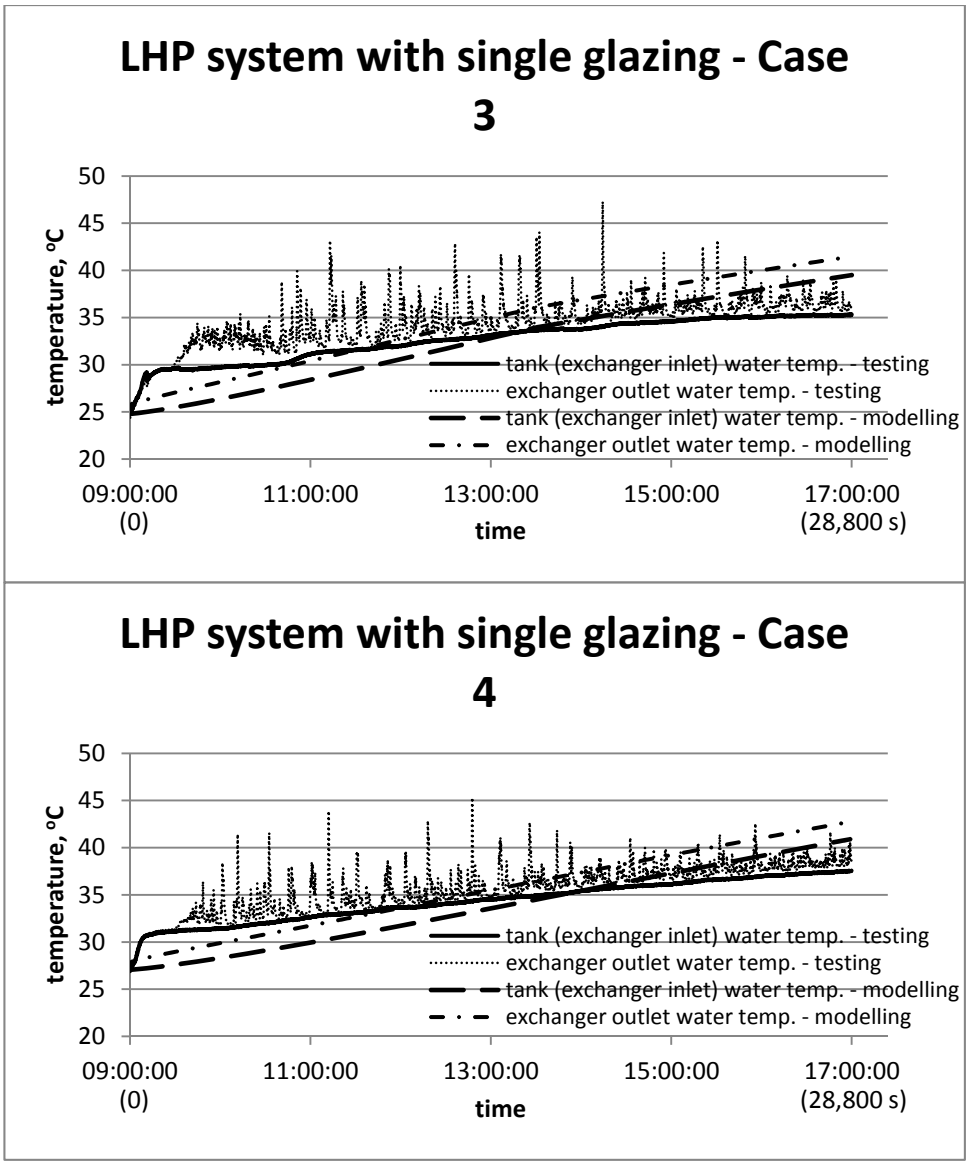

Fig. 6-15. Comparison of the testing and modelling water temperatures for the LHP system with single glazing.

Fig. 6-15 presents the comparison of the modelling and testing results of the temperatures of water in the tank and exchanger outlet. As regards the two cases, it was found that the testing results were slightly higher than the modelling results at the earlier hours of operation during the day and reversed later in the day. Theoretically, the final temperatures of the water could reach 40^{o}C, but the actual measurement figures were about 4-5^{o}C lower. The fluctuation of the temperatures of the water in the exchanger outlet may also be caused by the slow response of the working fluid in the heat pipes loop.

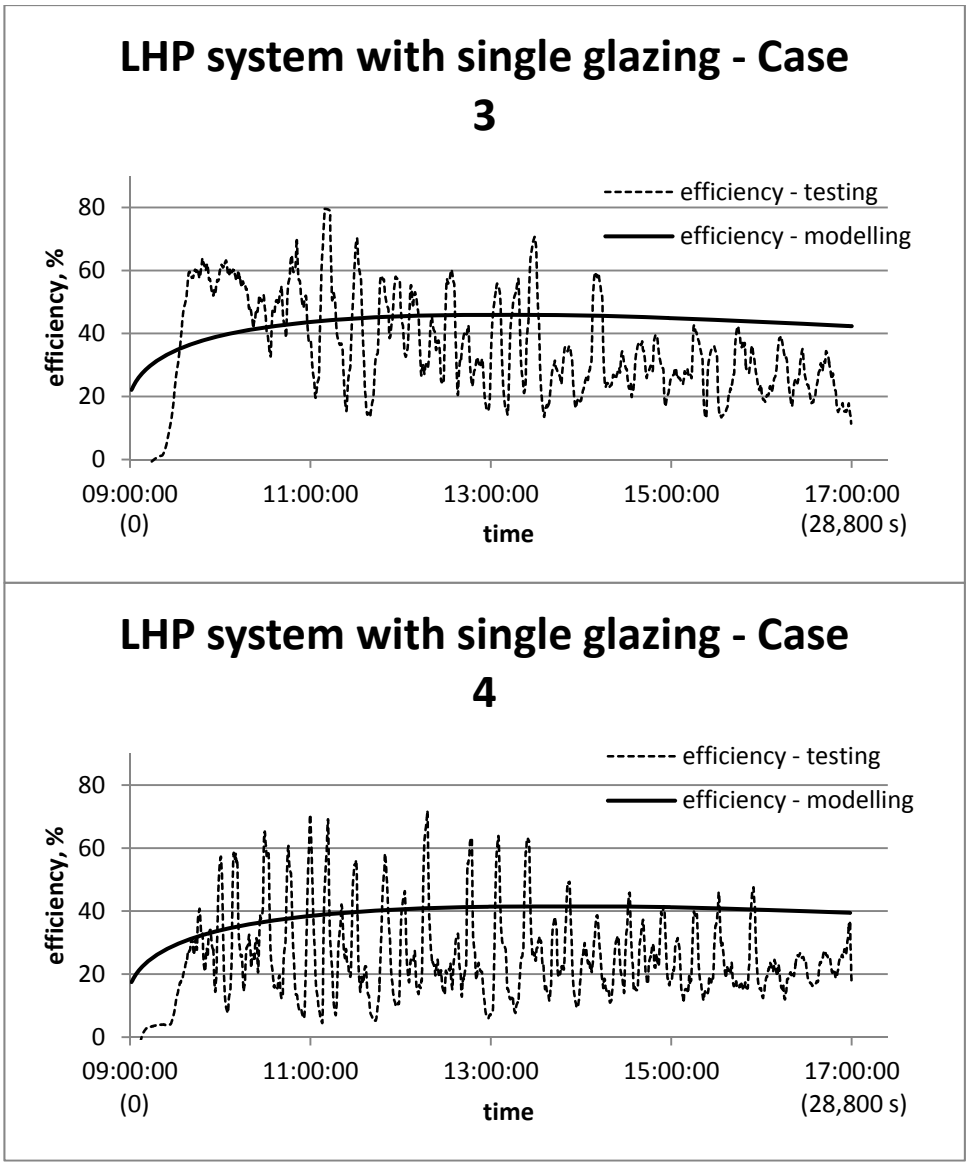

Fig. 6-16. Comparison of the testing and modelling efficiencies of the LHP system with single glazing.

The testing and modelling results of the solar efficiency of the LHP system with single glazing are shown in Fig. 6-16. The efficiencies were found to rise and fall gradually with the average testing and modelling values of 36.0% and 43.0% for Case 3 and 30.9% and 38.6% for Case 4, respectively. It can also be found that, in the later hours, the modelling efficiencies were higher than the testing ones. The occurrence of the errors could be considered from two aspects, i.e., theoretical and experimental. From the theoretical point of view, some simplifications/assumptions made in the model setup, e.g., inaccurate calculations of the heat transfer between the absorbers and surrounding, and

inappropriate omissions of the effect of slow response of the heat transfer fluid volume in the heat pipes loop, may be the potential reasons for the errors. From the experimental point of view, a number of factors, e.g., heat losses occurring in the transport lines due to the insufficient insulations during tests, and a lower than the expected heat transfer rate within the flat-plate heat exchanger, may cause the derivation of the measured figures from modelling.

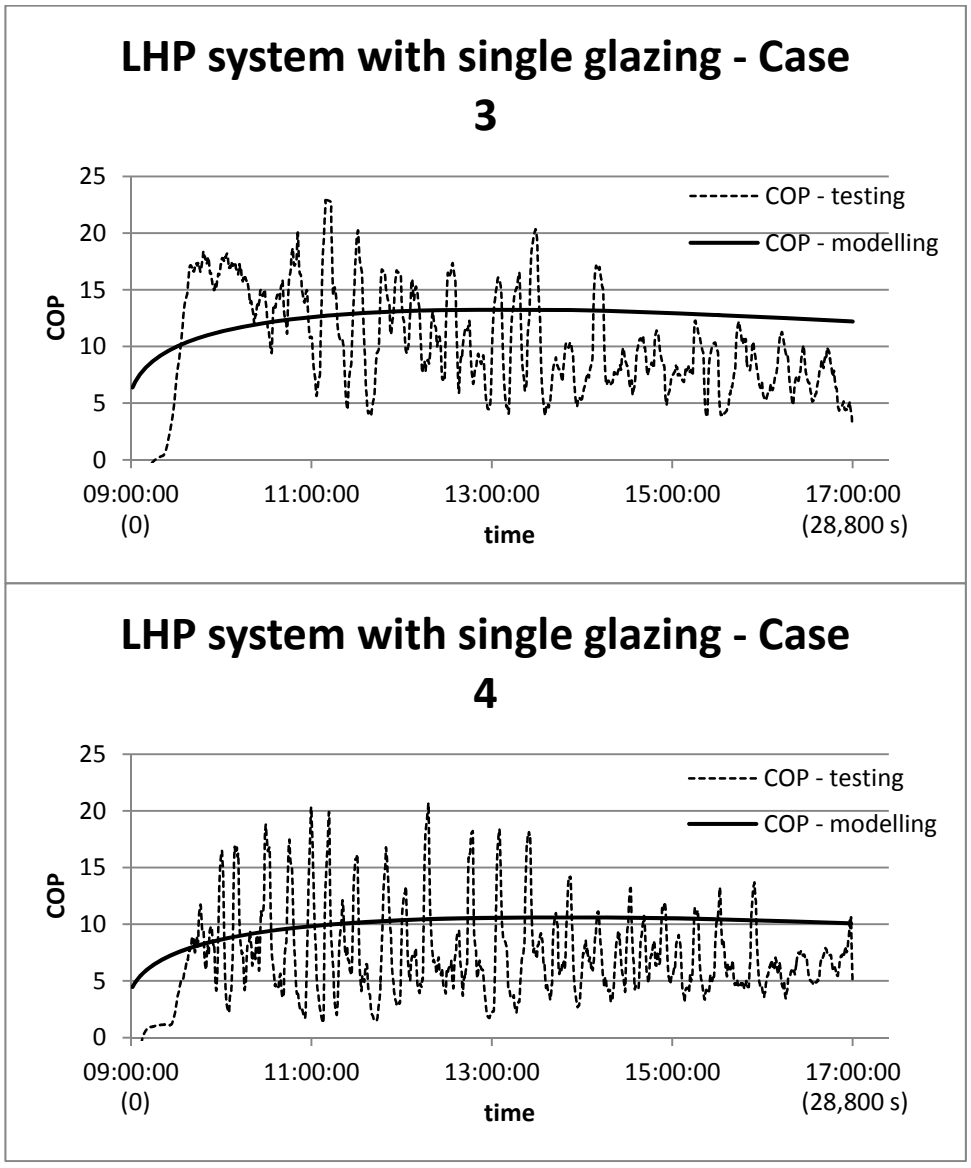

Fig. 6-17. Comparison of the testing and modelling COPs of the LHP system with single glazing.

Fig. 6-17 shows that the testing and modelling system COPs rose and fell during the whole-day operation with averages of 10.5 and 12.4 for Case 3 and

8.9 and 9.8 for Case 4, respectively. The differences between both were caused by several factors, e.g., heat losses occurring in the vapour/liquid transport lines, a lower than expected heat transfer rate within the flat-plate heat exchanger as well as some simplifications made in the model setup.

6.3 Summary

In this chapter, a prototype solar LHP system and its associated testing rig were constructed, simulated and tested at the SRB (Sustainable Research Building) Laboratory, University of Nottingham, in order to examine its dynamic performance during the whole-day operation. The solar collector was sized at the gross area of 1 m^2 comprising 14 mesh-screen wicked pipes. The operating characteristics of the LHP system, including the temperatures of the heat transfer fluid and circulation water, were obtained through measurement by the thermocouple probes. The system efficiency and COP could be determined by presetting the radiation of 816 W/m^2 and water flow rate of 1.6 l/min. Two types of glass covers, i.e., evacuated tubes and single glazing, were applied to the prototype, and each configuration was tested on two different days. Experimental results were in general agreement with the simulation data with the average discrepancy of 7.2%, which indicated that the established model was able to predict the performance of the LHP system with reasonable accuracy. The testing results would also help identify the real behaviour of the system, suggest the optimum operating condition and optimise the geometrical size of the LHP configuration.

For the prototype solar system with both glass covers, the loop heat pipe experienced a fast growth in the temperature of the heat transfer fluid in the start-up stage and afterwards reached its steady state. As to the similar level of heat transport capacity, the temperature of water could be raised by around 13.5^oC for the absorbers covered with the evacuated tubes and 10.0^oC with the single glazing under a fixed water flow rate of 1.6 l/min. Theoretical efficiencies of the evacuated tube system were 48.0% and 47.0% for the two-day operations. However, the testing efficiencies of the evacuated tube system configuration averaged 48.8% and 46.7% for the two cases. The modelling and testing efficiencies of the solar system in the single glazing configuration were

43.0% and 36.0% for the first-day operation and 38.6% and 30.9% for the second-day operation, respectively. The average modelling and testing COPs of the evacuated tube system were 13.0 and 14.0 for Case 1 and 12.7 and 13.4 for Case 2, and the average modelling and testing COPs of the single glazing LHP system were 12.4 and 10.5 for Case 3 and 9.8 and 8.9 for Case 4, respectively. The possible reasons for these differences could be generalised as:

- Slow thermal response of the system during operation owing to the large internal space of the LHP and small volume of the heat transfer fluid in occupation.
- Heat losses occurring in the vapour/liquid transport lines.
- A lower than expected heat transfer rate within the flat-plate heat exchanger.
- Several simplifications made in the model setup.

It can also be concluded that the evacuated tube based system presented better performance than the single glazing based one.

Chapter 7: Annual operational performance, economic and environmental evaluations of the solar façade LHP system with evacuated tubes

7.0 Overview

In this chapter, the annual operational performance of the solar LHP system with evacuated tubes will be studied by implementing the real weather data of Beijing, China into the computer model developed in Chapters 5 and 6. The system's operational parameters, i.e., heat transfer fluid temperature, tank water temperature, solar efficiency and system COP, will be simulated and analysed on a typical day for each month of the year. It was found that the service water temperature was able to reach the required level of 40^{o}C from July to December, and the highest temperature of 55^{o}C occurred in September. The heat transfer fluid temperature rose and fell during the single-day operation. The solar conversion efficiency was higher in summer, while the system COP was higher in winter.

The economic and environmental issues related to the evacuated tube solar LHP system will also be analysed through comparison of this system with a conventional flat-plate solar water heating system. The analytical results indicated that during its 15-year lifetime, the reduction in energy bills would be around £854.20, and the associated carbon dioxide emission cut would be 13.23 tonnes. It can also be concluded that the cost payback period would be 9.9 years.

This part of research will clarify the practicality and potential benefits to be achieved in converting this technology to a commercial product.

7.1 Prediction of the annual operational performance of the solar LHP system with evacuated tubes under real weather conditions

As to the satisfactory agreement achieved between the numerical program and laboratory testing results, as well as the fact that the evacuated tube was the preferred system configuration as indicated in Chapter 6, the annual operational performance of the evacuated tube solar LHP system under real

weather conditions will be predicted by using the computer model developed in Chapter 5. The input parameters, including the characteristic parameters of the system components and weather data, will be described as follows.

7.1.1 Summary of the characteristic parameters of the components of the solar LHP system with evacuated tubes

The optical, thermal and geometrical parameters of the components of the solar LHP system in the configuration of evacuated tubes, which were initially designed in Chapter 3 and then optimised in the following Chapters 4, 5 and 6, are summarised from Table 7-1 to Table 7-4.

Table 7-1. Specification of the evacuated tubes.

Evacuated tubes – borosilicate glass 3.3			
Transmittance	0.93	Length (m)	1.5
Emissivity	0.02	Outer diameter (m)	0.058
Thickness (m)	0.003	Inner diameter (m)	0.047
Number	55	Thermal conductivity (W/(m·K))	1.2

Table 7-2. Specification of the wicked heat absorbing pipes.

Absorbers – copper (with coating of nickel)			
Emissivity	0.1	Absorptivity	0.98
Heat absorbing pipes – copper			
Number	55	Outer diameter (m)	0.0162
Length (m)	1.5	Inner diameter (m)	0.0158
Thermal conductivity (W/(m·K))	383.8		
Two-layer mesh-screen wicks – copper			
Length (m)	1.5	Total thickness (m)	$7.5*10^{-4}$
Number of pores	9,158	Diameter of pores (m)	$3.86*10^{-5}$

Table 7-3. Specification of the vapour/liquid headers and transport lines.

Vapour/liquid headers – stainless steel			
Length (m)	3.73	Diameter (m)	0.08
Vapour/liquid lines – copper			
Length (m)	5	Diameter (m)	0.05

Table 7-4. Specification of the heat exchanger and water tank with pipelines.

Flat-plate heat exchanger – SWEP model: B10T Stainless Steel Condenser			
Length (m)	0.119	Plate thickness (m)	$3*10^{-4}$
Height (m)	0.289	Number of plates	50
Inner width of one channel (m)	$1.94*10^{-3}$	Plate thermal conductivity (W/(m·K))	16.3
Water piping – copper			
Length (m)	5	Diameter (m)	0.016
Water flow rate (m^3/s)	$3.2*10^{-4}$ (19.3 l/min)		
Water tank – Thermomax Direct Solar Storage Tank: 80 Gallons			
Capacity (m^3)	0.364 (80 gallons)		

7.1.2 Weather data

Weather data of different geographic locations could be extracted from the EnergyPlus database [7.1]. Considering the evacuated tube system vertically installed on the south-orientated building balcony at Beijing (China) with the latitude of 39.8°N and longitude of 116.47°E, the hour-based solar radiation and ambient temperature from 09:00:00 to 17:00:00 on a typical day for each month of the year are summarised in Tables 7-5 and 7-6. The instant figures of these two parameters could be calculated by using the interpolation approach. Table 7-7 presents the average daily wind velocity derived from the EnergyPlus database [7.1].

Table 7-5. Hourly solar radiation from 09:00:00 to 17:00:00 on 12 typical days (Unit: W/m^2) [7.1].

Hour of the day	**Jan**	**Feb**	**Mar**	**Apr**	**May**	**Jun**	**Jul**	**Aug**	**Sep**	**Oct**	**Nov**	**Dec**
09:00:00	56	166	225	178	91	71	68	119	242	315	242	81
10:00:00	391	433	424	340	234	165	174	271	417	524	519	422
11:00:00	628	632	588	478	355	281	295	403	560	681	704	651
12:00:00	775	766	703	573	439	362	381	496	657	778	814	785
13:00:00	844	834	760	616	474	399	423	541	697	812	850	838
14:00:00	837	834	754	602	458	387	415	532	678	780	814	812
15:00:00	754	765	687	532	392	328	359	470	600	685	704	707
16:00:00	591	630	562	414	284	228	261	362	472	530	519	513
17:00:00	333	430	390	262	146	100	132	220	306	322	242	205

Table 7-6. Hourly ambient temperature from 09:00:00 to 17:00:00 on 12 typical days (Unit: ^{o}C) [7.1].

Hour of the day	Jan	Feb	Mar	Apr	May	Jun	Jul	Aug	Sep	Oct	Nov	Dec
09:00:00	-2.6	0.3	5.8	14.9	22.7	25.8	26.8	25.3	20.5	15.2	6.3	0.4
10:00:00	-1.2	1.0	7.2	16.2	21.5	26.8	27.9	26.3	22.3	16.9	7.0	1.6
11:00:00	-0.5	2.8	8.6	17.1	25.2	27.8	28.5	27.1	22.8	17.8	9.1	2.6
12:00:00	0.3	4.1	9.5	17.8	25.7	28.7	29.0	27.9	23.6	18.5	9.8	3.7
13:00:00	1.0	4.0	9.9	18.6	23.5	29.6	29.7	28.5	24.5	19.1	9.3	3.9
14:00:00	0.9	5.0	10.7	19.0	26.7	29.7	29.8	28.5	24.7	18.8	10.0	4.1
15:00:00	0.5	4.8	10.6	19.0	26.3	29.7	29.7	28.3	24.6	18.2	9.0	2.9
16:00:00	0.1	3.7	10.0	18.6	23.8	29.6	29.6	28.1	24.2	18.2	7.5	2.5
17:00:00	-1.0	2.4	8.8	17.7	23.9	28.5	29.0	27.3	22.5	15.2	6.0	0.3

Table 7-7. Average daily wind speed for 12 months (Unit: m/s) [7.1].

	Jan	Feb	Mar	Apr	May	Jun	Jul	Aug	Sep	Oct	Nov	Dec
Wind speed	2.6	2.4	3.6	2.6	2.1	2.6	2.0	1.8	1.9	2.2	1.9	2.1

7.1.3 Simulation results and analyses

The initial temperature of water stored in the tank, as shown in Table 7-8, was the tap water temperature referred to as the temperature of ground water at the depth of 1.5 m, which can also be obtained from the EnergyPlus database [7.1]. Table 7-8 also indicates the simulation results of the water temperature for the evacuated tube solar system achieved on the 12 typical days, as well as the theoretical temperature rise over a single-day operation (8 hours from 09:00:00 to 17:00:00). It should be noted that during the prediction of the system performance, it is assumed that there is no tank water usage during the daylight.

Table 7-8. Summary of the initial and final water temperatures along with the temperature rise on the typical day for each month of the year [7.1].

Month of the year	Initial water temperature (^{o}C)	Final water temperature (^{o}C)	Temperature rise over a single day (^{o}C)
Jan	3.6	35.2	31.6
Feb	1.8	38.3	36.5
Mar	2.8	33.3	30.5
Apr	5.0	35.9	30.9
May	11.8	37.3	25.6
Jun	17.5	37.6	20.1
Jul	21.7	42.9	21.1
Aug	23.7	50.5	26.8
Sep	22.6	55.8	33.3
Oct	18.9	54.4	35.5
Nov	13.4	49.8	36.4
Dec	7.9	40.9	33.0

From Table 7-8, it can be seen that the temperatures of service water were higher than 40^{o}C for the typical days from July to December, which could satisfy the heat demand of hot water by the occupants. For the remaining six months from January to June, the water temperatures were lower than 40^{o}C, which may be caused by low levels of solar irradiance, high speed of wind and relatively low temperatures of ambient and tap water. The highest water temperature of 55.8^{o}C could be achieved in September, and the lowest one was at 33.3^{o}C in March. In terms of the temperature rise over a single day, the highest of 36.5^{o}C could be found in February.

In accordance with the optimal water flow rate of 19.3 l/min, the time interval of the water flowing between the exchanger and tank could be estimated at 8 seconds. The simulation results, i.e., heat transfer fluid temperature, tank water temperature, solar conversion efficiency and system COP, are presented from Fig. 7-1 to Fig. 7-4 for the typical day of each month. Fig. 7-1 also shows the variations of the instant solar radiation and ambient temperature in these selected days.

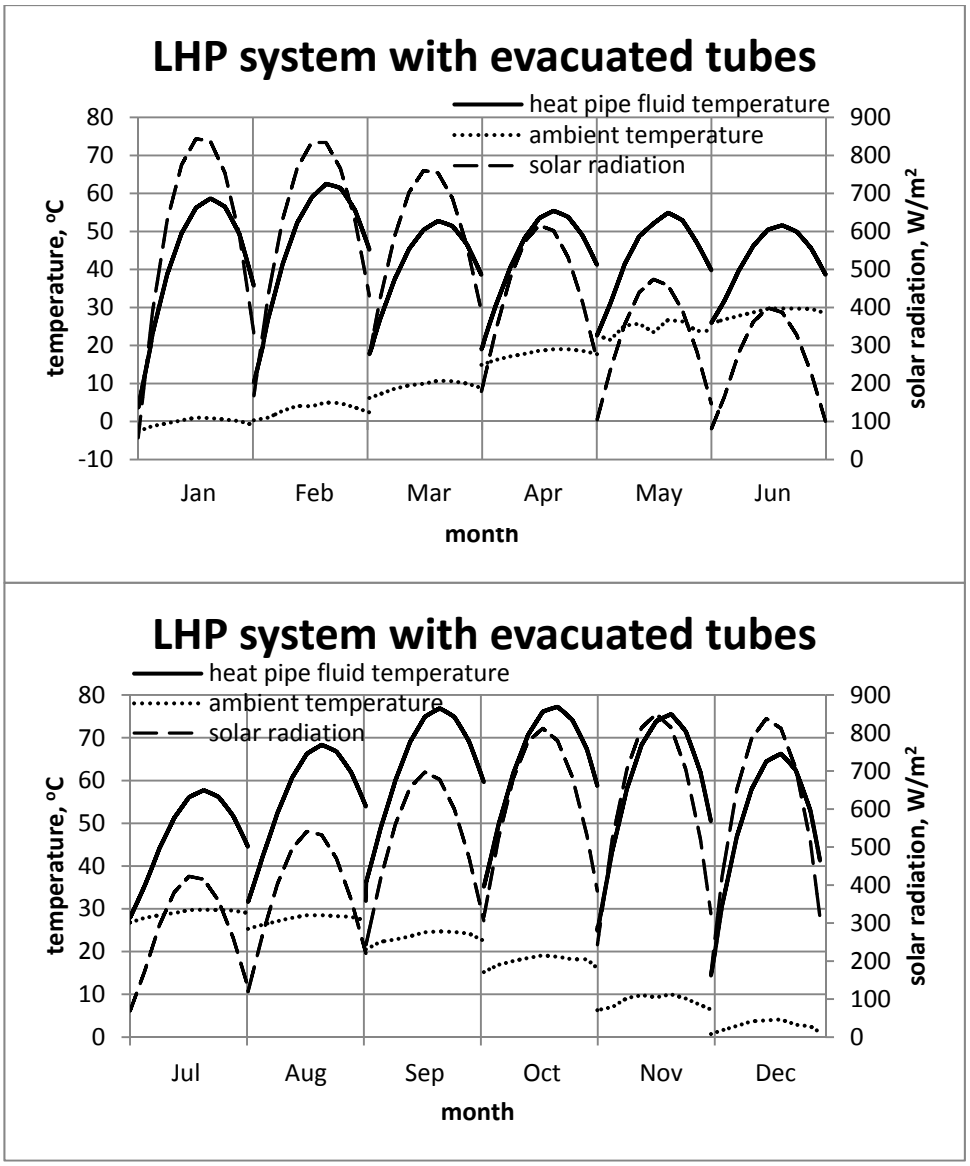

Fig. 7-1. Variation of the heat transfer fluid temperature along with the solar radiation and ambient temperature for the evacuated tube solar LHP system on the typical day for each month of the year.

The variation of the temperature of the working fluid within the heat absorbing pipes loop covered with the evacuated tubes is presented in Fig. 7-1. In the early hours of each day, the temperature increased dramatically to a maximum value, and then it reduced in the remaining operating period. In October, the heat pipe working fluid could reach a temperature of nearly 80^{o}C; while, in March, the highest temperature of the fluid was only 53^{o}C throughout the day. It can also be found that the heat transfer fluid temperature was primarily affected by the level of solar radiation.

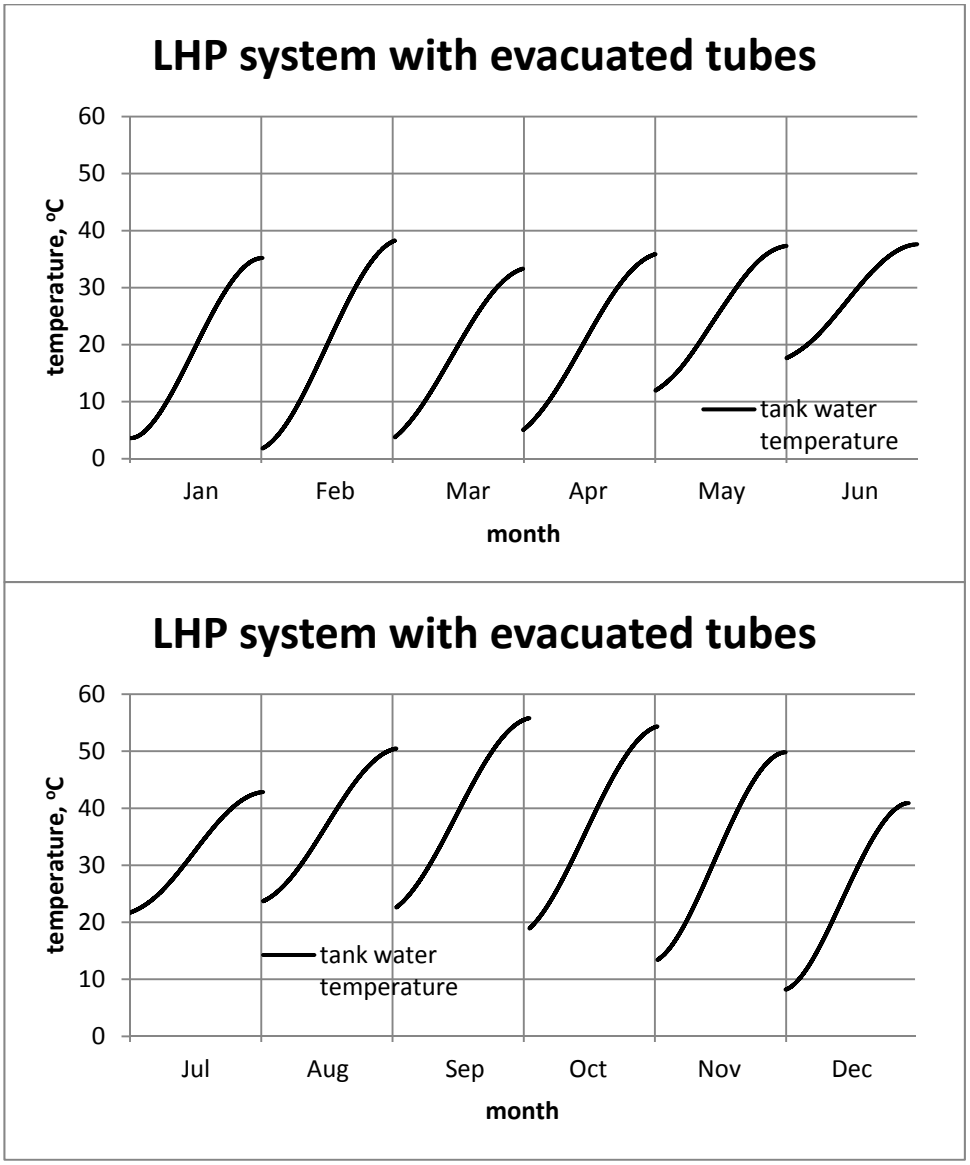

Fig. 7-2. Variation of the water temperature for the evacuated tube solar LHP system on the typical day for each month of the year.

Fig. 7-2 presents the variation of the temperature of water in the tank on the selected typical days. It was found that the water temperature steadily grew over the single day for the 12 months. However, the final water temperatures were lower than the expected 40^{o}C for the first-half-year months owing to the severe weather conditions. For the months from July to December, 40^{o}C could be achieved by employing the evacuated tube system, and the highest temperature of 55.8^{o}C was attained in September.

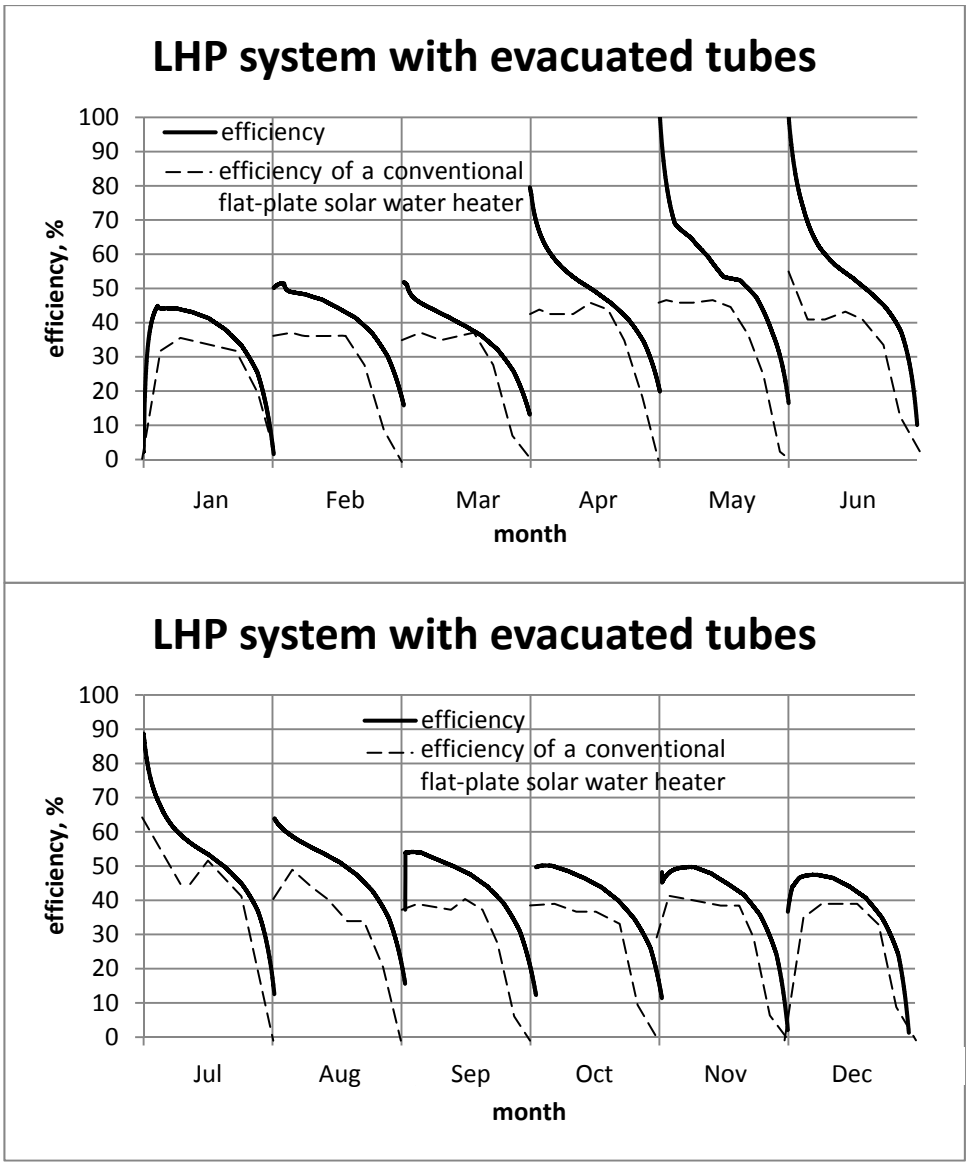

Fig. 7-3. Comparison of the solar conversion efficiency of the solar LHP system in the configuration of evacuated tubes with the conventional flat-plate solar water heating system for the 12 typical days.

The trend of variation of the solar conversion efficiency of the evacuated tube system is presented in Fig. 7-3 above, which was found to fall over the system's single-day operating period in summer. In May and June, 100% of the efficiency could be achieved at the beginning of the daily operation. During the winter season, the efficiencies were usually lower and less than 50% owing to higher heat losses occurring in the cold weather.

In order to evaluate the efficiency of this system, a conventional flat-plate solar water heater was used to compare against the system by using a simulation tool called T*SOL Pro from the Solar Design Company [7.2] and inputting the same parameters of the system to the simulation tool. As shown in Fig. 7-3 above, it was found that the efficiency of the flat-plate system was lower than the novel solar façade system in the configuration of evacuated tube. This may be due to the high heat loss through the single-layer flat-plate glass cover of the conventional solar water heating system to the ambient.

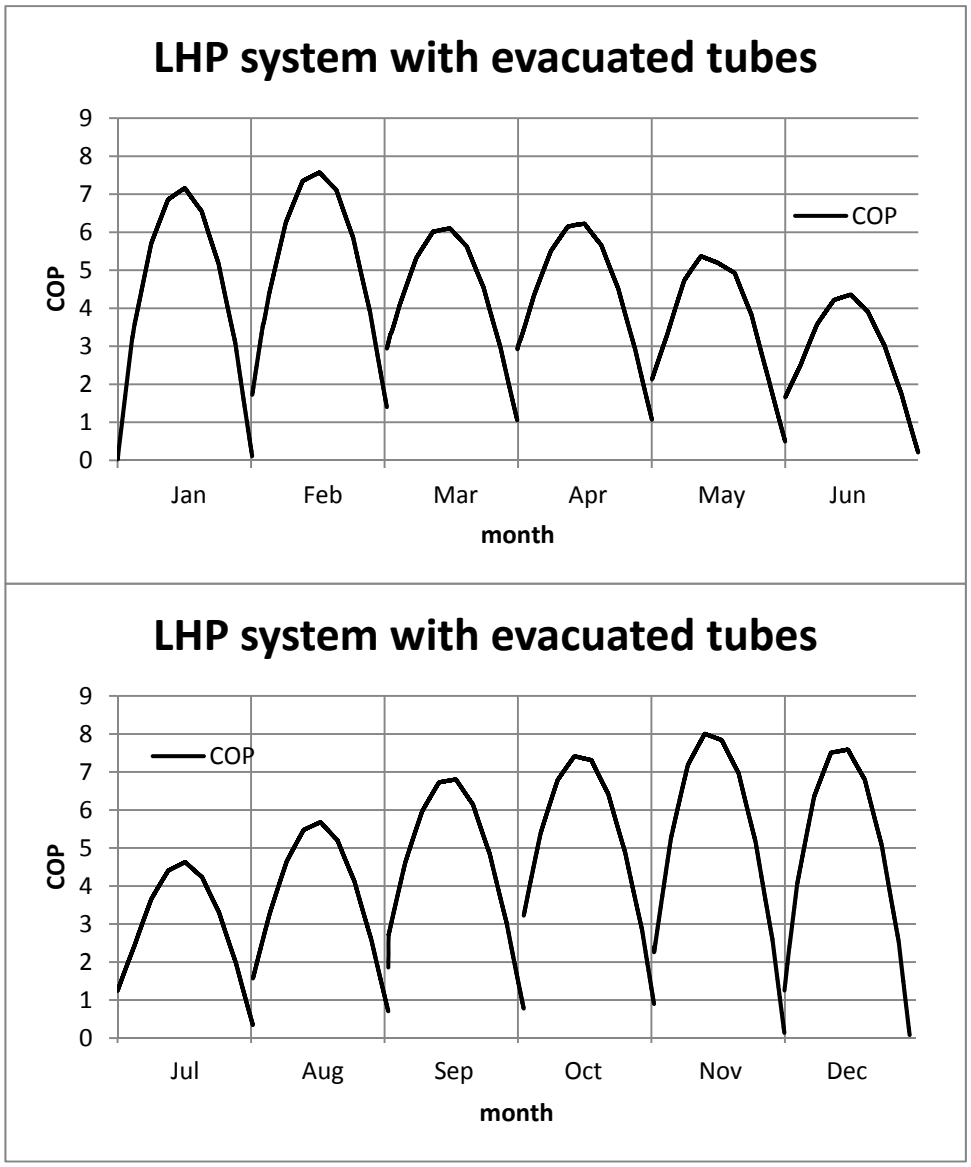

Fig. 7-4. Variation of the COP of the solar LHP system in the configuration of evacuated tubes for the 12 typical days.

Fig. 7-4 indicates that the system COP grew during the early hours of the day and then fell until the end of the whole-day operation for each month. It can be found that the evacuated tube system could achieve high COPs in winter with the highest value of 8 in November, which may be caused by the high levels of winter solar radiation striking the south-facing surface of the collector when the system operated under a fixed rate of 19.3 l/min for the water flowing across the electric pump.

7.2 Economic analysis

In order to understand the economic feasibility of converting this façade-based solar LHP technology to a commercial product, an economic analysis of this system in the configuration of evacuated tubes will be carried out through comparison with a conventional flat-plate solar system and an electric water heater.

7.2.1 Cost comparison of the solar façade LHP system in evacuated tube configuration with the conventional flat-plate solar system and electric water heater

A. Estimation of capital costs

(a) Capital cost of the novel evacuated tube system

The evacuated tube solar system was considered to have a life span of 15 years [7.3], and its capital cost could be calculated by summing up the prices of the system components, taking into account the appropriate sale profit and Value Added Tax (VAT) [7.4]. It should be noted that the unit costs of the system components were quoted from the selected product catalogue. In order to illustrate a direct cost comparison between the novel system and the conventional systems, the costs of the system components in different currencies were converted to British pounds. Details of the calculation for the cost of capital are presented in Table 7-9, and it can be concluded that the initial expense of the system is £2,029.09.

Table 7-9. Calculation of the capital cost of the evacuated tube solar LHP system.

System components	Unit cost (including labour, material and equipment costs) (£)	Quantity	Cost (£)
Evacuated tubes	1.24	55	68.20
Heat absorbing pipes/headers	1,018.25	1	1,018.25
Transport lines	3.65	10 m	36.50
Flat-plate heat exchanger	30.99	1	30.99
Water tank	185.93	1	185.93
Electric pump	160.18	1	160.18
Water piping	3.65	5 m	18.25
Backboard	4.34	5.7 m^2	24.74
Total cost (£)			1,543.04
Pre-tax profit (30% of total cost) (£)			462.91
VAT (5% of profit) (£)			23.15
Capital cost (£)			2,029.09

(b) Capital cost of the conventional flat-plate solar water heater

For comparison, a typical flat-plate solar water heating system in price of £1825.24 is installed and assumed to operate for 15 years [7.5].

(c) Capital cost of the conventional electric water heater

The conventional electric water heater is also expected to last for 15 years [7.5]. Compared to the evacuated tube solar system, the electric water heater is easy to install and thus could maintain the capital/installation cost to a minimum of £273.23 [7.6].

B. Calculation of annual operating costs

(a) Annual operating cost of the novel evacuated tube system

The annual operating cost of the solar façade LHP system includes the prices of electricity consumed by running the auxiliary heater and electric pump.

An auxiliary heater is regarded as the electric heater immersed in the tank. When the tank water had a final temperature of less than 40^{o}C after the solar system operated on a single day, the auxiliary heater will then be switched on to heat up the water until its temperature reached the expected 40^{o}C. The

auxiliary heater is particularly suitable for use in cold weather. Based on the simulation results in Section 7.1 and given the electricity price of 0.1351 £/kWh [7.7] and efficiency of 100% [7.5], the annual cost of the electricity consumed by the auxiliary heater could be calculated at £19.35, as shown in Table 7-10.

Table 7-10. Calculation of the annual electricity cost of the auxiliary heater of the novel evacuated tube system.

Month of the year	Initial water temperature (^{o}C)	Final water temperature (^{o}C)	Heat output of the novel solar system (MJ)	Electricity consumed by auxiliary heater (MJ)
Jan	3.6	35.2	740	112
Feb	1.8	38.3	773	37
Mar	2.8	33.3	716	156
Apr	5.0	35.9	700	93
May	11.8	37.3	599	63
Jun	17.5	37.6	457	54
Jul	21.7	42.9	495	0
Aug	23.7	50.5	629	0
Sep	22.6	55.8	754	0
Oct	18.9	54.4	831	0
Nov	13.4	49.8	826	0
Dec	7.9	40.9	773	0
Total (MJ)			8,291	516
Electricity cost (£)				19.35

The power consumption of the water electric pump can also be obtained from the simulation results in Section 7.1, and the average of 173 W is chosen. Assuming that the pump operates 1,952 hours each year, the annual electricity cost of running the pump could be determined at £45.62.

Summing up the two parts of costs yields a total annual operating cost of £64.97.

(b) Annual operating cost of the conventional flat-plate solar water heater

According to the calculation method illustrated above, the annual operating cost of the conventional flat-plate solar water heater could be estimated as in Table 7-11, which is at £105.91 from the sum of the electricity costs by running the auxiliary heater and water pump. It should be noted that the final water temperature for the conventional system was also calculated from the T*SOL Pro simulation tool [7.2].

Table 7-11. Calculation of the annual electricity cost of the auxiliary heater of the conventional flat-plate water heating system.

Month of the year	Initial water temperature (^{o}C)	Final water temperature (^{o}C)	Heat output of the conventional solar system (MJ)	Electricity consumed by auxiliary heater (MJ)
Jan	3.6	27.9	569	283
Feb	1.8	27.9	552	257
Mar	2.8	28.7	607	265
Apr	5.0	27.1	501	292
May	11.8	32.2	478	184
Jun	17.5	36.6	433	78
Jul	21.7	40.4	438	0
Aug	23.7	42.4	438	0
Sep	22.6	47.6	567	0
Oct	18.9	45.9	633	0
Nov	13.4	38.3	565	39
Dec	7.9	31.0	541	210
Total (MJ)			6,324	1,606
Electricity cost (£)				60.29

(c) Annual operating cost of the conventional electric water heater

The conventional electric water heater is 100% efficient and used to heat up the 180-litre water required by a 3-member family from its initial temperature to the expected 40^{o}C, and the annual operating cost could be calculated at £283.51 by using the same method illustrated above.

C. Assumption of the annual maintenance costs

The maintenance costs of the solar systems for both novel and conventional ones are 2% of the initial system cost [7.8] due to their low maintenance requirement, whereas the maintenance cost of the electric water heater is considered to be 0, as electric heating is a reliable technology and no moving parts would be broken down or worn out during its 15-year life cycle.

7.2.2 Estimations of the cost payback period and life cycle cost saving

Based on the above considerations, the cost payback period of the façade-based solar LHP water heating system in the configuration of evacuated tubes relative to the conventional electric water heater could be calculated as [7.8]:

$$PP_{sf} = \frac{C_{c,sf} - C_{c,el}}{(C_{o,el} - C_{o,sf}) + (C_{m,el} - C_{m,sf})} \quad (7\text{-}1)$$

The cost saving of the solar façade LHP system in energy bills during its 15-year life cycle could be calculated as:

$$CS_{sf} = \left(15 - PP_{sf}\right)\left(\left(C_{o,el} - C_{o,sf}\right) + \left(C_{m,el} - C_{m,sf}\right)\right) \quad (7\text{-}2)$$

The calculations suggest a cost payback period of 9.9 years and a life cycle cost saving of £854.20.

By applying the Eq. (7-1) and Eq. (7-2), the conventional flat-plate solar water heating system could also estimate its cost payback period of 11 years and the life cycle cost saving of £564.38. From the comparative analysis of these figures with that of the novel evacuated tube system, it could be identified that the evacuated tube system has a shorter cost payback period and a higher energy bills saving.

7.3 Environmental analysis

The annual CO_2 emission reduction could be determined from the annual electrical energy saving of the solar façade system over the conventional electric water heater, by multiplying a conversion factor [7.9].

$$CR_{sf} = cf_{co2}(Q_{el} - Q_{sf}) \quad (7\text{-}3)$$

On condition that 1 kWh of grid electricity converts to 0.54522 kg of CO_2, the annual CO_2 emission reduction of the solar façade system applied to the typical flat could be calculated at 0.882 tonnes. Considering the 15-year life cycle of the solar façade, 13.23 tonnes of carbon dioxide emission will be reduced.

Similarly, the analysis on the reduction of the CO_2 emission for the conventional flat-plate solar water heater could also be conducted, and a reduction of 10.75 tonnes could be achieved through its 15-year life cycle.

7.4 Summary

In this chapter, the annual operational performance of the façade-based LHP system with evacuated tubes was analysed under the real weather conditions by applying the computational program developed in Chapters 5 and 6. This part of research work will clarify the practicality and potential benefits to be achieved in converting this technology to a commercial product.

The weather data were extracted from the EnergyPlus database involving hourly solar radiation, hourly ambient temperature, average daily wind speed and initial water temperature. The instant figures of the parameters could be determined by the interpolation methods. It was found that the temperature of water in the tank could be heated up to 40^{o}C as required by the occupants from July to December. The highest water temperature was at 55^{o}C in September. The temperature of the heat transfer fluid increased during the earlier hours of operation in the day and then decreased. The solar conversion efficiency was high in summer, while the system COP was high in winter.

In comparison with a conventional electric water heater, the economic and environmental impacts of the solar water heating system in its life span of 15 years were analysed. It was found that the novel solar system could have the cost saving of £854.20 and CO_2 emission reduction of 13.23 tonnes over the 15 years. The estimated cost payback period of the system would be 9.9 years. It

was also found that the novel system had the potential to be cost-effective and environmentally-friendly through comparison with a conventional flat-plate solar water heating system.

Chapter 8: Conclusions and further work

8.1 Summary of the research work

This research investigated a novel façade-based solar loop heat pipe (LHP) water heating system, which is expected to have the potential to overcome the difficulties associated with the existing solar water heaters, thus creating a façade integrated, low cost, highly efficient and aesthetically appealing solar heating structure.

This research started from a comprehensive review in relation to several areas of research, including solar water heating and loop heat pipe technologies. This review illustrated the current status and global potential of the solar thermal market and revealed the problems existing in the solar water heaters. This review introduced the working principle and classifications of the solar water heating system, as well as its associated mathematical analysis and practical applications in buildings. This review also described the basic concept of the LHP device and thoroughly studied the performance characteristics of the LHP technology through the analytical modelling and experimental testing. Thus, a novel façade-based solar LHP water heating system was proposed.

This research further involved the conceptual design of the novel solar façade, based on a typical 3-member flat in Beijing, China. The working principle of the proposed system was described. The system components, i.e., glass covers, wicked heat absorbing pipes, vapour/liquid headers, transport lines, flat-plate heat exchanger, backboard, pump, water tank and pipelines, were initially designed from three aspects of size, quantity and material or selected from the market product catalogue.

This research investigated the operating limits (heat transport capacity) of the LHP system by developing a computer model. Six potential limits for the operation of the LHP device, i.e., capillary, entrainment, viscous, boiling, sonic and filled liquid mass, were considered. With the specified system structure, variations of these limits with several system structural and operational parameters, including the heat transfer fluid temperature, heat absorbing pipe

diameter, wick structure and exchanger-to-pipes height difference, were investigated. This helped identify the governing limit of the system and optimise the geometrical parameters of the LHP configuration.

This research also investigated the dynamic performance of the solar LHP system by developing a computer model on the basis of the heat balance mechanism. This implied that, at a certain time interval, the four processes of heat transfer in the LHP system, i.e. solar energy absorbed by the collector, heat energy transported across the LHP, heat energy transferred from the condensation section of the LHP to the passing water, and heat energy received by the tank water, were in the equalisation condition. The iteration process was activated by the trial-and-error method. In order to verify the computer model, two previously published papers were applied by inputting the same data of the papers into the modelling.

This research further involved the construction and testing of a prototype solar façade LHP system and its associated testing rig at the SRB (Sustainable Research Building) Laboratory, University of Nottingham. The solar collector of the prototype was sized at a gross area of 1 m^2 consisting of 14 mesh-screen wicked pipes. Two types of glass covers, i.e., evacuated tubes and single glazing, were applied to the prototype, and each configuration was tested on two different days for 8 hours from 09:00:00 to 17:00:00. The operating characteristics of the system configuration, including the temperatures of the heat transfer fluid and circulation water, were obtained through the measurement by the thermocouple probes during the tests. The system efficiency and COP could be determined by presetting the radiation of 816 W/m^2 and water flow rate of 1.6 l/min. Experimental results helped validate the simulation results, identify the real behaviour of the system, suggest the favourite operating condition and optimise the geometrical size of the system components.

This research finally analysed the annual operational performance of the façade-based solar LHP system with evacuated tubes and evaluated its economic and environmental impacts. By employing the validated computer

model, the performance characteristics of the system, including the heat transfer fluid temperature, water temperature, solar conversion efficiency and system COP, were examined under real weather conditions. The simulation results contributed to the reductions of energy bills and carbon emissions associated with the building's hot water production and supply in comparison with a conventional flat-plate solar water heating system and an electric water heater.

8.2 Conclusions

Conceptual design: Regarding the working principle of the proposed solar system, it could be divided into the outdoor and indoor parts, which were connected via the transport lines. The outdoor part, consisting of the glass cover, wicked heat absorbing pipes and headers, was capable of absorbing solar energy and vaporising the heat transfer fluid. The indoor part was composed of the heat exchanger, tank, electric pump and water piping, which could transfer the absorbed heat to the service water through the condensation of the evaporated heat transfer fluid.

Operating limits: Capillary was indicated as the governing limit of the LHP system heat transfer among the six limits, i.e., capillary, entrainment, viscous, boiling, sonic and filled liquid mass. The mesh-screen wick structure was able to achieve a higher heat transfer than the sintered power; therefore, it was a favoured choice for the system configuration. In order to achieve an enhanced system performance, the operation of the system should maintain a high temperature of heat transfer fluid, and have a large diameter for the heat absorbing pipe and a large exchanger-to-pipes height difference.

For the absorbing pipes fitted with mesh-screen wicks, their diameters fixed to 16 mm, the temperature of the heat transfer fluid controlled at 60^{o}C and the exchanger-to-pipes height difference at 1.5 m, the system could achieve the heat transport capacity of 2,362 W/m^2, which was higher than the required heat transfer of 855 W/m^2. This setting could be considered as the optimal system configuration and operating conditions, when it was applied for building's solar water heating in Beijing, China.

Theoretical analysis and computer simulation: In terms of the comparison between the previous testing and modelling data and results of this modelling, adequate accuracies of 87.1% and 91.3% were obtained for the two groups of data, indicating that this model could be used to predict the dynamic performance of the LHP device. Errors may be caused by the predications of the thermal conductance and internal heat transfer coefficients, and inaccuracy in the calculations of the heat exchange with the ambient by natural convection.

Experimental testing and model verification: With regards to the comparison between the experimental results and simulation data, a general agreement with an average discrepancy of 7.2% was acquired, which indicated that the established model was able to predict the performance of the LHP system with reasonable accuracy.

For the solar system in the configurations of evacuated tubes and single glazing, the loop heat pipe experienced a fast growth in the heat transfer fluid temperature in the start-up stage and afterwards reached its steady state. As for the similar level of heat transport capacity, the temperature of water could be raised by around 13.5^{o}C for the absorbers covered with the evacuated tubes and 10.0^{o}C with the single glazing under a fixed water flow rate of 1.6 l/min. Theoretical efficiencies of the evacuated tube system were 48.0% and 47.0% for the two-day operations, and the corresponding testing efficiencies were 48.8% and 46.7%, respectively. The modelling efficiencies of the solar system in the single glazing configuration were 43.0% and 38.6% for the two cases. However, the testing efficiencies of the single glazing system were 36.0% and 30.9% respectively. For the COPs, the evacuated tube system could theoretically achieve 13.0 and 12.7 for the two cases, and the average testing figures were 14.0 and 13.4, respectively. The single glazing system reached the COPs of 12.4 and 9.8 theoretically and 10.5 and 8.9 experimentally. The possible reasons for these differences may be due to the slow thermal response of the heat transfer fluid in the LHP, heat losses occurring in the transport lines, a lower than expected heat transfer rate within the flat-plate heat exchanger and several simplifications made in the model setup. In conclusion, the evacuated

tube based system presented better performance than the single flat-plate based one.

Annual operational performance, economic and environmental evaluations: For the optimised configuration of the solar façade system with evacuated tubes, the temperature of the heat transfer fluid within the LHP increased in the early hours of the system's operating period and decreased afterwards. The temperature of water in the tank rose gradually during a single-day operation and could reach the expected 40^{o}C from July to December. The highest water temperature of 55.8^{o}C was achieved in September. The solar conversion efficiency of the system was found to be high in summer, while the system COP was high in winter.

Compared with a conventional electric water heater, the novel system was able to reduce the energy bills of £854.20 and CO_2 emissions of 13.23 tonnes over its life cycle of 15 years. Its cost payback period was estimated at 9.9 years. It was also concluded that the novel system had the potential to be cost-effective and environmentally-friendly through comparison with the conventional flat-plate solar water heater.

8.3 Further work

Although substantial work has been carried out during this research, there are still quite a few opportunities to develop this project, in order to improve the performance of the system further. These may be indicated as follows:

8.3.1 Further optimisation/modification to the system configurations

Although some essential geometrical parameters of the system components were examined and optimised and the enhanced system performance was achieved, some other characteristic parameters should also be analysed, particularly the size of the liquid feeder. The liquid feeder is capable of controlling the liquid supplement from the liquid header to the wicks of the heat absorbing pipes. Thus, a proper size of the liquid feeder would improve the heat transfer performance of the loop system.

Another consideration is the amount of heat transfer fluid filled into the LHP. It was noticed that a certain amount of liquid accumulated at the bottom of the vapour header during the tests, resulting in a reduced amount of working fluid evaporating/condensing in the loop. In order to solve this problem, the positions of the vapour/liquid headers may be modified. Once this problem is resolved, the performance of the system heat transfer will be significantly improved.

8.3.2 Tests under real weather conditions and long-term schemes

Laboratory-based testing could not imitate the actual system operation owing to the limitations of the laboratory conditions. Therefore, further tests may be carried out to evaluate the operational performance of the system under real weather conditions. In addition, tests may also be performed under long-term schemes, i.e., seasonal or annual, to identify the real behaviour of the system. The testing results can be used to verify the annual operational performance data predicted by the computer model.

8.3.3 Developing a computer model to simulate the start-up stage of the LHP device

Although the start up of the LHP device involves a series of complex heat, mass and energy transfer processes, an experimentally-correlated model may be developed to specify the start-up mode. This will help understand the start-up phenomenon of the LHP device, save on the start-up time, and improve the start-up performance of the novel solar façade.

References

Chapter 1: Introduction

[1.1] Energy - consumption by fuel, 1965-2008 (XLS), Statistical review of world energy 2009, BP, 31st July 2006, retrieved 2009-10-24.

[1.2] Global energy review in 2009, Enerdata Publication.

[1.3] Peak uncertainty, when will we run out of fossil fuels, <http://www.science20.com/absentminded_professor/peak_uncertainty_when_will_we_run_out_fossil_fuels-70294>, [2011-09-27].

[1.4] National Academy of Sciences, National Academy of Engineering, Institute of Medicine, National Research Council, Understanding and responding to climate change, 2008 Edition, National Academies Reports, 2008.

[1.5] Solar heating and cooling for a sustainable energy future in Europe (Revised), European Solar Thermal Technology Platform (ESTTP), <http://www.estif.org/fileadmin/estif/content/projects/downloads/ESTTP_SRA_RevisedVersion.pdf>, 2009.

[1.6] Solar thermal action plan for Europe: Heating & cooling from the Sun, European Solar Thermal Industry Federation (ESTIF), 2007.

[1.7] G. Boyle, Renewable energy: Power for a sustainable future, Second Edition, Oxford University Press, UK, 2004.

[1.8] X.Q. Zhai, R.Z. Wang, Y.J. Dai, J.Y. Wu, Q. Ma, Experience on integration of solar thermal technologies with green buildings, Renewable Energy 33 (2008) 1904-1910.

[1.9] X.Q. Zhai, R.Z. Wang, Experience on solar heating and cooling in China, Renewable and Sustainable Energy Reviews 12 (2008) 1110-1128.

[1.10] D. Jaehnig, C. Isaksson, Solar integration: Five easy ways to incorporate solar thermal into conventional heating systems, Renewable Energy World, November-December 2006, 66-72.

[1.11] M. Yoshikawa, Solar heat collector system, United States Patent No. 4901537, Date of Patent: 20th February 1990.

[1.12] A.G. Hestnes, Building integration of solar energy systems, Solar Energy 67 (1999) 181-187.

[1.13] X. Zhao, S.B. Riffat, Prefabrication in house constructions, International Journal of Low Carbon 21 (2007) 45-51.
[1.14] S. Launay, V. Sartre, J. Bonyour, Parametric analysis of loop heat pipe operation: A literature review, International Journal of Thermal Science 45 (2007) 621-636.

Chapter 2: Literature review

[2.1] C. Philibert, Barriers to technology diffusion: The case of solar thermal technologies, Organisation for Economic Cooperation and Development/International Energy Agency (OECD/IEA), October 2006.
[2.2] W. Weiss, F. Mauthner, Solar heat worldwide: Markets and contribution to the energy supply 2009, 2011 Edition, IEA Solar Heating & Cooling Programme, May 2011.
[2.3] W. Weiss, I. Bergmann, R. Stelzer, Solar heat worldwide: Markets and contribution to the energy supply 2007, 2009 Edition, IEA Solar Heating & Cooling Programme, May 2009.
[2.4] IEA, World energy outlook 2008, OECD/IEA, 2008.
[2.5] IEA, Renewables for heating and cooling, OECD/IEA, 2007.
[2.6] W. Weiss, P. Biermayr, Potential of solar thermal in Europe, ESTIF, 2009.
[2.7] M. Rantil, Solar heating – Kilowatts or megawatts, Presentation at the REWP Technology & Policy Seminar, IEA, Paris, France, 5th April 2006.
[2.8] IEA, Renewable energy – Market and policy trends in IEA countries, OECD/IEA, 2004.
[2.9] Renewable Energy Policy Network for the 21st Century (REN21), Renewables 2010, Global Status Report, 2010.
[2.10] ESTIF, Sun in action II – A solar thermal strategy for Europe, Volume 1: Market overview, perspectives and strategy for growth, ESTIF, April 2003.
[2.11] IEA, Renewables information 2005, OECD/IEA, 2005.
[2.12] F. Karen, K. Neumann, Removing barriers to solar energy use in Santa Barbara county, Community Environmental Council, Santa Barbara, CA, 2004.
[2.13] G. Boyle, Renewable energy: Power for a sustainable future, Second Edition, Oxford University Press, UK, 2004.
[2.14] Solar water heating system, <http://www.solardirect.com/swh/swh.htm>, [2011-09-27].

[2.15] S.R. Hastings, M. Wall, Sustainable solar housing, Volume 2 – Exemplary buildings and technology, Earthscan, London, UK, 2007.

[2.16] N.V. Ogueke, E.E. Anyanwu, O.V. Ekechukwu, A review of solar water heating systems, Journal of Renewable and Sustainable Energy 1 (2009) 1-21.

[2.17] N.M. Nahar, Capital cost and economic viability of thermosyphonic solar water heaters manufactured from alternate materials in India, Renewable Energy 26 (2002) 623-635.

[2.18] A.-J.N. Khalifa, Forced versus natural circulation solar water heaters: A comparative performance study, Renewable Energy 14 (1998) 77-82.

[2.19] Comparison – Tubes vs. plate, <http://www.nrg-solar.co.uk/index.php?option=com_content&task=view&id=144&Ite>, [2011-06-14].

[2.20] F. Struckmann, Analysis of a flat-plate solar collector, 2008 MVK160 Heat and Mass Transport, Project Report, Lund Sweden, 8th May 2008.

[2.21] J.A. Duffie, W.A. Beckman, Solar engineering of thermal processes, John Wiley & Sons, 1980.

[2.22] S.A. Kalogirou, Solar thermal collectors and applications, Progress in Energy and Combustion Science 30 (2004) 231-295.

[2.23] K. Voss, Solar energy in building renovation – Results and experience of international demonstration buildings, Energy and Buildings 32 (2000) 291-302.

[2.24] ISIS Demonstration Housing Project in Freiburg, Germany, IEA-SHC Task 28/ECBCS Annex 38: Sustainable Solar Housing, <http://www.iea-shc.org/task28/publications/index.html>, [2011-05-19].

[2.25] House W – Demonstration House in the Czech Republic, IEA-SHC Task 28/ECBCS Annex 38: Sustainable Solar Housing, <http://www.iea-shc.org/task28/publications/index.html>, [2011-05-19].

[2.26] Plus Energy House in Thening, Austria, IEA-SHC Task 28/ECBCS Annex 38: Sustainable Solar Housing, <http://www.iea-shc.org/task28/publications/index.html>, [2011-05-19].

[2.27] Sunny Woods, Zurich, Switzerland, IEA-SHC Task 28/ECBCS Annex 38: Sustainable Solar Housing, <http://www.iea-shc.org/task28/publications/index.html>, [2011-05-19].

[2.28] W. Weiss, I. Stadler, Facade integration – A new and promising opportunity for thermal solar collectors, IEA-SHC Task 26, Industry Workshop, 2nd April 2001, 59-63.

[2.29] P.D. Dunn, D.A. Reay, The heat pipes, Physics in Technology 4 (1973) 187-201.

[2.30] D. Reay, P. Kew, Heat pipe, Fifth Edition, Elsevier, London, UK, 2006.

[2.31] D. Butler, F. Ku, T. Swanson, Loop heat pipes and capillary pumped loops – An applications perspective, Space Technology and Applications International Forum – STAIF 2002, 49-56.

[2.32] Yu.F. Maydanik, Review: Loop heat pipes, Applied Thermal Engineering 25 (2005) 635-657.

[2.33] M. Groll, M. Schneider, V. Sartre, M.C. Zaghdoudi, M. Lallemand, Thermal control of electronic equipment by heat pipes, Revue Générale de Thermique 37 (1998) 323-352.

[2.34] D.B. Sarraf, W.G. Anderson, Heat pipes for high temperature thermal management, Proceedings of IPACK2007, ASME InterPACK'07, Vancouver, Canada, 2007.

[2.35] G.P. Peterson, An introduction to heat pipes: Modelling, testing, and applications, Wiley-Interscience Press, 1994.

[2.36] K.C. Leong, C.Y. Liu, G.Q. Lu, Characterisation of sintered copper wicks used in heat pipes, Journal of Porous Materials 4 (1997) 303-308.

[2.37] C. Godet, C. Tantolin, M.C. Zaghdoudi, Use of heat pipe cooling systems in the electronics industry, <http://www.electronics-cooling.com/2004/11/use-of-heat-pipe-cooling-systems-in-the-electronics-industry/>, 2004.

[2.38] A. Engelhardt, Pushing the boundaries of heat pipe operation, <http://www.electronics-cooling.com/2008/11/pushing-the-boundaries-of-heat-pipe-operation/>, 2008.

[2.39] J. Rosenfeld, Ultra-lightweight magnesium heat pipes for spacecraft thermal management, Internal Documentation, Thermacore Inc, 2006.

[2.40] G.S. Hwang, M. Kaviany, W.G. Anderson, J. Zuo, Modulated wick heat pipe, International Journal of Heat and Mass Transfer 50 (2007) 1420-1434.

[2.41] T. Kaya, T.T. Hoang, Mathematical modelling of loop heat pipes, American Institute of Aeronautics and Astronautics (AIAA), Paper No. AIAA 99-0477, 1999, 1-10.

[2.42] Z.J. Zuo, A. Faghri, A network thermodynamic analysis of the heat pipe, International Journal of Heat and Mass Transfer 41 (1998) 1473-1484.

[2.43] L. Bai, G. Lin, D. Wen, Modelling and analysis of start-up of a loop heat pipe, Applied Thermal Engineering 30 (2000) 2778-2787.

[2.44] M. Pauken, J.I. Rodriguez, Performance characterisation and model verification of a loop heat pipe, Society of Automotive Engineers (SAE), Paper No. 2000-01-0108, 2000.

[2.45] T.T. Hoang, K.H. Cheung, R.W. Baldauff, Loop heat pipe testing and analytical model verification at the US Naval Research Laboratory, SAE International Paper No. 04ICES-288, 2004.

[2.46] R.R. Riehl, Comparing the behaviour of a loop heat pipe with different elevations of the capillary evaporator, SAE International Paper No. 2004-01-2510, 2004.

[2.47] K.J. Zan, C.J. Zan, Y.M. Chen, S.J. Wu, Analysis of the parameters of the sintered loop heat pipe, Heat Transfer – Asian Research 33 (2004) 515-526.

[2.48] R.R. Riehl, T. Dutra, Development of an experimental loop heat pipe for application in future space missions, Applied Thermal Engineering 25 (2005) 101-112.

[2.49] V.V. Vlassov, R.R. Riehl, Modelling of a loop heat pipe for ground and space conditions, SAE International Paper No. 2005-01-2935, 2005.

[2.50] S. Launay, V. Platel, S. Dutour, J.-L. Joly, Transient modelling of loop heat pipes for the oscillating behaviour study, Journal of Thermo-physics and Heat Transfer 21 (2007) 487-495.

[2.51] T. Kaya, R. Pérez, C. Gregori, A. Torres, Numerical simulation of transient operation of loop heat pipes, Applied Thermal Engineering 28 (2008) 967-974.

[2.52] B.J. Huang, H.H. Huang, T.L. Liang, System dynamics model and start-up behaviour of loop heat pipe, Applied Thermal Engineering 29 (2009) 2999-3005.

[2.53] S. Wang, W. Zhang, X. Zhang, J. Chen, Study on start-up characteristics of loop heat pipe under low-power, International Journal of Heat and Mass Transfer 54 (2011) 1002-1007.

[2.54] A. Faghri, Heat pipe science and technology, First Edition, Taylor & Francis Group, 1995.

[2.55] J. Zhuang, Loop heat pipes for solar energy water heater, People's Republic of China Patent No. 101922814 A, Date of Patent: 22nd December 2010, <http://ip.com/sipoen/101922814>.

[2.56] New type solar water heater, <http://www.me.ntu.edu.tw/~nec/en/en_e_03.htm>, [2011-09-22].

Chapter 3: Conceptual design of the façade-based solar LHP water heating system

[3.1] Chemists discover freezing point of super-cooled water, <http://www.technologyreview.com/blog/arxiv/26985/>, [2011-09-27].

[3.2] G. Boyle, Renewable energy: Power for a sustainable future, Second Edition, Oxford University Press, 2004.

Chapter 4: Operating limits of the façade-based solar LHP water heating system

[4.1] D. Reay, P. Kew, Heat pipe, Fifth Edition, Elsevier, 2006.

[4.2] S.B. Riffat, X. Zhao, P.S. Doherty, Analytical and numerical simulation of the thermal performance of 'mini' gravitational and 'micro' gravitational heat pipes, Applied Thermal Engineering 22 (2002) 1047-1068.

[4.3] A. Faghri, Heat pipe science and technology, First Edition, Taylor & Francis Group, 1995.

[4.4] S.W. Chi, Heat pipe theory and practice, McGraw-Hill, New York, US, 1976.

[4.5] M. Yoshikawa, Solar heat collector system, United States Patent No. 4901537, Date of Patent: 20th February 1990.

[4.6] Ratios of specific heat, <http://www.engineeringtoolbox.com/specific-heat-ratio-d_608.html>, [2009-09-27].

[4.7] V.G. Levich, Physicochemical hydrodynamics, American Journal of Physics 31 (1963) 892.

[4.8] I. Muraoka, F.M. Ramos, V.V. Vlassov, Analysis of the operating characteristics and limits of a loop heat pipe with porous element in the condenser, International Journal of Heat and Mass Transfer 44 (2001) 2287-2297.

[4.9] Weather data, <http://apps1.eere.energy.gov/buildings/energyplus/cfm/weather_data3.cfm/region=2_asia_wmo_region_2/country=CHN/cname=China>, [2011-05-20].

Chapter 5: Theoretical analysis and computer simulation of the dynamic performance of the façade-based solar LHP water heating system

[5.1] S.B. Riffat, X. Zhao, P.S. Doherty, Developing a theoretical model to investigate thermal performance of a thin membrane heat-pipe solar collector, Applied Thermal Engineering 25 (2005) 899-915.

[5.2] Weather data, <http://apps1.eere.energy.gov/buildings/energyplus/cfm/weather_data3.cfm/region=2_asia_wmo_region_2/country=CHN/cname=China>, [2011-05-20].

[5.3] US Department of Energy, DOE fundamentals handbook: Thermodynamics, heat transfer and fluid flow, Volume 2 of 3, DOE-HDBK-1012/2-92, Washington D.C., US, 1992, 6-30.

[5.4] P.D. Dunn, D.A. Reay, Heat pipes, Third Edition, Pergamon Press, New York, US, 1982.

[5.5] S.W. Chi, Heat pipe theory and practice, McGraw-Hill, New York, US, 1976.

[5.6] W. Wagner, H. Kretzschmar, International steam tables: Properties of water and steam, Second Edition, Springer-Verlag, Germany, 2008.

[5.7] The basics of two-phase flow, <http://www.personal.psu.edu/jhm/470/lectures/3.html>, [2011-09-27].

[5.8] J.H. Lienhard IV, J.H. Lienhard V, A heat transfer textbook, Third Edition, Phlogiston Press, US, 2008.

[5.9] US Department of Energy, DOE fundamentals handbook: Thermodynamics, heat transfer and fluid flow, Volume 3 of 3, DOE-HDBK-1012/3-92, Washington D.C., US, 1992, 31-36.

[5.10] C.H. Blanchard, Coefficient of performance for finite speed heat pump, Journal of Applied Physics 51 (1980) 2471-2472.

[5.11] L. Bai, G. Lin, D. Wen, Modelling and analysis of start-up of a loop heat pipe, Applied Thermal Engineering 30 (2010) 2778-2787.

[5.12] T. Kaya, R. Pérez, C. Gregori, A. Torres, Numerical simulation of transient operation of loop heat pipes, Applied Thermal Engineering 28 (2008) 967-974.

Chapter 6: Experimental testing and model verification of the façade-based solar LHP water heating system

[6.1] K insulated thermocouple, <http://uk.rs-online.com/web/p/products/3971488/>, [2011-07-12].

[6.2] Manual on the Use of Thermocouples in Temperature Measurements. ASTM, 1974.

[6.3] K unscreened PVC extension cable, <http://uk.rs-online.com/web/p/products/2363820/?origin=PSF_412657|acc>, [2011-07-12].

[6.4] R1/8 press gauge, <http://uk.rs-online.com/web/p/gauges-for-pneumatics/4055616/>, [2011-07-12].

[6.5] General purpose low power data loggers, <http://www.datataker.com/products/dt500.html>, [2011-07-12].

[6.6] Weather data, <http://apps1.eere.energy.gov/buildings/energyplus/cfm/weather_data3.cfm/region=2_asia_wmo_region_2/country=CHN/cname=China>, [2011-05-20].

[6.7] SR11 pyranometer, <http://www.hukseflux.com/products/radiationMeasurement/sr11.html>, [2011-07-12]

[6.8] Acrylic water flow meter, <http://uk.rs-online.com/web/p/flow-sensors-switches-indicators/3610199/>, [2011-07-12].

Chapter 7: Annual operational performance, economic and environmental evaluations of the solar façade LHP system with evacuated tubes

[7.1] Weather data, <http://apps1.eere.energy.gov/buildings/energyplus/cfm/weather_data3.cfm/region=2_asia_wmo_region_2/country=CHN/cname=China>, [2011-05-20].

[7.2] Software for solar thermal, <http://www.solardesign.co.uk/tsol.php>, [2011-12-05].

[7.3] Solar water heating system, <http://www.solardirect.com/swh/swh.htm>, [2011-09-27].

[7.4] Solar water heating, <http://www.energysavingtrust.org.uk/Generate-your-own-energy/Solar-water-heating>, [2011-08-11].

[7.5] Benefits of electric heating, <http://www.dimplex.co.uk/corporate_information/benefits_of_electric_heating.htm>, [2011-08-11].

[7.6] Economic benefits, <http://thermotechs.com/Advantages_and_Costs.php>, [2011-05-30].

[7.7] Retail price index: Fuels components monthly figures (QEP 2.1.3), <http://www.decc.gov.uk/en/content/cms/statistics/prices/prices.aspx>, [2011-04-28].

[7.8] S. Kalogirou, Economic analysis of solar energy systems using spreadsheets, Proceedings of the World Renewable Energy Congress IV, Denver, Colorado, US, 1996, 1303-1307.

[7.9] 2010 guidelines to Defra/DECC's GHG conversion factors for company reporting, <http://www.carbontrust.co.uk/cut-carbon-reduce-costs/calculate/carbon-footprinting/Pages/conversion-factors.aspx>, [2011-05-23].